Progress in Retinal and Eye Research xxx (xxxx) xxx

Contents lists available at ScienceDirect

Progress in Retinal and Eye Research

journal homepage: www.elsevier.com/locate/preteyeres

The OCT angular sign of Henle fiber layer (HFL) hyperreflectivity (ASHH) and the pathoanatomy of the HFL in macular disease

Prithvi Ramtohul [a,b], Diogo Cabral [b,c], SriniVas Sadda [d], K. Bailey Freund [b,e], David Sarraf [f,*]

[a] Centre Hospitalier Universitaire de l'Hôpital Nord, chemin des Bourrely, 13015, Marseille, France
[b] Vitreous Retina Macula Consultants of New York, New York, NY, United States
[c] CEDOC, NOVA Medical School, Universidade NOVA de Lisboa, Lisbon, Portugal
[d] Doheny Image Reading Center, Doheny Eye Institute, University of California Los Angeles (UCLA) Affiliated, Department of Ophthalmology, Los Angeles, CA, United States
[e] Department of Ophthalmology, NYU Grossman School of New York, New York, United States
[f] Stein Eye Institute, University of California Los Angeles, Los Angeles, CA, United States

ARTICLE INFO

Keywords:
Angular sign of HFL hyperreflectivity
Henle fiber layer
Macula
Multimodal imaging
Optical coherence tomography
Photoreceptor
Retina

ABSTRACT

The Henle fiber layer (HFL) is comprised of bundles of unmyelinated photoreceptor axons intermingled with outer Müller cell processes. The photoreceptor axons extend from the cell bodies located in the outer nuclear layer and radially project toward the outer plexiform layer, the inner third of which includes the synaptic junctional complexes and the outer two-thirds of which includes the HFL. The oblique path of the HFL provides unique structural and reflectance properties and this radial anatomy is highlighted in many macular disorders including those with macular star exudation and HFL hemorrhage. Recent investigations using multimodal imaging techniques, especially cross sectional and *en face* optical coherence tomography (OCT), have provided new perspectives regarding HFL disruption in retinal diseases. The aim of this review is to highlight the pathoanatomy and multimodal imaging, especially OCT, associated with HFL disruption that is present in various macular diseases. After describing the current knowledge of the embryology, anatomy, and physiology of the HFL, we review the existing imaging modalities that allow *in vivo* visualization of the HFL in the healthy and diseased retina. Finally, we report the clinical and imaging findings of acute HFL alteration in various macular disorders, including degenerative, inflammatory, and vascular conditions. Also, we propose a novel and signature OCT biomarker indicative of acute photoreceptor disruption involving the HFL, termed the "angular sign of HFL hyperreflectivity" (ASHH) of macular disease, to unify the pathoanatomy common to these various macular disorders and to provide clarity regarding the underlying pathogenesis.

1. Introduction

The human macula, a 6-mm-diameter area centered on the fovea, is defined by numerous clinically relevant layers, sublayers, and potential spaces (Curcio et al., 2011). As classically described by Polyak, the macula includes the retinal nerve fiber layer (RNFL), ganglion cell layer, inner plexiform layer (IPL), inner nuclear layer (INL), outer plexiform layer (OPL), outer nuclear layer (ONL), photoreceptor inner and outer segments or bacillary layer, and the retinal pigment epithelium (RPE) (Curcio et al., 2011; Polyak, 1941; Ramtohul et al., 2021b). The macular OPL is comprised of two sub-layers: the inner one-third synaptic portion that includes the bipolar and horizontal cell neurites and the cone pedicles and rod spherules; and the outer two-third axonal portion (i.e., the dendritic portion or Henle fiber layer, HFL) that contains bundles of unmyelinated cone and rod axons intermingled with outer Müller cell processes (Curcio et al., 2011; Fine and Yanoff, 1979; Polyak, 1941).

The human fovea has evolved under selective pressure and adaptive processes favoring high spatial resolution and optimal optical properties. The extreme centripetal packing of cone photoreceptors in the fovea externa and the centrifugal displacement of inner retinal layers in the fovea interna are the critical ontogenic stages for the development of high-acuity vision with reduced retinal light scattering at neuronal and vascular interfaces, respectively (Davenport, 1960; Hendrickson and Yuodelis, 1984; Polyak, 1957; Walls, 1942). These 2 ontogenic processes lead to the formation of the radially-oriented HFL (Provis et al., 1998). The distinctive architecture of the HFL has direct pathoanatomical implications, including macular star formation in exudative and

* Corresponding author. Stein Eye Institute, University of California Los Angeles, 100 Stein Plaza, Los Angeles, CA, 90095-7002, United States.
E-mail address: dsarraf@ucla.edu (D. Sarraf).

https://doi.org/10.1016/j.preteyeres.2022.101135
Received 16 August 2022; Received in revised form 8 October 2022; Accepted 12 October 2022
1350-9462/Published by Elsevier Ltd.

List of abbreviations

AAOR	acute annular outer retinopathy
AMN	acute macular neuroretinopathy
ANCA	antineutrophil cytoplasmic antibody
APMPPE	acute posterior multifocal placoid pigment epitheliopathy
ARPE	acute retinal pigment epitheliitis
ASHH	angular sign of HFL hyperreflectivity
AZOOR	acute zonal occult outer retinopathy
BALAD	bacillary layer detachment
CAR	cancer-associated retinopathy
DCP	deep capillary plexus
FA	fluorescein angiography
FAF	fundus autofluorescence
HFL	Henle fiber layer
HLA	human leukocyte antigen
ICGA	indocyanine green angiography
ICP	intermediate capillary plexus
INL	inner nuclear layer
IPL	inner plexiform layer
OCT	optical coherence tomography
OCTA	optical coherence tomography angiography
ONBL	outer neuroblast layer
ONL	outer nuclear layer
OPL	outer plexiform layer
RNFL	retinal nerve fiber layer
RPE	retinal pigment epithelium
SD-OCT	spectral domain optical coherence tomography
SVP	superficial vascular complex
WG	weeks of gestation

inflammatory retinopathies, radially-oriented cystoid macular edema, and radial or petaloid HFL hemorrhage in local (e.g. branch and central retinal vein occlusion) and systemic venous disorders (e.g. intracranial hemorrhage) and macular telangiectasia type 2 (Au et al., 2018; Baumal et al., 2020; Bringmann et al., 2022b; Dreyer et al., 1984; Gass, 1977; Gaudric et al., 2022; Leber, 1916). Recent advances in multimodal imaging techniques, especially cross sectional and *en face* optical coherence tomography (OCT), have provided new insights into the pathophysiology of the HFL in retinal diseases (Au et al., 2018, 2022; Baumal et al., 2020; Lujan et al., 2011; Mrejen et al., 2013; Otani et al., 2011).

The aim of this review is to summarize the evidence supporting the involvement of the HFL in various macular disorders. A true appreciation of the pathoanatomy of the HFL cannot be complete without an in depth understanding of the basic elements of the HFL in healthy retina. After describing the current knowledge of the embryology, anatomy, and physiology of the HFL, we review the existing imaging modalities allowing *in vivo* visualization of the HFL in healthy and diseased retina. Finally, we report the clinical and imaging findings of acute HFL alteration in various macular diseases, including degenerative, inflammatory, and vascular disorders. Also, we describe a novel and signature OCT feature that is a biomarker of acute photoreceptor disruption involving the HFL, termed the "angular sign of HFL hyperreflectivity" (ASHH) of macular disease, to unify the pathoanatomy common to these various macular disorders, to provide clarity regarding the underlying pathogenesis and to guide clinicians to the correct diagnosis.

2. Embryology, anatomy and physiology of the Henle fiber layer

2.1. Embryology and developmental dynamics

2.1.1. Histologic development of the Henle fiber layer in the human fovea

Understanding of the embryologic development of the human macula primarily originated from the descriptive report by Bach and Seefelder in 1914 that included anatomical drawings that were refigured by Ida Mann in 1964 (Bach and Seefelder, 1914; Mann, 1964). Subsequently, several histological reports analyzed the morphogenesis of macular development in pre- and postnatal human retinas (Abramov et al., 1982; Hendrickson and Yuodelis, 1984; Yuodelis and Hendrickson, 1986). Well-fixated human retinas spanning the developmental spectrum of the macula were studied and details of the formation and maturation of the HFL were described (Hendrickson et al., 2012; Yuodelis and Hendrickson, 1986). At around 10–11 weeks of gestation (WG), the developing retina comprises 2 layers, the inner and outer neuroblastic layers, separated by the transient layer of Chievitz which disappears by the sclerad migration of the inner neuroblastic cells (Bach and Seefelder, 1914; Bringmann et al., 2018; Mann, 1964; Provis et al., 1998; Smelser et al., 1973). The inner neuroblastic layer gives rise to the retinal ganglion cells, amacrine cells, and Müller cells. The outer neuroblastic layer evolves into bipolar cells, horizontal cells, and photoceptors (Bringmann et al., 2018; Smelser et al., 1973). At 15–16 WG, spherical photoreceptor inner segments appear at the outermost part of the outer neuroblastic layer (Narayanan and Wadhwa, 1998). At 22 WG, the foveal OPL becomes well defined but remains relatively thin compared to older fetuses (Yuodelis and Hendrickson, 1986). Between 19 and 24 WG, the cone inner segments elongate and the cilium is discernible (Narayanan and Wadhwa, 1998; Provis et al., 1998; Yuodelis and Hendrickson, 1986). At 24–25 WG, the rod outer segments develop from the distal ends of each cilium. At this period, the cone and rod inner segments are interconnected by protoplasmic projections (Narayanan and Wadhwa, 1998; Yuodelis and Hendrickson, 1986). The foveal cone outer segments are not present until 38 WG (Bringmann et al., 2018; Yuodelis and Hendrickson, 1986). Between 24 and 26 WG, the base of the cone displaces at an angle laterally away from the nucleus, indicating the formation of the HFL comprised of short photoreceptor axons and parallel pale-staining cell processes representing outer Müller cell processes (Yuodelis and Hendrickson, 1986). Elaboration of the HFL by the foveal cones reflects the degree of separation of these cones from the bipolar cells with which they are synaptically connected. This separation results from the centripetal displacement of the foveal cones and the centrifugal extension of the foveal bipolar cells (Provis et al., 1998). The rod cell bodies populate between the cone nuclei and pedicles, outside the rod-free zone (central 1500–1800 μm), causing the cone axons to lengthen (Hendrickson et al., 2012). Between 28 and 29 WG, the length of the photoreceptor axons markedly increases and is directly attributable to the continued centripetal displacement of cones (Hendrickson and Yuodelis, 1984). Between 34 and 36 WG, the elongated photoreceptor axons end in a prominent synaptic pedicle (Hendrickson and Yuodelis, 1984). At birth, the cones of the foveal slope have very long axons running through the HFL, making the OPL a much thicker layer (Hendrickson et al., 2012). By 13–15 months postpartum, all the central foveal cones are extremely elongated and thinned, compared to newborns, with long axons extending laterally from the foveal pit to end in a wide and flattened cup-like cone pedicle (Hendrickson and Yuodelis, 1984). In this first postnatal year, synaptic pedicles disappear over the foveal pit as all INL neurons are displaced peripherally, thereby eliminating the OPL entirely from the foveal center (Hendrickson et al., 2012). At 45 months postpartum, the inner portion of the foveola is composed of the cone axons which run along the inner limiting membrane at an angle approaching 90° to the axis of the cone inner and outer segments (Yuodelis and Hendrickson, 1986). During the following years, eyeball growth is associated with the elongation of the HFL and the stretching of the retinal tissue (Gong et al., 2016; Hendrickson, 2005; H. Lee et al., 2015). The foveal cone axons further elongate as cone packing

into the fovea occurs after birth; long axons are prominent as they radiate away from the center (Hendrickson et al., 2012). Postnatal changes of the central fovea (up to 16 years of age) also include a decreased thickness of the HFL in the foveola and increased thickness of the HFL in the foveal walls (between 0.3 and 1.5 mm from the foveal center) (H. Lee et al., 2015). The OPL around the fovea is much thicker than in the periphery, where it contains mainly synaptic contacts (Hendrickson et al., 2012).

2.1.2. Radial and peripheral extension of the Henle fiber layer

The radial extension of the HFL reflects the displacement between the inner and outer retina during foveal development (Provis et al., 1998). The centrifugal displacement of the inner retina has a shorter duration and starts after 28 WG, long after the beginning of the centripetal displacement of the outer retina (fetal week 8), and is complete between 9 and 45 months postnatally (Dubis et al., 2012; Yuodelis and Hendrickson, 1986). Conversely, the centripetal displacement of the outer retina continues for several years postnatally (Bringmann et al., 2018). Therefore, the radial extension of the HFL is proportionally more

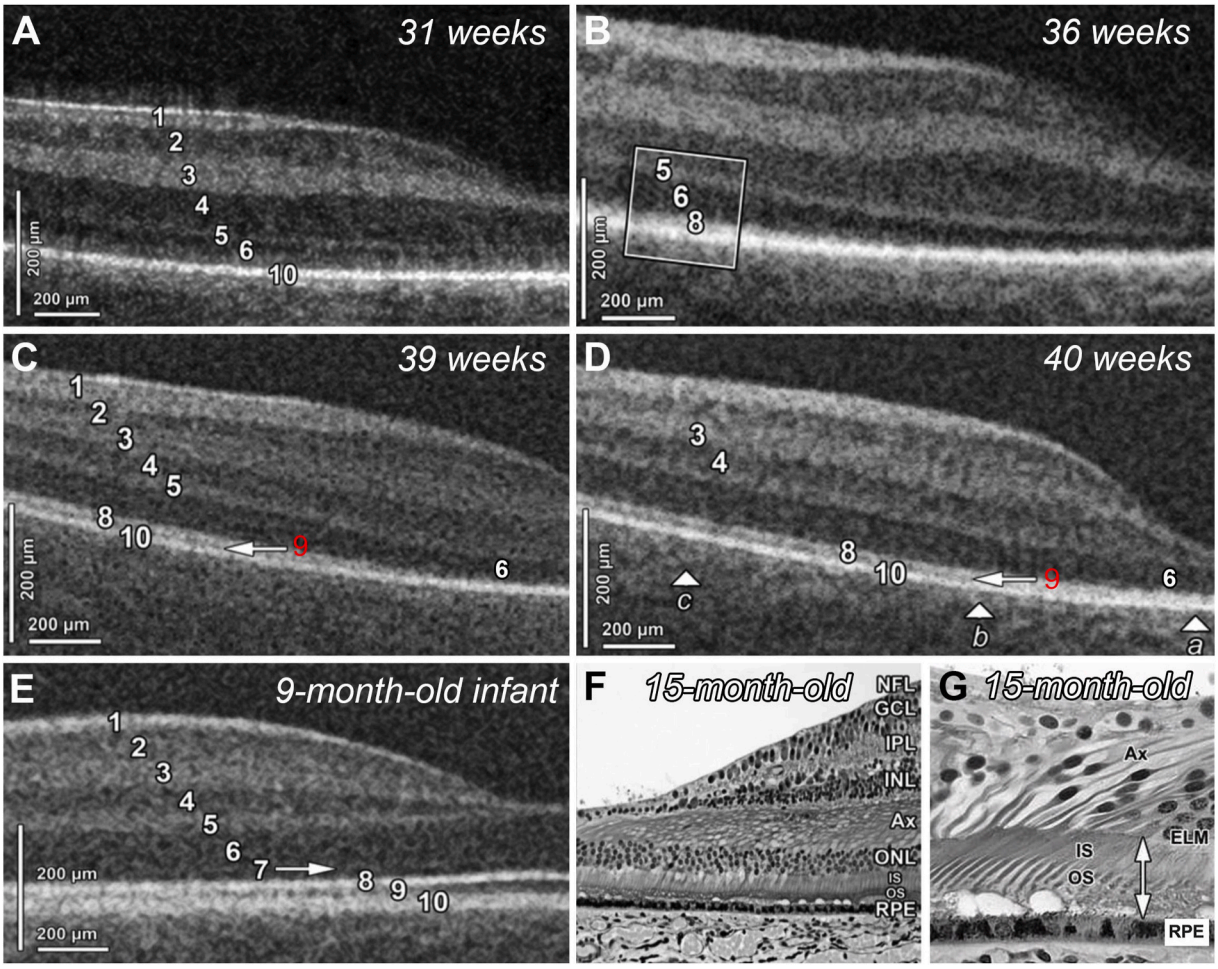

Fig. 1. Dynamics of foveal maturation from 31 weeks post-menstrual age (preterm infants) to 15 months of age: analysis on optical coherence tomography and histology. Adapted from He et al. (2022); Vajzovic et al. (2012).

A. Optical coherence tomography (OCT) B-scan from a 31 weeks postmenstrual age (PMA) infant eye. At this stage, the ganglion cell layer (GCL), inner plexiform layer (IPL), and inner nuclear layer (INL) are clearly evident at the fovea, whereas the outer plexiform layer (OPL) and outer nuclear layer (ONL) are very thin. The ellipsoid zone (EZ) is not visible. Layers are defined as follows: 1 = retinal nerve fiber layer (RNFL); 2 = ganglion cell layer (GCL); 3 = inner plexiform layer (IPL); 4 = inner nuclear layer (INL); 5 = outer plexiform layer (OPL); 6 = outer nuclear layer (ONL); 10 = retinal pigment epithelium (RPE)/Bruch's complex.

B. At 36 weeks PMA, the EZ (Band 8) is barely detectable in the perifovea and absent in the fovea. Layers are defined as follows: 5 = OPL; 6 = ONL; 8 = EZ.

C. At 39 weeks PMA, OCT B-scan from a full-term infant shows a very thin band 6 (ONL) in the fovea and band 8 (EZ) is nearly absent at the foveal center. Layers are defined as follows: 1 = RNFL; 2 = GCL; 3 = IPL; 4 = INL; 5 = OPL; 6 = Henle fiber layer + ONL; 8 = EZ; 9 = photoreceptor outer segments; 10 = RPE/Bruch's complex.

D. At 40 weeks PMA, OCT B-scan from a full-term infant shows the presence of the EZ (Band 8) at the foveal center. Layers defined as follows: 3 = IPL; 4 = INL; 6 = Henle fiber layer + ONL; 8 = EZ; 9 = photoreceptor outer segments; 10 = RPE/Bruch's complex. The annotations (a), (b), and (c) are not relevant for the current article but were displayed on the original figure.

E. At 9 months of age, OCT B-scan shows adult-like retinal layers. At this period, the foveal pit is wider than in the earlier phase. The thickening of OCT band 6 is attributable to cone packing and elongation of photoreceptor axons. The external limiting membrane (ELM) (horizontal white arrow) is more apparent. Layers defined as follows: 1 = retinal nerve fiber layer (RNFL); 2 = ganglion cell layer (GCL); 3 = IPL; 4 = INL; 5 = OPL; 6 = Henle fiber layer + ONL; 8 = EZ; 9 = photoreceptor outer segments; 10 = RPE/Bruch's complex.

F and G. Histology from a 15-month-old infant retina at the foveal center. The image in (G) is a magnified view of (F). Note the thickening of the photoreceptor axons in (F). Vertical double arrows in (G) show the length of the inner and outer segments of the photoreceptors (the distance between the ELM and RPE). Abbreviations: NFL = nerve fiber layer; GCL = ganglion cell layer; IPL = inner plexiform layer; INL = inner nuclear layer; Ax = photoreceptor axons; ONL = outer nuclear layer; ELM = external limiting membrane; IS = inner segment; OS = outer segment; RPE = retinal pigment epithelium/Bruch's membrane complex.

influenced by the wide displacement of the outer retina (Bringmann et al., 2018).

The *in utero* and postnatal development of the human macula has a prominent foveal-to-peripheral gradient (Hendrickson, 2016). Therefore, the horizontal extension or distance of the HFL from the foveal center is not uniform and two retinal loci only 2 mm apart may be at strikingly different stages of development (Bringmann et al., 2018; Hendrickson, 2016). In the human retina, the horizontal extension of the HFL is greatest in the temporal retina (mean ± SD: 2.51 ± 0.21 mm; n = 3) and smallest in the nasal retina (mean ± SD: 1.89 ± 0.29 mm); the extension in the superior and inferior retinas are between these two values (Bringmann et al., 2018; Curcio et al., 1987). The asymmetrical horizontal extensions of the HFL in the temporal and nasal retina suggest that the temporal retina is more stretched than the nasal retina during postnatal eyeball growth (Bringmann et al., 2018). A similar asymmetrical pattern of growth is demonstrated in macaque retina, where the postnatal dimension between the optic disc and the fovea remains constant although the area of the whole retina increases (Packer et al., 1990). This topographic distribution and radial asymmetry in the cardinal meridians reflect the greater cone and ganglion cell densities in the nasal than in the temporal retina (Curcio et al., 1987; Curcio and Allen, 1990; Perry and Cowey, 1988; Wässle and Boycott, 1991). Interindividual variability of the HFL density in young adult human eyes is well documented and may contribute to individual differences in visual acuity (Curcio et al., 1987).

2.1.3. Spectral domain optical coherence tomography analyses of Henle fiber layer morphogenesis

Spectral domain OCT (SD-OCT) is an additional valuable resource to study the dynamics of human foveal development after premature birth (Dubis et al., 2012; Maldonado et al., 2011; Vajzovic et al., 2012) (Fig. 1). In contrast with previous studies of postmortem human foveal specimens, SD-OCT imaging analyses can track retinal maturation in the same eye over time and can assess the variation in the timing of foveal development across individuals (Maldonado et al., 2011). The *in vivo* changes of the inner and outer retinal layers at the foveal center with OCT are consistent with cellular redistribution reported in histologic studies (Abramov et al., 1982; Hendrickson and Yuodelis, 1984; Isenberg, 1986; Yuodelis and Hendrickson, 1986). Moreover, the foveal region follows a developmental time course similar to that associated with *in utero* maturation (Dubis et al., 2012). Between 30 and 32 WG, the HFL is faintly visible on SD-OCT which correlates with the extremely short axons reported on histologic sections at this phase (Vajzovic et al., 2012). Between 40 and 42 WG, the HFL becomes thicker and forms an identifiable hyporeflective band separated from the ONL (Vajzovic et al., 2012). After birth, there is gradual thickening of the HFL which is attributable to central cone packing and increased axon length (Vajzovic et al., 2012). After 6 years, a thick HFL is present on the foveal shoulders and may appear hyperreflective depending on the angle of OCT scanning (Vajzovic et al., 2012).

2.2. Architecture of the Henle fiber layer in the macular area

2.2.1. From a frontal perspective

The HFL has a unique geometrical arrangement. From a frontal or *en face* view, the HFL displays a radial pattern arising centrifugally from the center of the fovea and extending through the parafovea (2500 μm from the fovea) and the perifovea (5500 μm from the fovea) (Polyak, 1941; Quinn et al., 2019). The HFL is absent in the near periphery (8500 μm from the fovea) and far periphery (26,000 μm from the fovea) (Quinn et al., 2019). The centrifugal extension of the HFL is asymmetrical in the cardinal meridians (Bringmann et al., 2018; Perry and Cowey, 1988). In the human retina, the horizontal extension of the HFL is longest in the temporal retina and shortest in the nasal retina; the extension in the superior and inferior retinas are between these two values (Bringmann et al., 2018; Curcio et al., 1987). Also, the length of the HFL components is not uniform and exhibits a complex eccentricity dependency (Drasdo et al., 2007; Perry and Cowey, 1988). The length of the vertically-oriented HFL components is 24% less than the horizontal HFL components (Drasdo et al., 2007; Perry and Cowey, 1988; Sjöstrand et al., 1999a, 1999b). The vertically-oriented HFL components in the superior and inferior hemi-meridians show similar lengths at comparable eccentricities with a slight curvature towards the optic disc reminiscent of the arcuate bundles of the RNFL (Perry and Cowey, 1988; Sjöstrand et al., 1999b). The length of the nasal HFL components is longer than the temporal HFL components at comparable eccentricities (Drasdo et al., 2007; Perry and Cowey, 1988). The radial pattern of the HFL is not apparent clinically in healthy retinas; however, the spoke-like accumulation of exudates forming a macular star can be attributed to the radial geometry and loose structure of the HFL according to historical textbooks (Duke-Elder, 1941; Elwyn, 1946; Friedenwald, 1952). The first clinical description in the literature was provided by Leber in 1916 under the term "*retinitis stellata*" (Leber, 1916).

2.2.2. From a cross-sectional perspective

On a cross-sectional view, the HFL displays regional variations of its angulation: at the foveal center, the HFL is short and entirely vertical; from the center of the fovea to the perifovea, the obliqueness of the striation increases so as to become almost horizontal (after an initial vertical tracking) resulting in the typical Z-shape pattern of the HFL; outside the perifovea, the obliqueness of the striation decreases with eccentricity so as to become almost vertical (Figs. 2 and 3) (Bringmann et al., 2018; Cao et al., 2021; Curcio et al., 2011; Polyak, 1941; Yamada, 1969). These topographic changes are associated with variations of the HFL thickness (Curcio et al., 2011). Histologically, the HFL rises to a maximum thickness at 0.4 mm eccentrically (72 μm nasal and 54.6 μm temporal to the foveal center) and declines from there to 13.5–20 μm at the macular edge (Curcio et al., 2011). The thicker nasal HFL may be related to the higher photoreceptor and ganglion cell densities in the nasal compared to the temporal retina (Curcio et al., 2011; Curcio and Allen, 1990; Finlay et al., 2008; Perry and Cowey, 1988; Wässle et al., 1989). At 1 mm eccentricity, the HFL accounts for 14.2–16.6% of the total neurosensory retina thickness (Curcio et al., 2011). With aging, the HFL becomes 21% thicker possibly due to an increase in the volume of Müller cells rather than photoreceptor axons, in contradistinction to the common expectation of atrophy of aging tissues (Curcio et al., 2011). Qualitative and quantitative *in vivo* OCT analyses of the HFL in healthy Asian and Caucasian population have reproduced these histology-based measurements of the HFL (Bagci et al., 2008; Curcio et al., 2011; Loduca et al., 2010; Ooto et al., 2011; Wang et al., 2020). Thickness of the HFL is significantly higher in men than women (Ooto et al., 2011; Wang et al., 2020). Increased thickness of the OPL with aging has also been corroborated *in vivo* (Wang et al., 2020). Associations between HFL thickness and axial length are heterogenous (Kim et al., 2019, 2020; Ooto et al., 2011; Ye et al., 2019).

2.3. Oxygenation and energy metabolism

The present article does not intend to repeat prior reviews describing the detailed anatomy and physiology of the retinal microvasculature, but will focus on the physiology and anatomy of oxygen consumption of the OPL (Hardarson, 2013; Linsenmeier and Zhang, 2017; J. Scharf et al., 2020; Wangsa-Wirawan and Linsenmeier, 2003; Yu et al., 2019; Yu and Cringle, 2001). Similarly, extensive reviews summarizing the enormous topic of the Müller cell in healthy and diseased retinas are already published (Bringmann et al., 2006, 2022b; Reichenbach and Bringmann, 2020; Vecino et al., 2016).

2.3.1. Organization of the human retinal capillary plexuses

Ex-vivo human models demonstrate that the human retinal capillary vasculature is comprised of three major laminar plexuses at different retinal depths: a superficial, intermediate and deep capillary plexus

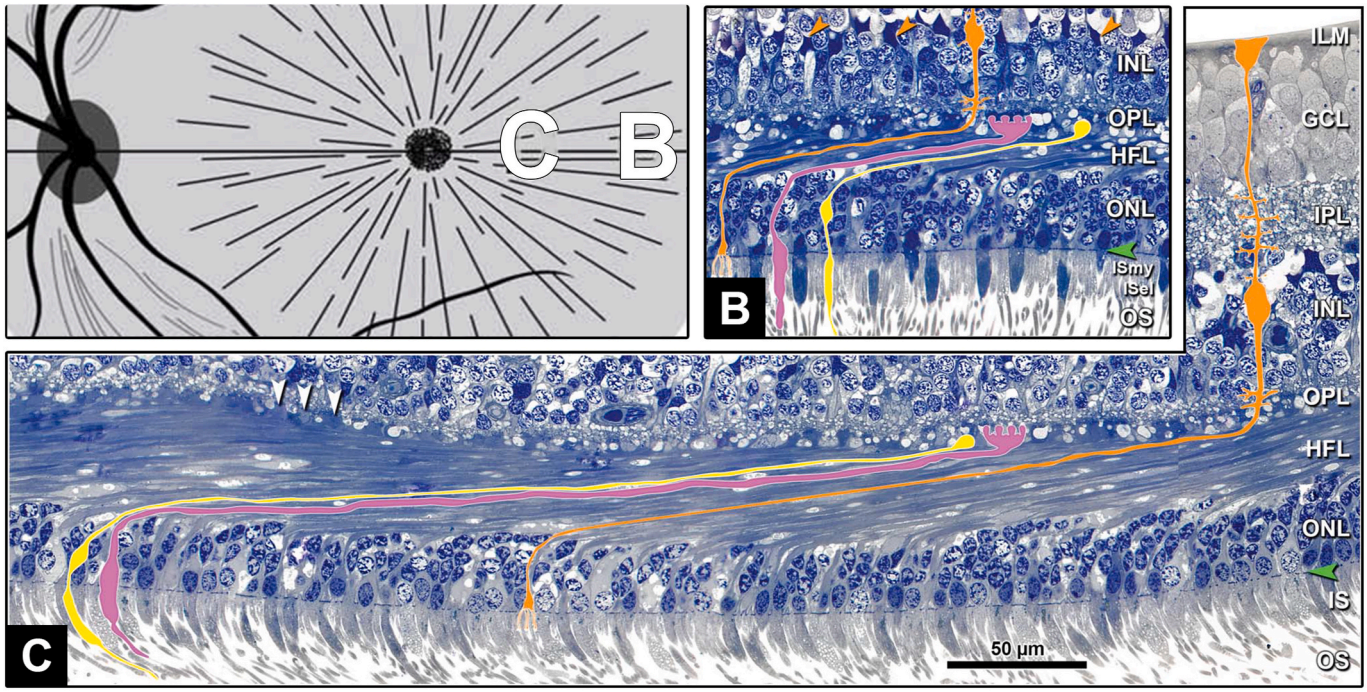

Fig. 2. Geometry of Henle fiber layer in a normal macula. Adapted from Li et al. (2018b).
A. The *en face* view of Henle fibers shows their radial dispersion from the foveal center. The annotations "B" and "C" indicate the locations of the sections in the image (B) and (C), respectively.
B. In the perifoveal area of the central section, the Henle fibers are longitudinally oriented but short. A Müller cell (orange), rod (yellow) and cone (pink) photoreceptor are shown. One fiber is 115-µm long (from external limiting membrane to outer surface of outer plexiform layer). The Müller cell bodies are annotated (orange arrowheads).
C. Close to the fovea in the central section, the Henle fibers are longitudinally oriented and long. One fiber is 350-µm-long (from external limiting membrane to outer surface of outer plexiform layer). Müller cell, orange; rod, yellow; cone, pink. Bar in (D) applies to all panels. Abbreviations: INL, inner nuclear layer; external limiting membrane: green arrowheads; IS, inner segment; ISmy, inner segment myoid; ISel, inner segment ellipsoid; OS, outer segment.

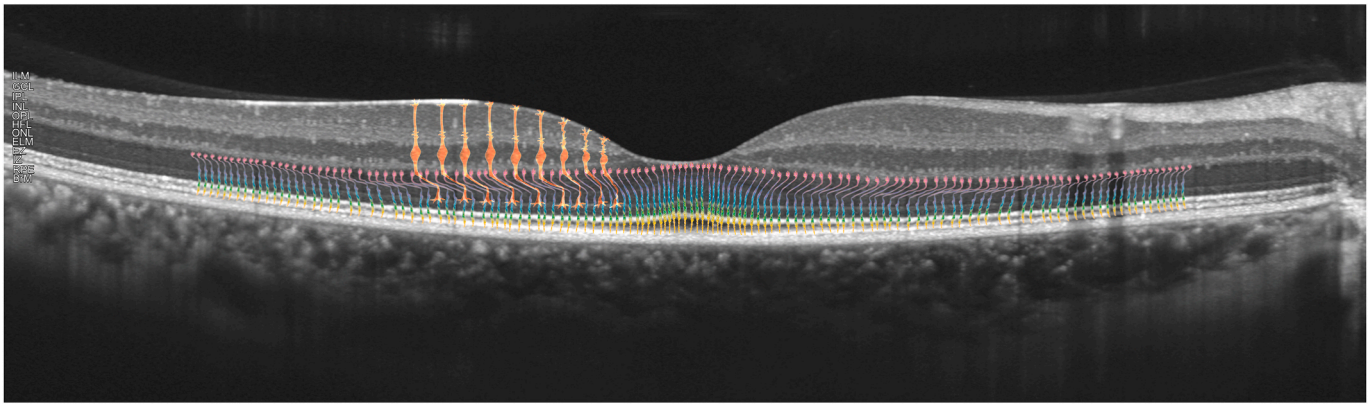

Fig. 3. Cross-sectional high-resolution OCT B-scan of a healthy 29-year-old man with schematized cone photoreceptors and Müller cells. The Henle fiber layer (HFL) displays regional variations of its angulation. At the foveal center, the HFL is short and perpendicular. From the center of the fovea to the perifovea, the oblique orientation of the striation increases so as to become almost horizontal centrally, resulting in the typical Z-shaped pattern of the HFL. Outside the perifovea, the oblique orientation of the striation decreases with eccentricity so as to become almost vertical. Schematic cone photoreceptor and Müller cell trajectories were prepared in reference to a retinal section immunostained with guanine nucleotide-binding protein β3 (GNB3), cellular retinaldehyde-binding protein (CRALBP), cytochrome-C antibodies, and glial fibrillary acidic protein (Cuenca et al., 2020). The schematized Müller cells are colored in orange. The 1: 1 ratio of photoreceptor axon to outer Müller cell process is not displayed to facilitate the interpretation. The schematized cells have been magnified. Annotation of the retinal layers is displayed. Abbreviations of the retinal layers: ILM: internal limiting membrane; GCL: ganglion cell layer; IPL: inner plexiform layer; INL: inner nuclear layer; OPL: outer plexiform layer; HFL: Henle fiber layer; ONL: outer nuclear layer; ELM: external limiting membrane; EZ: ellipsoid zone; IZ: interdigitation zone; RPE: retinal pigment epithelium; BrM: Bruch's membrane. High-Resolution OCT: Spectralis, Heidelberg Engineering, Heidelberg, Germany.

(DCP) (Michaelson, 1954; Toussaint et al., 1961). In the central macula, the DCP is located at the outer boundary of the INL bordering the OPL (Snodderly et al., 1992; Snodderly and Weinhaus, 1990). The DCP displays a typical planar configuration with a lobular organization characterized by the presence of a central vortex venule (Bonnin et al., 2015; Cabral et al., 2022; Park et al., 2016; Xu et al., 2019). Although the nature of the retinal blood flow remains debated, several animal models and human eye studies support a predominantly vertical or in series path

of blood flow wherein the DCP represents the major level of venous outflow (An et al., 2020; Cabral et al., 2020; Fouquet et al., 2017; Freund et al., 2018; Garrity et al., 2017; Ramtohul et al., 2022b; Shimizu and Ujiie, 1978; Snodderly et al., 1992; Yu et al., 2010). In the OPL, the Müller cell processes ensheath the capillaries of the DCP and are the sole mediator of the macroglia-vascular interaction at the DCP where astrocytes are absent (Hogan and Feeney, 1963; Schnitzer, 1988). Moreover, in the OPL, Müller cells form a honeycomb-like meshwork of processes that ensheath the photoreceptor synapses (Fig. 4) (Reichenbach et al., 1989).

2.3.2. Oxygen flux and consumption in the outer plexiform layer

The understanding of macular oxygen flux and consumption greatly originates from oxygen-sensitive microelectrodes inserted in the living animal retina, which remains the most accurate and direct experimental tool to measure the oxygen tension across each cellular layer (Linsenmeier and Zhang, 2017; Yu and Cringle, 2001). This technique allowed for the mapping of oxygen gradients with high spatial and temporal resolution in cat, rats, pigs, rabbits and monkeys (Ahmed et al., 1993; Alder et al., 1983; Ames et al., 1992; Birol et al., 2007; Cringle et al., 1991; Pournaras et al., 1989). Except for monkey fovea, the oxygen gradients in the outer retina show minor differences across species (Linsenmeier and Zhang, 2017). The dominant oxygen-consuming layers include the photoreceptor inner segments, the OPL and the deeper portion of the IPL (Yu and Cringle, 2001). Measuring the oxygen consumption of the inner segments is relatively easy; in fact, due to the avascular nature of the outer retina, the oxygen consumption of the inner segments can be determined using mathematical models based on Fick's law of diffusion (Avtar and Tandon, 2008; Cringle et al., 2002; Haugh et al., 1990; Seth et al., 2022; Yu et al., 2009). Determining the oxygen consumption of the OPL is more problematic due to the presence of vascular beds (Yu and Cringle, 2001). Measuring the oxygen consumption of the OPL requires occlusion of the retinal circulation and/or experiments involving changes in physiological conditions (i.e., modulation of the systemic blood pressure, exposure to hypoxia, hyperoxia or hypercapnia, alteration of light and darkness) (Cringle and Yu, 2002; Linsenmeier, 1986; Yu et al., 1999, 2005, 2007). In animals, the OPL has a high oxygen consumption rate, likely related to the synaptic activity of cone pedicles and rod spherules, and the high density of mitochondria (Linsenmeier and Zhang, 2017; Yu and Cringle, 2001, 2005). Oxygen consumption in the OPL shows a relative stability during light or dark adaptation (Birol et al., 2007; Linsenmeier, 1986; Linsenmeier and Braun, 1992). Under hyperoxic conditions, the oxygen consumption rate of the OPL increases significantly and gradually at all hyperoxic levels, indicating the potential for high oxygen consumption in the OPL (Cringle and Yu, 2002). In the monkey fovea, the oxygen tension ranges

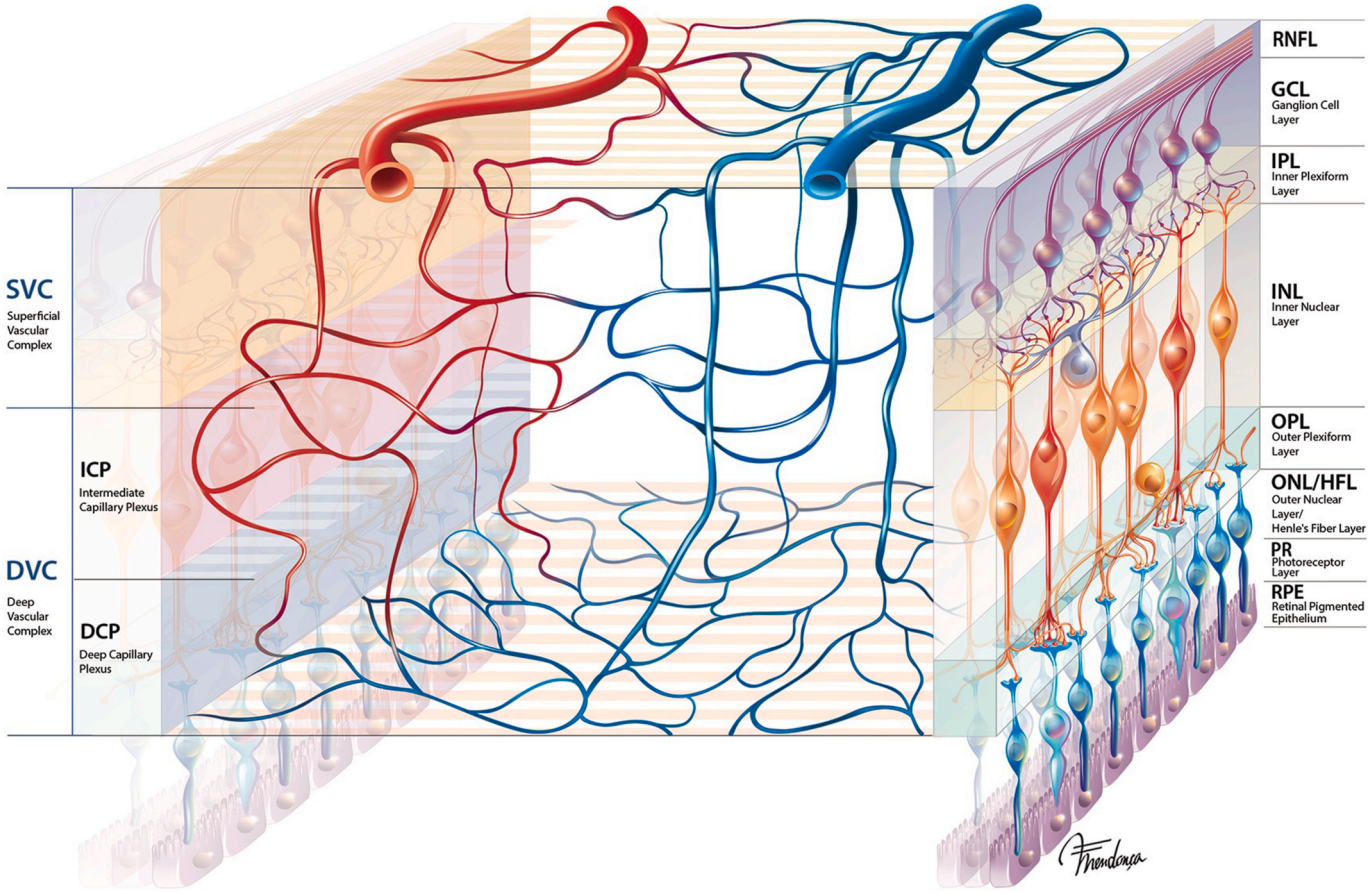

Fig. 4. Schematic representation of the parafoveal vascular network demonstrates the most frequently observed connectivity patterns observed with high-resolution OCT. Courtesy of Cabral et al. (Cabral et al., 2022). Superficial retinal arteries supply the deep capillary plexus (DCP) through large arteriolar connections to the superficial vascular complex (SVC) and intermediate capillary plexus (ICP). DCP inflow originates from small arterioles in the ICP. Venules originate from the convergence of capillaries in every plexus but the DCP is major level of venous outflow. DCP draining venules angle towards a superficial vein and typically receive ICP draining venules prior to reaching this target. The schematic representation demonstrates a hybrid model of flow between arteries and veins in the human parafovea, with a parallel circuit in the SVC and ICP and an in-series or vertical circuit through the DCP. Note that rod bipolar cells do not synapse directly with ganglion cells in human macula.

from 2 to 8 mmHg at the surface of the inner retina and reaches multiple peaks at the level of the IPL and OPL (up to 40 mmHg). These peaks occur with variable timing and amplitudes, indicating that the blood supply is very actively regulated to meet the local metabolic demands (Wangsa-Wirawan and Linsenmeier, 2003; Yu et al., 2005). The identification of the OPL as a major oxygen consumer in the middle retina accounts for its selective vulnerability to ischemic insults (Sarraf et al., 2013; Yu and Cringle, 2001); reduced perfusion pressure to the DCP which does not have a direct arterial supply from the major arterioles and is supplied by connectors from the intermediate capillary plexus (ICP) may be an additional factor explaining this vulnerability (An et al., 2020). After laser-induced retinal artery occlusion in the rat, the choroid becomes the only source of retinal oxygenation: under air-breathing conditions (20% O_2), the choroid supplies only a small proportion of the oxygen needs of the OPL; under moderate systemic hyperoxia (40% O_2), the oxygen uptake of the OPL exceeds that of the photoreceptor inner segments, which further indicates the potentially high oxygen demand of the OPL (Yu et al., 2007). However, the proportions of the OPL and HFL oxygen needs supplied by the choroid under physiologic and pathologic conditions in humans remain unexplored.

2.4. Optical properties, birefringence and macular pigment content

2.4.1. Birefringence property of the Henle fiber layer

The unique orientation and packing geometry, together with the packing arrangement of microtubules, cause the HFL to exhibit the optical property known as birefringence, a measure of phase retardation per unit distance. Analogous to a uniaxial crystal, axons in the HFL retard light in one orientation of polarization more than another (Brink et al., 1988; Cense et al., 2013; van Blokland, 1985). The birefringence values peak between two to three degrees eccentricity from the fovea, where the HFL density increases, and then decline with increasing eccentricity due to the cone axons re-orienting more parallel with the incident beam (Cense et al., 2013). There is no measurable birefringence of the HFL within the center of the fovea due to the parallel orientation of central cone photoreceptors relative to the incoming light source (Cense et al., 2013). It has been proposed that the Müller cells act as living optical fibers that guide light from the inner retinal surface through their main processes towards photoreceptor cell nuclei (Agte et al., 2011; Franze et al., 2007; Labin et al., 2014). Specialized intermediate filaments that traverse the entire length of the Müller cells and interact with the photoreceptor disk membrane have been suggested to confer cell transparency, although the exact mechanism is unknown (Makarov et al., 2017). These intermediate filaments have a diameter of 10–18 nm and are built of electrically conductive polypeptides (Khmelinskii et al., 2017; Ron et al., 2010). Spectral studies in animal retinas suggest that these intermediate filaments show the capacity to transfer light energy with a very high efficiency (~90%) (Makarov et al., 2017; Zueva et al., 2016, 2019, 2020).

2.4.2. Macular pigments in the Henle fiber layer and Haidinger's brush entoptic phenomenon

Macular pigment is a generic term that refers to the yellow xanthophyll pigment comprised principally of three isomeric carotenoids: lutein, zeaxanthin, and meso-zeaxanthin, (Bone et al., 1997; Landrum and Bone, 2001). The highest levels of macular pigment in the human body are found in the HFL at the fovea, with a sharp drop-off with increased eccentricity from the fovea (Bone and Landrum, 1992; Snodderly et al., 1984a; Trieschmann et al., 2008). Lutein is the dominant pigment in the peripheral macula, zeaxanthin in the mid-peripheral macula, and meso-zeaxanthin at the epicenter of the macula (Bone et al., 1997; Bone and Landrum, 1992; Snodderly et al., 1984a). The lutein: zeaxanthin ratio in the fovea is ~1:2.4 and it reverses in the peripheral macula, exceeding 2:1 (Bone et al., 1988). The absorption spectra of macular pigment overlap and peak at 460 nm (Bone et al., 1992; Pease et al., 1987). Due to their chemical structure, these carotenoids act as an optical filter for blue light and provide antioxidant protection by inhibiting peroxidation of long-chain poly-unsaturated fatty acids (Britton, 1995; Edge et al., 1997; Junghans et al., 2001; Khachik et al., 1997; Snodderly et al., 1984b; Sujak et al., 1999). Filtration of blue light reduces chromatic aberration and enhances visual acuity and contract sensitivity. Lutein and zeaxanthin reduce discomfort associated with glare and improve photostress recovery time, macular function, and neural processing speed (Hammond et al., 2014; Nolan et al., 2011; Stringham et al., 2004, 2011; Stringham and Hammond, 2007; Wenzel et al., 2006).

Macular carotenoid molecules have dichroic properties which may be ascribed to their unique orientation perpendicular to the plane of the cell membranes of the photoreceptor axons (Bone and Landrum, 1983, 1984; Hemenger, 1982; Mottes et al., 2022). This spatial distribution of dichroic macular pigments forms a radial polarizer embedded in the foveal region and is responsible for the entoptic phenomenon known as Haidinger's brushes (Haidinger, 1844; Mottes et al., 2022). We refer the reader to a recent review on Haidinger's brushes (Mottes et al., 2022). The Haidinger's brushes refer to the perception of the characteristic two-petal or bow-tie pattern resulting from the selective filtration of a linearly-polarized light by the radial polarizer formed by dichroic carotenoid pigments (Mottes et al., 2022). The contrast is maximum under blue light exposure, in correspondence with the peak of lutein absorption (458 nm). This entoptic phenomenon has direct clinical applications, including diagnosis and correction of eccentric fixation, and estimation of the fixation status (Cleary and Thompson, 2001; Sherman and Priestley, 1962) (see 3.2. *Scanning Laser Polarimetry*).

3. In vivo visualization of the Henle fiber layer on multimodal imaging

Due to the distinctive radial pattern arising centrifugally from the center of the fovea, the HFL can be indirectly identified on ophthalmoscopic examination or *en face* imaging in the setting of cystoid spaces, exudates, hemorrhages, or schisis of the HFL (Au et al., 2018; Baumal et al., 2020; Fragiotta et al., 2019; Gaudric et al., 2022). Optical coherence tomography uses infrared light to interferometrically derive optical reflectivity features *in vivo* with depth resolution (Lujan et al., 2011). Despite progresses in spectral domain OCT technology, the delineation of the HFL on cross-sectional images remains challenging, likely due to the inability to distinguish a change in reflectivity between the hyporeflective HFL and ONL (Lujan et al., 2011; Staurenghi et al., 2014). Changes in HFL reflectivity (from hyporeflectivity to hyperreflectivity) can be spontaneously induced by distortion of the outer retinal architecture (e.g., subretinal fluid) or elicited by deviation of the OCT beam (i.e., directional OCT) (Lujan et al., 2011; Mrejen et al., 2013). Recent advances in the optical axial resolution of OCT devices, including the High-Resolution OCT (High-Res OCT, Spectralis, Heidelberg Engineering, Heidelberg, Germany) may achieve precise delineation of the hyporeflective HFL from a non-titled scan. Improvement in automatic segmentation of HFL boundaries on OCT imaging may also provide additional insights into macular disease pathophysiology. Accurate quantification of the HFL thickness and volume may represent salient biomarkers of disease severity and progression.

3.1. Directional optical coherence tomography

A seminal paper published in 2004 comparing OCT images of monkey fovea to histology recognizes the HFL as a major layer of the retina (Anger et al., 2004). It also identifies the directional variability of the HFL reflectivity as the HFL orientation changes with eccentricity (Anger et al., 2004). Difficulty in HFL visualization by conventional OCT may be related to the absence of reflectivity change at the HFL/ONL interface (Lujan et al., 2011). Gao et *al.* first used a custom OCT setup to image off-axis macular photoreceptors and measure the contributions of photoreceptor components to the psychophysical Stiles-Crawford effect

(Gao et al., 2008; Snyder and Pask, 1973; Stiles et al., 1933). The potential interest of directional OCT to improve delineation of the HFL was highlighted by Lujan et *al.,* thereby allowing accurate evaluation of the thickness of the ONL, which is an important biomarker of retinal degeneration (Lujan et al., 2011, 2015). Directional OCT is a technique to contrast directionally reflective structures by recording images using an intent angle alteration of the incident beam (Lujan et al., 2011). Directional OCT of the HFL also relies on the Stiles-Crawford effect indicating that the tissue reflectivity is maximal when light is parallel to the physical orientation of the HFL (Fig. 5) (Gao et al., 2008; Lujan et al., 2011; Snyder and Pask, 1973; Stiles et al., 1933). Apart from ONL thickness measurements, the reflectivity properties of the HFL with directional OCT may provide valuable insights into disease processes affecting the HFL (D. J. Lee et al., 2018; Lujan et al., 2015; Mrejen et al., 2013; Otani et al., 2011; Ouyang et al., 2013b; Sjöstrand et al., 2017; Tong et al., 2016). Recent advances for investigating the scattering properties of directionally reflective tissue samples, including multi-directional OCT and volumetric directional OCT, may improve the applicability of directional OCT in clinical practice (Kesim et al., 2022; Ni et al., 2022; Ramrath et al., 2008; Wartak et al., 2017).

On SD-OCT, delineation of the HFL from the hyporeflective ONL is subtle, likely due to the inability to distinguish a change in reflectivity between the hyporeflective HFL and ONL (Staurenghi et al., 2014). High-Resolution OCT (High-Res OCT, Spectralis, Heidelberg Engineering, Heidelberg, Germany) is a novel device that increases the axial resolution of SD-OCT to 3 μm, enabling more precise evaluation of the retinal microstructure (Ramtohul et al., 2022a). Illustration of a High-Res OCT B-scan from a normal eye shows the demarcating transition between the HFL and ONL (Fig. 6). On directional OCT, the changes in reflectivity are confined to the HFL and do not extend downward to the ONL and photoreceptor inner and outer segments.

3.2. Scanning laser polarimetry

As mentioned earlier, the HFL possesses form birefringence, a measure of phase retardation per unit distance, due to its unique regularity and geometry (Brink et al., 1988; van Blokland, 1985). Polarization sensitive imaging can use the presence or absence of phase retardation as a biomarker of tissue changes. In healthy eyes, the interaction of polarized light with macular birefringence results in the macular cross, also known as a macular bow tie sign, which is a windmill-shaped pattern centered on the fovea (Brink et al., 1988; Elsner et al., 2008). This macular bow tie pattern has been used to localize the fovea in normal subjects, monitor fixation and eye tracking in infants, and characterize damages due to age-related macular degeneration, epiretinal membrane, and central serous chorioretinopathy (Elsner et al., 2007; Gramatikov, 2017; Gramatikov et al., 2006, 2007; Hunter et al., 1999; Irsch et al., 2014; Miura et al., 2005, 2007; VanNasdale et al., 2009). The intensity of the macular bow tie birefringence can be used to quantitatively model the foveal structure, and assess cone photoreceptor

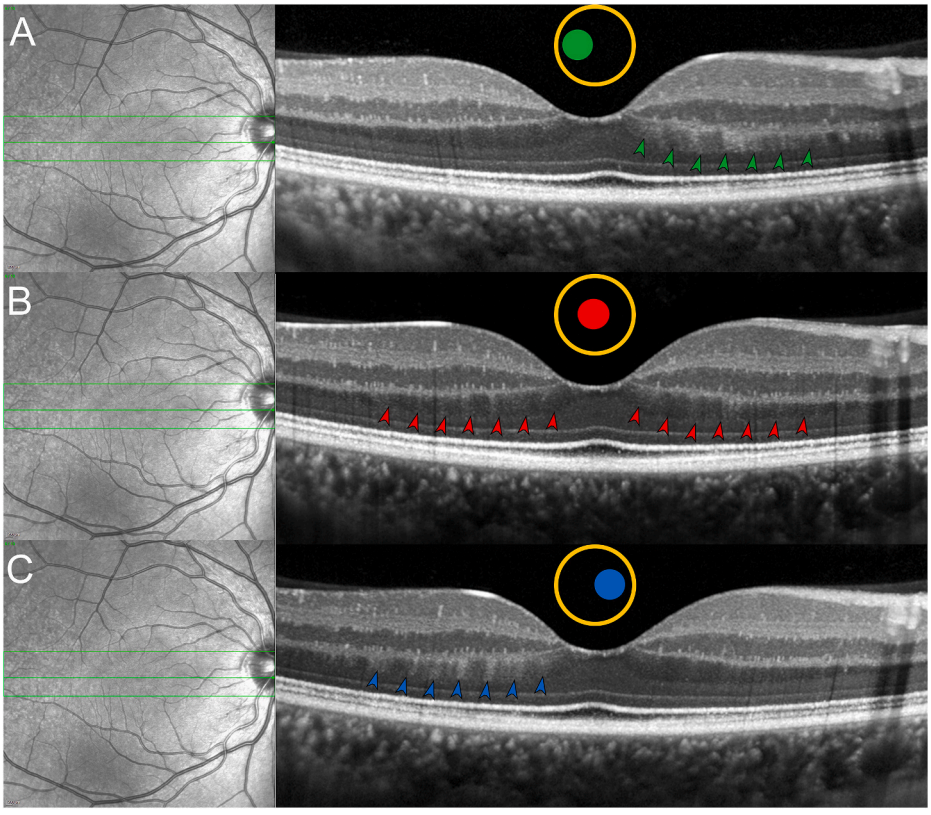

Fig. 5. Directional high-resolution OCT in a healthy 29-year-old man.
The reference OCT B-scan is acquired through the center of the pupil (non-tilted OCT B-scan). In order to acquire OCT scans from the same retinal locations, the built-in auto-alignment feature of the device was used by assignment of the first acquired image as the "reference scan" and the assignment of the following tilted scans as its "follow-up" scans. In directional scans, the retinal image is tilted to the desired quadrant (nasal and temporal quadrants) before acquisition by modifying the pupil entry position of the OCT light beam. To obtain a tilted image on desired direction, the arm of the OCT is deviated laterally. The scan is titled until an adequate hyperreflective Henle fiber layer (HFL) was observed (about 15° between the horizontal line and the imaginary line that passes through the retinal pigment epithelium band). With this technique, the reflectivity of the HFL is increased which facilitates delineation of the HFL from the hyporeflective outer nuclear layer.
A. High-resolution foveal OCT B-scan (Spectralis, Heidelberg Engineering, Heidelberg, Germany) acquired through the left side of the pupil results in hyperreflectivity of the HFL on the nasal half of the macula (*green arrowheads*) while the temporal HFL remains hyporeflective. Note that the distinctive Z-shaped configuration of the HFL is not at all apparent on the nasal half of the macula. The green line in the near-infrared reflectance image indicates the location of the high-resolution OCT B-scan. The pupil entry position of the B-scan is depicted by the colored spot location within the circle.
B. Same eye-tracked high-resolution foveal OCT B-scan acquired through the center of the pupil shows the hyporeflective HFL with a clear demarcation from the outer nuclear layer (ONL) (*red arrowheads*). The green line in the near-infrared reflectance image indicates the location of the high-resolution OCT B-scan. The pupil entry position of the B-scan is depicted by the colored spot location within the circle.
C. High-resolution foveal OCT B-scan acquired through the right side of the pupil results in hyperreflectivity of the HFL on the temporal half of the macula (*blue arrowheads*) while the nasal HFL remains hyporeflective. Note that the distinctive Z-shaped configuration of the HFL is not at all apparent on the temporal half of the macula. The green line in the near-infrared reflectance image indicates the location of the high-resolution OCT B-scan. The pupil entry position of the B-scan is depicted by the colored spot location within the circle.

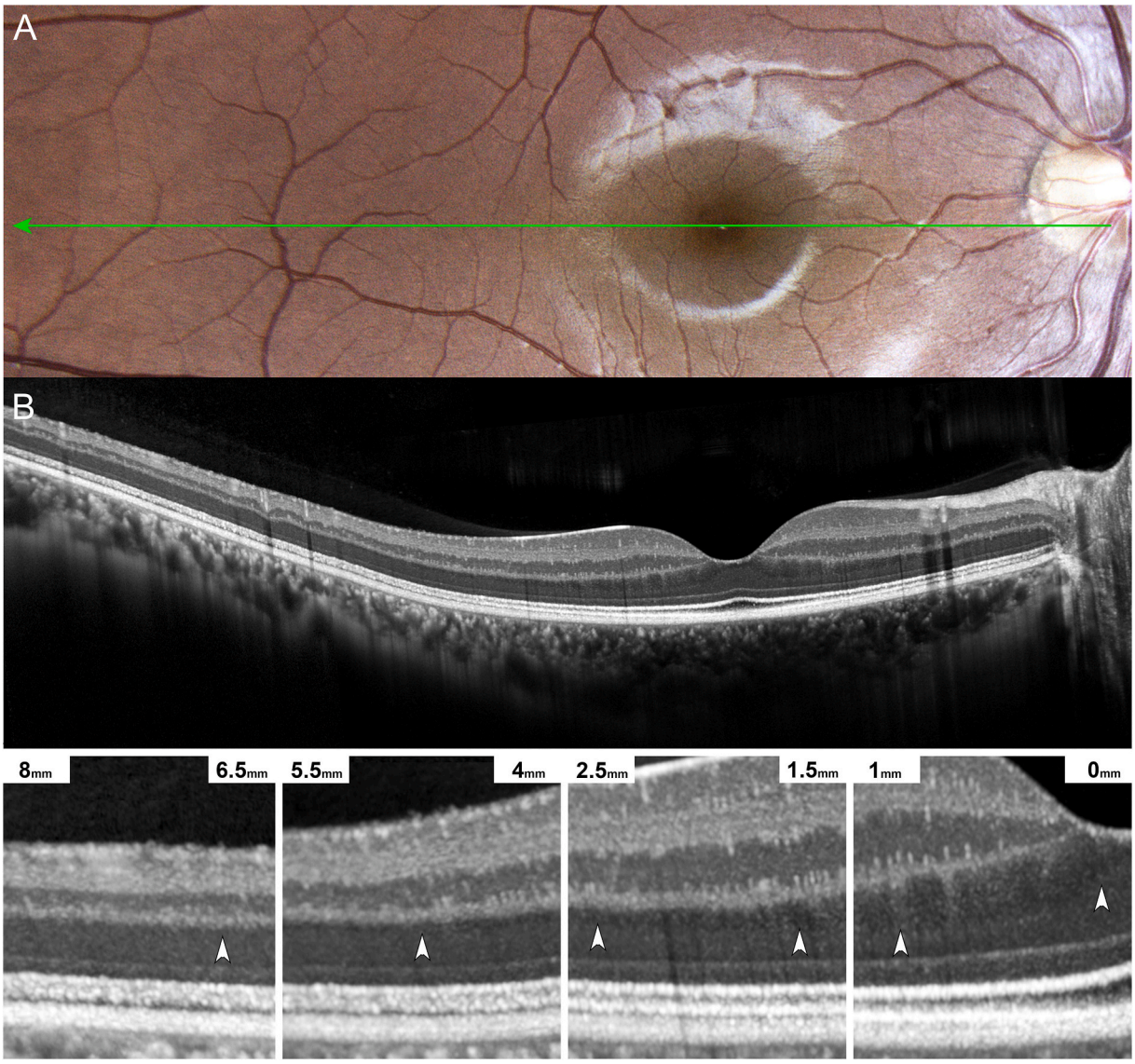

Fig. 6. High-resolution OCT of the normal Henle fiber layer (HFL).
A. Confocal color fundus photography of the right eye in a healthy 29-year-old man. The green line indicates the position of the High-Resolution OCT B-scan in (B). B. Cross-sectional High-Resolution OCT scan (Spectralis, Heidelberg Engineering, Heidelberg, Germany) through the fovea shows regional variations of the thickness of the hyporeflective HFL. The thickness of the HFL is maximal in the parafoveal area and higher in the nasal compared to the temporal fovea. There is a progressive disappearance of the HFL in the temporal macula. The insets below the panel (B) are magnified views of the High-Resolution OCT B-scans at different eccentricities from the foveal center. Subtle hyperreflective lines crossing the HFL are seen in the magnified view of the fovea (between 0 and 1 mm) and may represent increased reflectivity of the HFL due to angulation of HFL bundles in the foveal slope. The distance from the foveal center is displayed in millimeter. The white arrowheads indicate the transition between the hyporeflective HFL and the outer nuclear layer.

density and repartition (Elsner et al., 2008). This is based on the principle that the ratio of cone cell bodies to cone axons is consistently 1:1 in the foveal region (Elsner et al., 2008). Similarly, qualitative alteration of the bow tie reflex producing a concentric macular ring sign or fingerprint sign has been recognized in patients with foveal hypoplasia, epiretinal membrane and vitreoretinal traction, Alport syndrome, Vogt-Koyanagi-Harada (VKH) disease, and even in normal eyes (Bringmann et al., 2022a; Cornish et al., 2014; Degli Esposti et al., 2020; Griffin et al., 2021; Jadon et al., 2022; Missaka et al., 2022; Ramtohul et al., 2020a; Ramtohul and Denis, 2019; Rotsos et al., 2021; Sisk et al., 2020). This finding can be elicited with various modalities including scanning laser polarimetry, scanning laser ophthalmoscopy, and polarized infrared imaging. Several mechanisms have been proposed, including verticalization of the HFL, localized intracellular edema in the HFL, outer retinal distortion by choroidal thickening, distortion of the HFL by intra- and/or subretinal fluid in VKH disease, development of Newton's rings (i.e., interference between light reflected from adjacent flat and curved surfaces), or compression of the HFL by tractional vitreoretinal disorders (Degli Esposti et al., 2020; Griffin et al., 2021; Missaka et al., 2022; Rotsos et al., 2021). Reproduction of this concentric macular ring pattern can be performed with *en face* OCT segmented at the level of HFL, which suggests that altered geometry of the HFL can qualitatively impair its birefringent properties (Fig. 7) (Griffin et al., 2021; Li et al., 2021; Missaka et al., 2022; Ramtohul et al., 2020a; Rotsos et al., 2021).

3.3. Structure-function relationships in glaucoma: implication of the Henle fiber layer

Structure-function correlation is a topic of significant interest in the

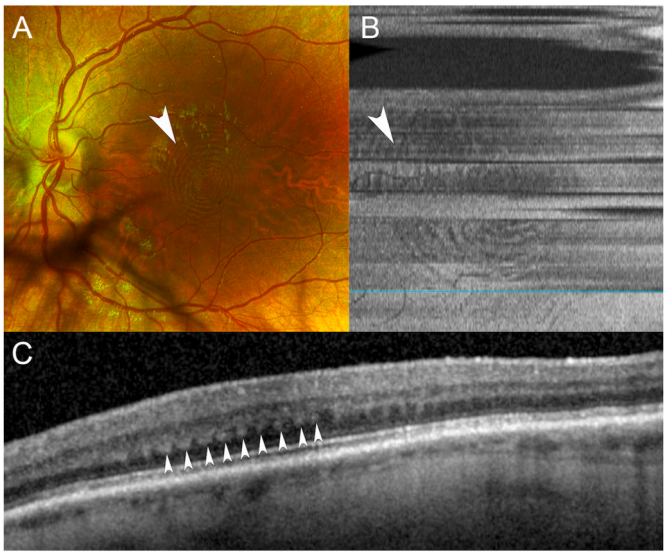

Fig. 7. Multimodal imaging of the concentric macular ring sign in foveal hypoplasia. Adapted from Ramtohul et al. (2020a).
A. Ultra-widefield fundus photography (Optos PLC, Dunfermline, UK) of the left eye of a 4-year-old-child diagnosed with Chediak-Higashi syndrome and nystagmus. Note the concentric macular rings centered on the fovea (*white arrowhead*).
B. En face OCT image (Cirrus HD-5000 OCT, Carl Zeiss Meditec, Jena, Germany) at the level of the Henle fiber layer (HFL) shows a similar concentric macular ring pattern around the hypoplasic fovea (*white arrowhead*). A 20-μm-thick ellipsoid zone-based contour positioned at the depth of the HFL was used to obtain *en face* OCT image.
C. Spectral domain OCT B-scan (Spectralis, Heidelberg Engineering, Heidelberg, Germany) shows a vertically-oriented HFL with alternating hypo- and hyperreflective bands (*white arrowheads*). Note the foveal hypoplasia.

field of glaucoma research (Denniss et al., 2019; Hood et al., 2007; Kim et al., 2010, 2015; Lee et al., 2017; W. J. Lee et al., 2018; Miraftabi et al., 2016; Na et al., 2012; Nilforushan et al., 2012; Rao et al., 2011; Sato et al., 2013). It is generally accepted that evaluating both structure and function could result in more efficient and timely detection of glaucomatous damage and progression (Mohammadzadeh et al., 2020). Macular OCT is the imaging modality of choice to assess the retinal ganglion cell complex, which comprises the RNFL, GCL, and IPL (Cho et al., 2010; Greenfield et al., 2003; Kim et al., 2010; Raza et al., 2011; Wang et al., 2009). The unique HFL geometry connecting the inner and outer retina in the macular region needs to be considered when comparing structural and functional measurements in glaucoma. Due to the radial displacement of the retinal ganglion cells from their input photoreceptors, a given central visual field location may correspond to a different area of the retina (Drasdo et al., 2007; Hood and Kardon, 2007). This displacement diminishes with eccentricity, becoming minor at around 10 visual degrees from the fovea (Drasdo et al., 2007; Turpin et al., 2015). Different numerical models based on histologic measurements of HFL components have been proposed (Drasdo et al., 2007; Hood and Kardon, 2007; Sjöstrand et al., 1999b). Several studies support that adjustment for the average displacement of the retinal ganglion cells in the central macula improves the structure-function relationships in glaucoma (Cho et al., 2010; Hood, 2017; Nouri-Mahdavi et al., 2019; Raza et al., 2011). Several anatomical factors, including the foveal shape, fovea-disc axis angle, or temporal raphe location may affect the spatial and temporal aspects of structure-function relationships in glaucoma (Amini et al., 2014; Bedggood et al., 2017; Sepulveda et al., 2016).

4. OCT angular sign of HFL hyperreflectivity (ASHH) of macular disease

Traditionally, the description of OCT patterns in macular diseases often includes terms related to the anatomical structures affected, the changes of reflectivity (hyperreflective versus hyporeflective), and the shape of the lesions on cross-sectional or *en face* views. The HFL has an angular shape in the macula and is comprised of tubular structures, the orientation and optical properties of which render the HFL virtually indistinguishable from the ONL with OCT of normal eyes. Alterations in the HFL reflectivity are associated with changes in the orientation of the incident OCT light beam either primarily during the acquisition or secondary to structural changes causing uneven orientation of HFL. Therefore, it is likely that disruption of the HFL may affect its reflectivity and facilitate its detection on OCT. However, on directional OCT, these changes in reflectivity are confined to the HFL and do not extend downward to the ONL and ellipsoid (EZ) and interdigitation zones (IZ).

In certain macular diseases, including acute macular neuroretinopathy (AMN) and acute posterior multifocal placoid pigment epitheliopathy (APMPPE), a distinctive hyperreflective lesion mirroring the angulation of the HFL and further extending from the OPL to the EZ/IZ has been reported on OCT. Mrejen et *al.* elegantly illustrated curvilinear hyperreflective lesions of the outer retina in APMPPE and first proposed inflammatory disruption of the HFL as the underlying mechanism (Mrejen et al., 2016). Similarly, Fawzi et *al.* identified hyperreflective lesions of the OPL/HFL on OCT, attributed to disruption of the photoreceptor axons, as an early finding of AMN (Fawzi et al., 2012).

Certain authors in the literature have erroneously adopted the acronym "AMN" to describe changes on OCT featuring HFL hyperreflectivity in other retinal diseases. However, these AMN-like lesions can be secondary to a myriad of different diseases that have etiologies, risk factors, multimodal imaging features, clinical implications and management distinct from the disease entity AMN.

In this section, we introduce the OCT "Angular Sign of HFL Hyperreflectivity" (ASHH) to provide a novel descriptive OCT terminology that is a diagnostic feature unifying various macular diseases and is the result of disruption of the whole photoreceptor length, including the HFL. This sign aims to encompass presumed acute insults of the macular photoreceptor cell compartments, including synaptic terminals, photoreceptor axons, nuclei, inner and outer segments. Concurrent involvement of the outer Müller cell processes which run through the HFL is plausible and may contribute to ASHH. Acutely, this OCT finding refers to the hyperreflective lesion mirroring the angulation of the HFL and extending from the OPL to the EZ/IZ. Resolution of ASHH typically occurs in few weeks and can lead to a legacy of OPL, HFL and ONL thinning, and varying degrees of EZ/IZ disruption. Due to the unique geometry of the HFL, the shape of ASHH on cross-sectional OCT is influenced by its location and eccentricity: (1) foveal-centered lesion follows the vertical-oriented HFL; (2) parafoveal ASHH follows the obliqueness of the HFL; (3) perifoveal ASHH follows the more vertical-oriented HFL. Moreover, the typical angular appearance of this feature may not be apparent on a single OCT B-scan due to scan position and direction. Radial acquisition patterns on OCT may help to highlight the angular nature of this lesion.

The etiology may be related to an ischemic, inflammatory, thermal or mechanical insults to the photoreceptor and outer Müller cell processes although no clinical-histopathological description exists. This finding can be associated with functional consequences including paracentral or central scotoma, although central visual acuity may remain intact. Prognosis and treatments are variable and related to the underlying disorder. While ASHH is a signature OCT finding that is caused by a limited number of macular disorders, multimodal imaging may be critical for more precise definitive diagnosis and to elucidate the exact etiologic mechanism. ASHH is distinct from hyperreflective lesions (e.g., pigment, hemorrhage, exudate) migrating or accumulating through the HFL. The aim of this section is to provide clinicians a restricted catalog of

retinal diseases associated with ASHH on OCT in order to orient further investigations and treatments and to guide accurate diagnosis. A summary of the presumed pathogenesis is shown is Fig. 8. We also review alternative disorders associated with hyperreflective lesions migrating or accumulating through the HFL.

4.1. Acute macular neuroretinopathy

Acute macular neuroretinopathy (AMN) is a relatively rare condition, originally described by Bos and Deutman as dark-reddish, wedge-shaped lesions pointing toward the fovea in young women taking oral contraceptives (Bos and Deutman, 1975). Although the initial description localized the lesions to the superficial retinal layers, subsequent reports using OCT demonstrated outer retinal involvement with the earliest detectable sign affecting the posterior border of the OPL (Baumüller and Holz, 2012; Fawzi et al., 2012; Ramtohul et al., 2020b). Subsequent downward hyperreflectivity of the HFL, ONL, EZ and IZ is typical and is mostly evident for lesions in the fovea or parafovea where the oblique orientation of the HFL is maximal (Baumüller and Holz, 2012; Fawzi et al., 2012; Iovino et al., 2021; Ramtohul et al., 2020b). Resolution of the ASHH in AMN is often followed by OPL/HFL and ONL thinning and varying degrees of EZ/IZ disruption (Fawzi et al., 2012). Fundus autofluorescence (FAF), fluorescein (FA) and indocyanine green angiography (ICGA) in patients with AMN are usually unremarkable (Bhavsar et al., 2016). Near-infrared reflectance (NIR) imaging shows round, tear-drop or petaloid hyporeflective parafoveal lesions that can gradually expand over time and correlate with scotoma and co-localize with EZ/IZ disruption (Fig. 9) (Bhavsar et al., 2016; Casalino et al., 2019; Fawzi et al., 2012). Although several environmental risk factors have been identified, including flu-like illness and the use of oral contraceptives or vasoactive substances and more recently COVID-19 infection or vaccination, systemic and laboratory work-up are largely unremarkable (Bhavsar et al., 2016; David and Fivgas, 2021; Ng et al., 2021; Preti et al., 2022). AMN is a self-limited disorder often with spontaneous recovery of visual acuity. However, persistent visual field deficits have been reported in more than 50% of patients (Bhavsar et al., 2016). There is no specific treatment and no consensus regarding the discontinuation of risk factors such as hormonal contraceptives after AMN (Bhavsar et al., 2016; Fawzi et al., 2012; Turbeville et al., 2003).

4.1.1. Pathogenesis

The nature of the primary insult in AMN remains uncertain and both ischemic and inflammatory disruption have been suggested. Recent studies using OCT-angiography (OCTA) provide new insights into the pathophysiology of AMN. Projection-resolved OCTA demonstrates reduced DCP flow signal co-localizing with ASHH on OCT (Chu et al., 2018). Recently, using non-linear transformation to correct the projection of AMN lesions in the DCP for HFL length and orientation, we observed a high prevalence of either capillary vortices or complete flow defects within the centroid of AMN lesions, supporting a distal ischemic insult at the level of the capillary vortex in AMN (Fig. 10) (Cabral et *al.* under review). Notably, shadowing artifacts on OCTA induced by the hyperreflectivity of the early AMN lesions may account for discrepancies in prior OCTA studies with early reports indicating choriocapillaris flow deficits (Ashraf et al., 2017; Thanos et al., 2016).

Analysis of the chronological sequence of ASHH on OCT may also provide insights into AMN pathogenesis (Fawzi et al., 2012). Prior OCT reports of early AMN presentation indicated primary hyperreflective lesion of the OPL/HFL which subsequently extends downward to affect the ONL, EZ and IZ (Baumüller and Holz, 2012; Fawzi et al., 2012; Ramtohul et al., 2020b). This well-documented temporal sequence in AMN may support an early alteration of the proximal division of photoreceptor cells, possibly the synaptic terminal and photoreceptor axons of the HFL, that originates due to impairment of the most distal aspect of the DCP. Subsequent involvement of the ONL, EZ, and IZ suggests a retrograde diffusion to the more distal component of photoreceptor cells, including photoreceptor nuclei and inner and outer segments (retrograde pathway of photoreceptor disruption) (Fig. 11).

It is interesting that several other disorders including dengue maculopathy, whiplash maculopathy, and contusion maculopathy have been associated with ASHH and AMN-like features on OCT. It may be more accurate to describe these disorders as ones associated with ASHH, and not AMN, as the etiology of the HFL abnormalities may be different from classical AMN.

4.2. Dengue maculopathy

Ocular manifestations of dengue fever are not entirely rare, with a prevalence of dengue maculopathy among patients hospitalized with dengue infection estimated to be 10% (Su et al., 2007). The reported manifestations of dengue maculopathy include foveolitis, macular hemorrhage and edema, vascular occlusions and vasculitis, cotton wool spots, perifoveal telangiectasia and microaneurysms (Ng and Teoh, 2015). Several reports describe the occurrence of ASHH on OCT, attributed to AMN, in patients with dengue fever (Aggarwal et al., 2017; Akanda et al., 2018; Guardiola et al., 2022; Li et al., 2015; Munk et al., 2016; Ooi et al., 2016). Outer retinal alterations including OPL/ONL thinning and EZ/IZ disruption, typical of resolved ASHH, can also complicate this disease and co-localize with a persistent scotoma (Akanda et al., 2018; Fang et al., 2017). Further, OCTA investigations demonstrate DCP flow signal deficits in patients with ASHH and dengue infection, suggesting HFL ischemia (Agarwal et al., 2019; Aggarwal et al., 2017). Additional multimodal images show hyporeflective wedge-shaped lesions on NIR, and largely unremarkable FAF, FA, and ICGA (Aggarwal et al., 2017; Akanda et al., 2018; Guardiola et al., 2022; Li et al., 2015; Munk et al., 2016). There is no effective treatment for dengue maculopathy and there are no randomized controlled trials to date (Ng and Teoh, 2015). Although systemic steroid therapy can be prescribed, it is still unclear as to whether this is of any real benefit to the patient (Agarwal et al., 2019; Li et al., 2015; Ng and Teoh, 2015).

4.2.1. Pathogenesis

Pathophysiology of dengue maculopathy is unknown but both immune-mediated and ischemic processes are suspected (Carr et al., 2017; Chanthick et al., 2018; Ng and Teoh, 2015; Soe et al., 2017; Su et al., 2007). Capillary endothelial dysfunction or occlusion of precapillary arterioles due to immune complex deposition may explain retinal capillary ischemia in dengue maculopathy (Chanthick et al., 2018). Recent OCTA studies reported flow signal deficits at the level of the superficial and deep capillary plexuses (Agarwal et al., 2019). Persistent visual scotomas may be related to ischemic damage (Agarwal et al., 2019). DCP ischemia, at the most distal aspect, leading to retrograde disruption of the photoreceptor synapses and axons, as with classical AMN, may be a possible explanation for ASHH in dengue maculopathy.

4.3. Whiplash maculopathy

Whiplash maculopathy refers to acute macular changes due to rapid acceleration/deceleration movements of the head and neck typically during a car accident and resulting in mild reduction of visual acuity (Kelley et al., 1978). A single histopathologic study reported serous RPE detachments and retinoschisis between the photoreceptor nuclei and their inner segments, possibly related to shear stress forces (Parsons et al., 2005). Ophthalmoscopy may show retinal hemorrhages (Patel et al., 2016; Pham et al., 2007). Acute OCT findings include intraretinal and subretinal fluid, and ASHH attributed to AMN (Cappello et al., 2021; Chronopoulos et al., 2014; Nentwich et al., 2013; Patel et al., 2016; Sigona et al., 2015; Villard et al., 2019). On NIR, parafoveal hyporeflective lesions co-localize with ASHH and EZ loss noted on OCT (Cappello et al., 2021; Patel et al., 2016). Follow-up OCT of resolved ASHH may show a legacy of EZ/IZ disruption corresponding to persistent

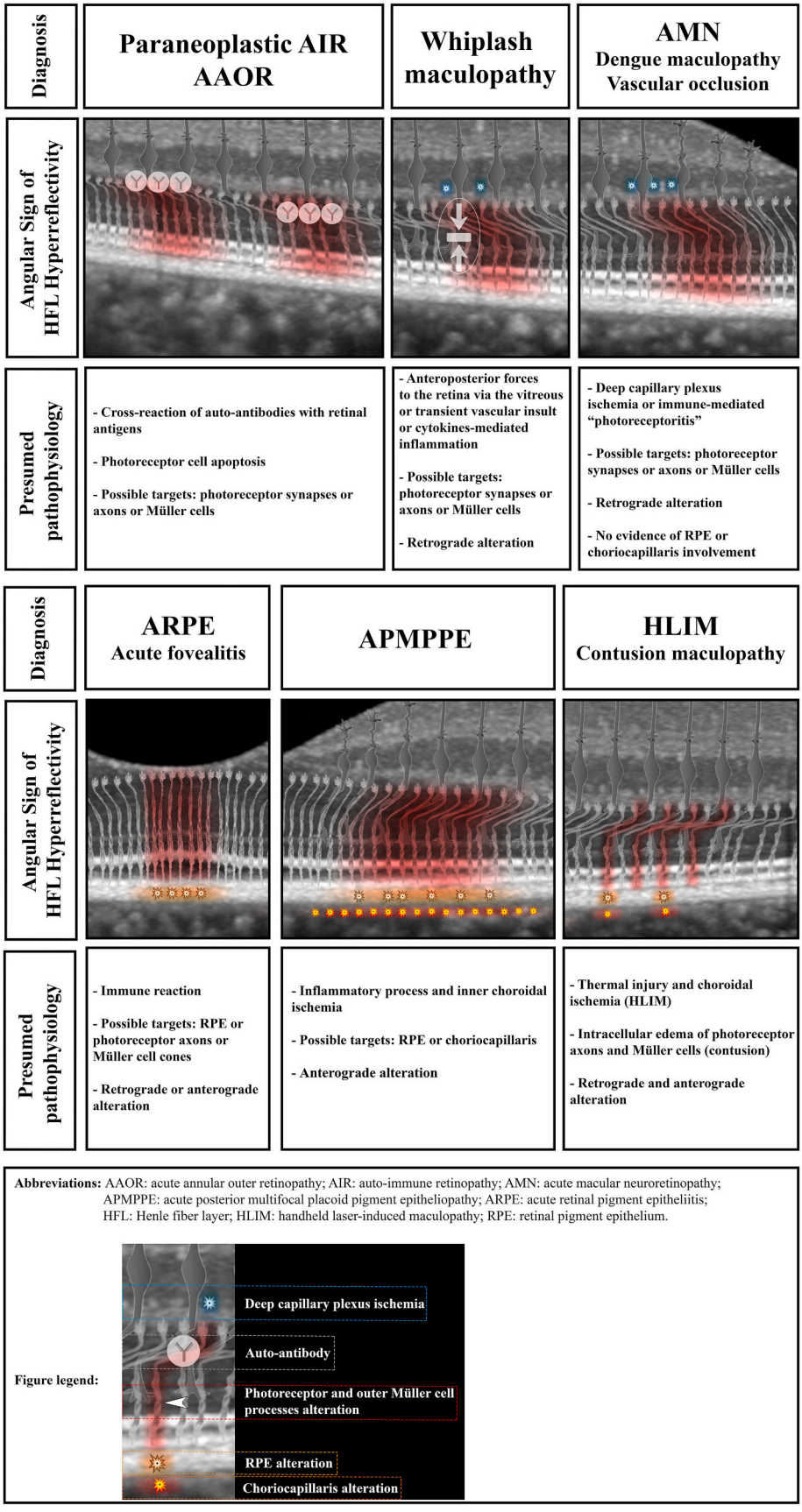

Fig. 8. Schematic representation of the pathogenesis of the Angular Sign of Henle Fiber Layer Hyperreflectivity (ASHH) in macular disease.

In paraneoplastic autoimmune retinopathy, tumor-derived or systemic mediated auto-antibodies cross-reacting with retinal antigens and leading to cell apoptosis is the current accepted theory (Adamus et al., 2004). In acute annular outer retinopathy (AAOR) viral infection of the photoreceptors followed by a host immune response has been suggested response (retrograde pathway of photoreceptor disruption) (Gass and Stern, 1995).

In whiplash maculopathy, transmission of the anteroposterior forces to the retina via the vitreous, transient vascular insult, and cytokine mediated inflammation have been proposed (Cappello et al., 2021; Parsons et al., 2005). Due to the similarities of the imaging features with classical acute macular neuroretinopathy (AMN), a retrograde pathway of photoreceptor disruption is plausible.

In AMN, both ischemic insult targeting the deep capillary plexus (DCP) and inflammatory disruption of photoreceptor synapses and axons with retrograde alteration of inner and outer segments have been suggested (Ramtohul and Freund, 2020).

In dengue maculopathy, both immune-mediated and ischemic processes are suspected (Carr et al., 2017; Chanthick et al., 2018; Ng and Teoh, 2015; Soe et al., 2017; Su et al., 2007). Capillary endothelial dysfunction or occlusion of precapillary arterioles due to immune complex deposition has been suggested as the underlying mechanisms of retinal capillary ischemia in dengue maculopathy (Chanthick et al., 2018). DCP ischemia, at the most distal aspect, leading to retrograde disruption of the photoreceptor synapse and axons, as with classical AMN, may be a possible explanation for ASHH in dengue maculopathy.

In retinal vascular disorders associated with ASHH, disruption of the DCP on optical coherence tomography angiography (OCTA) has been reported (Carroll et al., 2020; Iovino et al., 2021; Ong et al., 2021). Moreover, recent description of AMN-like lesions and retinal venulitis in patients treated with checkpoint inhibitors further suggests that disruption of the venous side of the retinal plexuses, at the most distal aspect of the DCP, may trigger ASHH (retrograde pathway of photoreceptor disruption) (Ramtohul and Freund, 2020).

In acute retinal pigment epitheliitis (ARPE), immune reaction targeting the retinal pigment epithelium (RPE) has been proposed (Krill and Deutman, 1972). Recent investigations using optical coherence tomography (OCT) demonstrate hyperreflective lesions affecting the outer neurosensory retina, suggesting that the latter, and not the RPE, may be the primary site of inflammation (Baillif et al., 2011; Cho et al., 2011; De Bats et al., 2013; Hall et al., 2012; Hsu et al., 2007; Iu et al., 2017; Krill and Deutman, 1972; Merkoudis and Granstam, 2013). In acute fovealitis, transient inflammation affecting the foveolar cellular components (cones and/or Müller cell cones) has been postulated (Ledesma-Gil and Spaide, 2022). Anterograde and retrograde pathways of photoreceptor disruption are pathophysiologic candidates.

In acute posterior multifocal placoid pigment epitheliopathy (APMPPE), a primary inflammatory process targeting the RPE (Gass, 1968) or the choriocapillaris has been suggested (Bird and Hamilton, 1972; Deutman et al., 1972; Van Buskirk et al., 1971). On OCT, ASHH may result from primary choroidal ischemia and inflammation with

subsequent alteration of the proximal part of the photoreceptor cells, including the Henle fiber layer (HFL) components (Mrejen et al., 2016). As opposed to typical retrograde diffusion of the lesion in AMN, this hypothesis in APMPPE may also suggest an anterograde pathway of alteration of the whole photoreceptor length starting distally. Although this chronological sequence has not been thoroughly reported in APMPPE, the occurrence of ASHH in areas of prior choroidal ischemia as assessed by indocyanine green angiography (ICGA) and OCTA may support this concept (Burke et al., 2017; Klufas et al., 2017). Alternatively, Steptoe et *al.* proposed that ASHH may represent retrograde axonal flow disruption of the photoreceptor axons triggered by a viral infection (Steptoe et al., 2022).

In handheld laser-induced maculopathy (HLIM), thermal injury of the HFL components and choroidal ischemia may contribute to the ASHH genesis (Bhavsar et al., 2020; Tran et al., 2020). Anterograde and retrograde pathways of photoreceptor disruption are pathophysiologic candidates.

In contusion maculopathy, direct transmission of the forces to the outer retina has been suggested. In fact, histologic studies of primate and human eyes note the presence of damaged photoreceptor outer segments and RPE cells and intracellular edema of photoreceptor axons and glial elements (Hart and Blight, 1979; Kohno et al., 1983; Mansour et al., 1992; Sipperley et al., 1978). Anterograde and retrograde pathways of photoreceptor disruption are pathophysiologic candidates.

Abbreviations: AAOR: acute annular outer retinopathy; AIR: auto-immune retinopathy; AMN: acute macular neuroretinopathy; APMPPE: acute posterior multifocal placoid pigment epitheliopathy; ARPE: acute retinal pigment epitheliitis; HLIM: handheld laser-induced maculopathy; RPE: retinal pigment epithelium.

scotoma on visual field testing (Cappello et al., 2021; Chronopoulos et al., 2014; Patel et al., 2016). No treatment is required as spontaneous functional and anatomical resolution occurs within few weeks (Villard et al., 2019).

4.3.1. Pathogenesis

Pathophysiologic mechanisms of retinal damage in whiplash maculopathy are not completely understood and include transmission of the anteroposterior forces to the retina via the vitreous, transient vascular insult, and cytokine mediated inflammation (Cappello et al., 2021; Parsons et al., 2005). Due to the similarities of the imaging features with classical AMN, a retrograde pathway of photoreceptor disruption is plausible.

4.4. Contusion maculopathy

Morphologic OCT changes associated with closed-globe injuries vary from increased EZ/IZ reflectivity to more severe disruption of the OPL, ONL, EZ/IZ and RPE layers (Ahn et al., 2013; Oh et al., 2011; Souza-Santos et al., 2012). On OCT, ASHH can be observed early in the course of contusion maculopathy in association with disruption of the EZ/IZ and RPE layers (Fig. 12) (Ahn et al., 2013; Boss et al., 2017; Li et al., 2018a; Mishra et al., 2019; Oh et al., 2011; Souza-Santos et al., 2012). These lesions have been attributed to AMN (Chinskey et al., 2015). Resolution may be associated with severe outer retinal atrophy and even full-thickness macular hole (Ahn et al., 2013; Li et al., 2018a; Souza-Santos et al., 2012).

4.4.1. Pathogenesis

The pathophysiology of ASHH in contusion maculopathy is speculative and may include direct transmission of the forces to the outer retina. In fact, histologic studies of primate and human eyes note the presence of damaged photoreceptor outer segments and RPE cells and intracellular edema of photoreceptor axons and glial elements (Hart and Blight, 1979; Kohno et al., 1983; Mansour et al., 1992; Sipperley et al., 1978). Anterograde and retrograde pathways of photoreceptor disruption are pathophysiologic candidates.

4.5. Retinal vascular diseases

Recently, Iovino et *al.* reported a case series of patients presenting with coincidental paracentral acute middle maculopathy (PAMM) and ASHH (attributed to AMN) in association with retinal vascular disorders, including central retinal vein and artery occlusions, idiopathic retinal vasculitis, and Purtscher's retinopathy (Fig. 13) (Iovino et al., 2021). ASHH has also been reported in patients with sickle cell disease (Ong et al., 2021). All these cases demonstrate flow signal deficit at the level of the DCP on OCTA, suggesting HFL ischemia (Iovino et al., 2021; Ong et al., 2021). Chronic cocaine use can also be associated with DCP flow signal deficit on OCTA and ASHH on OCT (Carroll et al., 2020).

4.5.1. Pathogenesis

The pathophysiology of ASHH in retinal vascular disorders is unclear but recent reports using OCTA provide further insights into the plausible mechanisms resulting in ASHH genesis. In fact, disruption of the DCP on OCTA is a common finding in patients with ASHH secondary to retinal vascular diseases (Carroll et al., 2020; Iovino et al., 2021; Ong et al., 2021). Moreover, recent description of AMN-like lesions and retinal venulitis in patients treated with checkpoint inhibitors further suggests that disruption of the venous side of the retinal plexuses, at the most distal aspect of the DCP, may trigger ASHH (retrograde pathway of photoreceptor disruption) (Ramtohul and Freund, 2020).

4.6. Acute posterior multifocal placoid pigment epitheliopathy

Acute posterior multifocal placoid pigment epitheliopathy (APMPPE), first described by Gass in 1968, is a rare, idiopathic, self-limited, inflammatory condition typically affecting healthy adults who present with transient acute central or paracentral vision loss related to multiple creamy white or yellow placoid outer retinal and RPE lesions (Gass, 1968). One third of the patients report a preceding viral or flu-like illness prior to symptom onset (Gass, 1968; Holt et al., 1976). With more advanced retinal imaging, including ICGA and more recently OCT and OCTA, it is clear that this disease is primarily the result of inner choroidal or choriocapillaris ischemia likely originating from an inflammatory etiology (Burke et al., 2017; Dhaliwal et al., 1993; Dolz-Marco et al., 2017; Howe et al., 1995; Klufas et al., 2017; Mrejen et al., 2016; Yuzawa et al., 1994). Cross-sectional and *en face* OCT can also capture the classic pattern of morphologic alterations affecting the RPE, photoreceptors, and outer retina (Goldenberg et al., 2012; Klufas et al., 2017). An SD-OCT classification scheme of APMPPE was devised in 2012 and includes 4 stages: (1) early dome-shaped elevation of the EZ/IZ, now known as bacillary layer detachment or BALAD (Ramtohul et al., 2021a, 2021b), (2) separation between the EZ/IZ and the RPE with mild subretinal fluid, (3) disruption of the EZ/IZ and RPE thickening, and (4) progressive restoration of the EZ/IZ and RPE reflectivity with possible permanent alterations (Goldenberg et al., 2012). Hyperreflective outer retinal lesions mirroring the angulation of the HFL, representing the characteristic ASHH, were first described by Mrejen et *al.* and subsequently reported by others and represents an acute sign of disease (Fig. 14) (Bigaut et al., 2019; Burke et al., 2017; Mrejen et al., 2016; Steptoe et al., 2022).

There are various infectious conditions that can be associated with placoid disorders such as APMPPE, including tuberculosis, group A Streptococcus, syphilis, Borrelia, dengue fever, mumps, coxsackie B, adenovirus, and COVID-19. Additional associations include post vaccination (varicella, hepatitis A and B, meningococcal C, yellow fever, typhoid, influenza, COVID-19), and inflammatory disorders such as

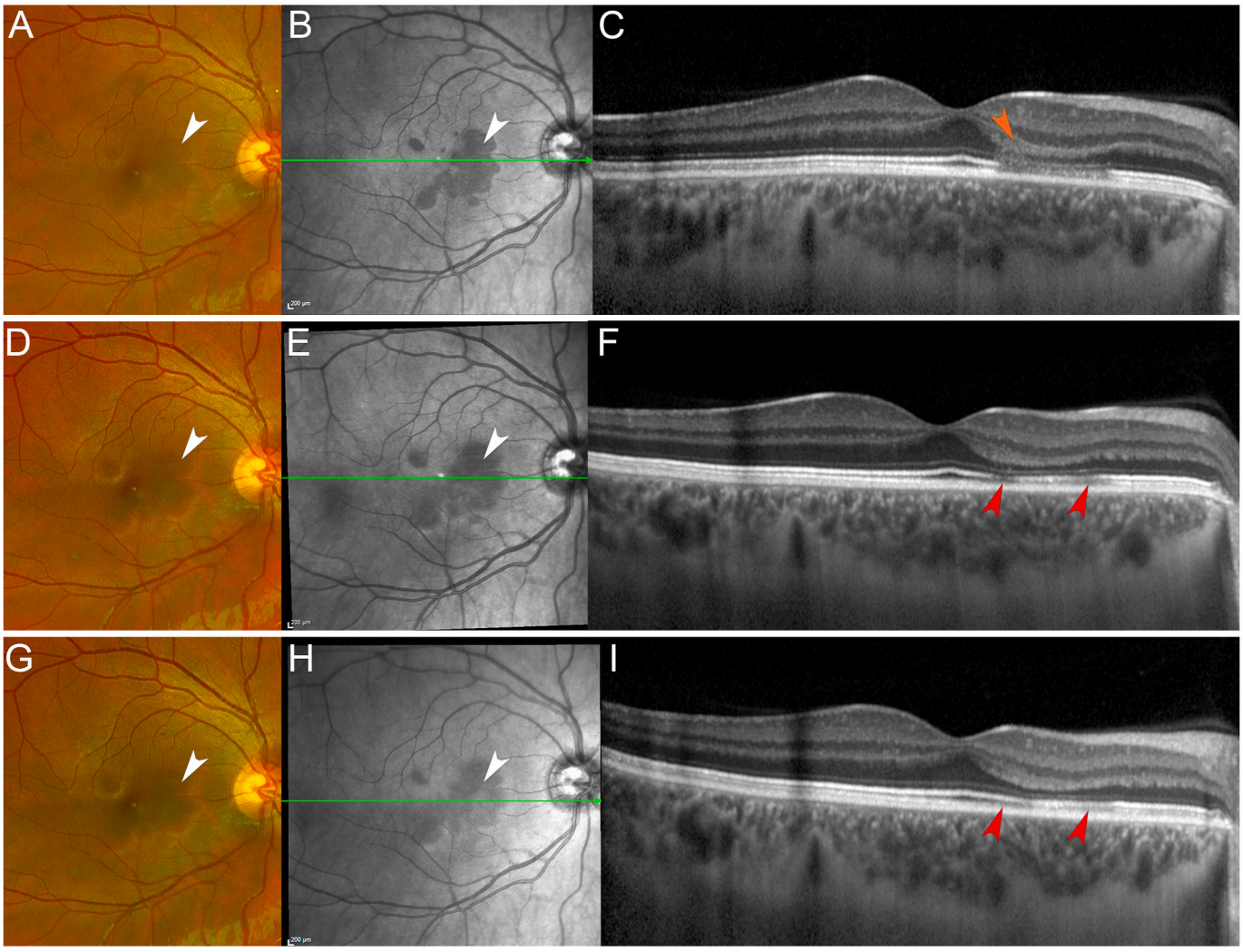

Fig. 9. Longitudinal multimodal imaging of acute macular neuroretinopathy in a 28-year-old patient.
A. Pseudocolor fundus photography (Optos PLC, Dunfermline, UK) of the right eye shows dark-reddish, petaloid-shaped lesions in the macula (*white arrowhead*).
B. Near-infrared reflectance image shows hyporeflective petaloid lesions in the macula with sharp borders (*white arrowhead*). The green line indicates the location of the spectral domain optical coherence tomography (SD-OCT) B-scan in (C).
C. SD-OCT B-scan (Spectralis, Heidelberg Engineering, Heidelberg, Germany) shows the angular sign of Henle fiber layer (HFL) hyperreflectivity (ASHH) (*orange arrowhead*). Note that the typical angular pattern is barely apparent likely due to the OCT B-scan position and direction through the lesion.
D. At 4-month follow up, the pseudocolor fundus photograph shows increased visibility of the dark-reddish macula lesions (*white arrowhead*).
E. At 4-month follow up, the near-infrared reflectance image shows enlargement of the hyporeflective lesions with blurred margins (*white arrowhead*). The green line indicates the location of the SD-OCT B-scan in (F).
F. At 4-month follow up, SD-OCT B-scan shows decreased hyperreflectivity of the HFL with thinning of the outer nuclear layer (ONL). Note the persistent focal attenuation of the ellipsoid and interdigitation zone (EZ/IZ) bands (*red arrowheads*).
G. At 10-month follow up, the pseudocolor fundus photograph shows the dark-reddish macula lesions that remain stable (*white arrowhead*).
H. At 10-month follow up, the near-infrared reflectance image shows reduction of the hyporeflective lesions with blurred margins (*white arrowhead*). The green line indicates the location of the SD-OCT B-scan in (I).
I. At 10-month follow up, SD-OCT B-scan shows ONL thinning and progressive restoration of the EZ/IZ reflectivity (*red arrowheads*).

sarcoidosis, ulcerative colitis, juvenile rheumatoid arthritis, anti-neutrophil cytoplasmic antibody (ANCA)-associated vasculitis, granulomatosis with polyangiitis, polyarteritis nodosa, thyroiditis, acute nephritis, erythema nodosum, familial Mediterranean fever (Al Mousa and Koch, 2016; Anderson et al., 1996; Atas et al., 2021; Azar et al., 1975; Borruat et al., 1998; Bridges et al., 1995; Chiquet et al., 1999; Darugar et al., 2011; Di Crecchio et al., 2001; Georgakopoulos et al., 2016; Goldhardt et al., 2016; Hsu et al., 2003; Jacklin, 1977; Kraemer et al., 2022; Laatikainen and Immonen, 1988; Lowder et al., 1996; Matsuo et al., 2002; Olguín-Manríquez et al., 2021; Wolf et al., 1992). Association with human leukocyte antigen (HLA)-DR2 and HLA-B7 suggests an immunogenetic susceptibility (Wolf et al., 1990).

Patients with APMPPE or other placoid variant diseases (e.g., persistent placoid maculopathy, relentless placoid chorioretinitis, serpiginous chorioretinopathy) should be questioned for neurological symptoms and urgently referred for evaluation if positive. Various neurological complications can occur during the course of APMPPE, including aseptic meningitis, meningoencephalitis, cerebral vasculitis, cerebral and spinal cord infarction, recurrent strokes, cerebral nerve III and VI palsy, and cerebral venous sinus thrombosis (Berger et al., 2019; Bigaut et al., 2019; Case et al., 2015; Castro et al., 2016; Gibelalde et al., 2009; Jaramillo et al., 2009; Kersten et al., 1987; Kline et al., 2007; Knox, 2021; Luneau et al., 2009; Matamala et al., 2013; O'Halloran et al., 2001; Pillar et al., 2021; Weinstein et al., 1988; Yunker et al.,

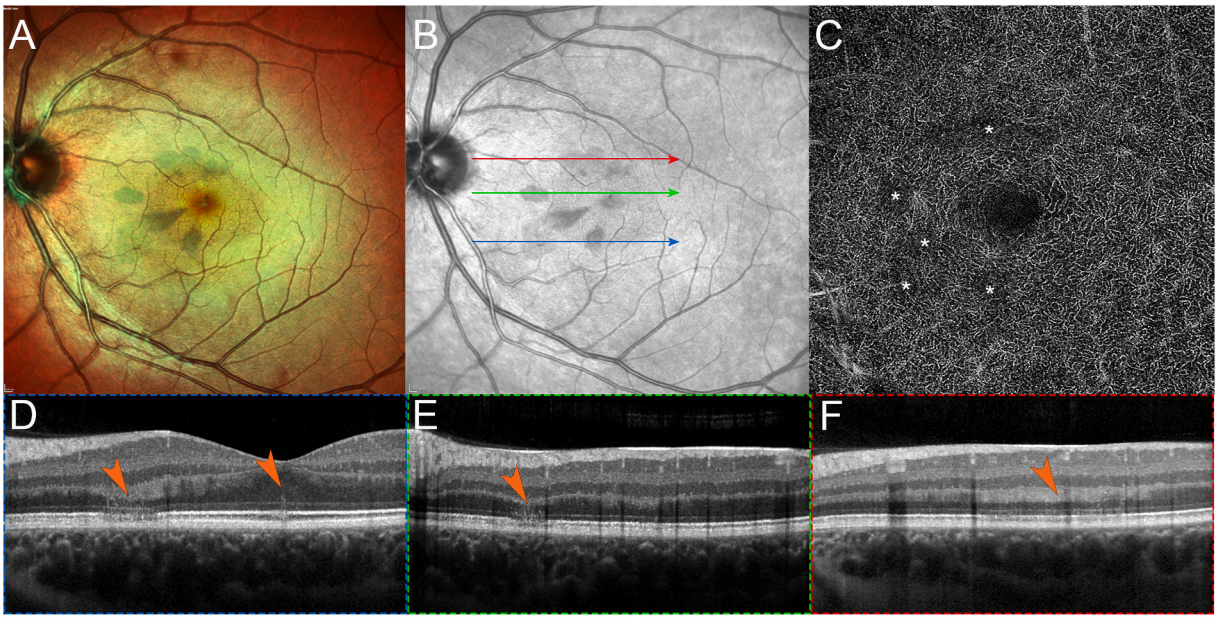

Fig. 10. Multimodal imaging of acute macular neuroretinopathy in a 27-year-old patient.
A. Multicolor image (Spectralis, Heidelberg Engineering, Heidelberg, Germany) of the left eye shows multiple dark-reddish tear-drop lesions with the apices pointing toward the fovea.
B. Near-infrared reflectance image shows hyporeflective lesions. The blue, green, and red lines indicate the position of the OCT B-scans in (D), (E), and (F), respectively.
C. En face OCT-angiography (Plex Elite 9000, Carl Zeiss Meditec, Inc, Dublin, CA) segmented at the level of the deep capillary plexus shows flow signal deficits (*asterisks*) suggestive of ischemia.
D-F. Cross-sectional High-Resolution OCT scans (Spectralis, Heidelberg Engineering, Heidelberg, Germany) show multiple angular signs of Henle fiber layer hyperreflectivity (ASHH) (*orange arrowheads*). Note the vertically oriented ASHH in the fovea in (D). The blue, green, and red dashed boxes correspond to the scan locations illustrated in (B).

2008). Fatal cerebral complications associated with APMPPE can very rarely occur (El Sanhouri et al., 2012; Hammer et al., 1989; Maamari et al., 2019; Wilson et al., 1988).

There is no current consensus on the treatment, although favorable outcomes are reported after steroid therapy (Oliveira et al., 2020). Immunosuppressive therapy should be considered in severe, persistent or recurrent cases, or in patients with central nervous system involvement (El-Markaby et al., 2012). Systemic work-up and treatment of underlying systemic conditions should also be considered (O'Halloran et al., 2001). Choroidal neovascularization is not an uncommon complication of placoid retinopathies, especially persistent placoid maculopathy and careful surveillance with OCT and OCTA is necessary so that prompt anti-vascular endothelial growth factor (VEGF) therapy can be initiated if necessary (Fogel Levin et al., 2022).

4.6.1. Pathogenesis

The exact pathophysiology of APMPPE was initially proposed to be a primary inflammatory process targeting the RPE (Gass, 1968) or the choriocapillaris (Bird and Hamilton, 1972; Deutman et al., 1972; Van Buskirk et al., 1971). ICGA and OCTA studies have confirmed that inner choroidal ischemia is the primary etiology (Burke et al., 2017; Howe et al., 1995; Klufas et al., 2017).

In APMPPE, ASHH may result from primary choroidal ischemia and inflammation with subsequent alteration of the proximal part of the photoreceptor cells, including the HFL components (Mrejen et al., 2016). As opposed to typical retrograde extension of the lesion as in classical AMN, an anterograde pathway in APMPPE may be relevant due to choriocapillaris ischemia causing alteration of the photoreceptor inner and outer segments with extension through the HFL towards the OPL. Although this chronological sequence has not been thoroughly reported in APMPPE, the occurrence of ASHH in areas of prior choroidal ischemia as assessed by ICGA and OCTA may support this concept (Burke et al., 2017; Klufas et al., 2017). Alternatively, Steptoe et *al.* proposed that ASHH may represent retrograde axonal flow disruption of the photoreceptor axons triggered by a viral infection (Steptoe et al., 2022).

4.7. Acute retinal pigment epitheliitis and acute fovealitis

Acute retinal pigment epitheliitis (ARPE) is a rare, idiopathic, self-limited, inflammatory maculopathy, first described by Krill and Deutman in 1972, and affecting young healthy adults (Krill and Deutman, 1972). ARPE is characterized by acute vision loss with central scotoma and characteristic funduscopic perifoveal findings of fine pigment stippling surrounded by hypopigmented halos (Krill and Deutman, 1972). Approximately, 20% of patients present with prodromal flu-like symptoms prior to disease onset (Cho et al., 2014). Acutely, the characteristic OCT feature is a dome-shaped hyperreflective haze at the level of EZ/IZ (Iu et al., 2017). Subsequently, ARPE patients may display fovea-centered ASHH on OCT associated with varying degrees of EZ/IZ alterations, hyporeflective gap at the IZ, and RPE disruption (Aydoğan et al., 2015; Cho et al., 2014; De Bats et al., 2013; Hall et al., 2012; Li et al., 2019; Roy et al., 2021). Resolution of the acute findings can by followed by persistent defects of the EZ/IZ with RPE alterations (Cho et al., 2014; Iu et al., 2017). Typically, FAF is either normal or shows discrete hyperautofluorescent spots in the macula (Aydoğan et al., 2015; De Bats et al., 2013; Roy et al., 2021). FA shows hyperfluorescence at the fovea due to transmission defect without any leakage, and ICGA is either unremarkable or shows subtle hyperfluorescent patches in the fovea (Aydoğan et al., 2015; Baillif et al., 2011; Cho et al., 2014; De Bats et al., 2013; Iu et al., 2017; Li et al., 2019; Roy et al., 2021). ARPE is associated with a favorable visual prognosis, and treatment is usually not required (Cho et al., 2014; Iu et al., 2017). More rarely, acute coxsackie A virus infection can cause ARPE (Colucciello, 2022) and masqueraders of ARPE

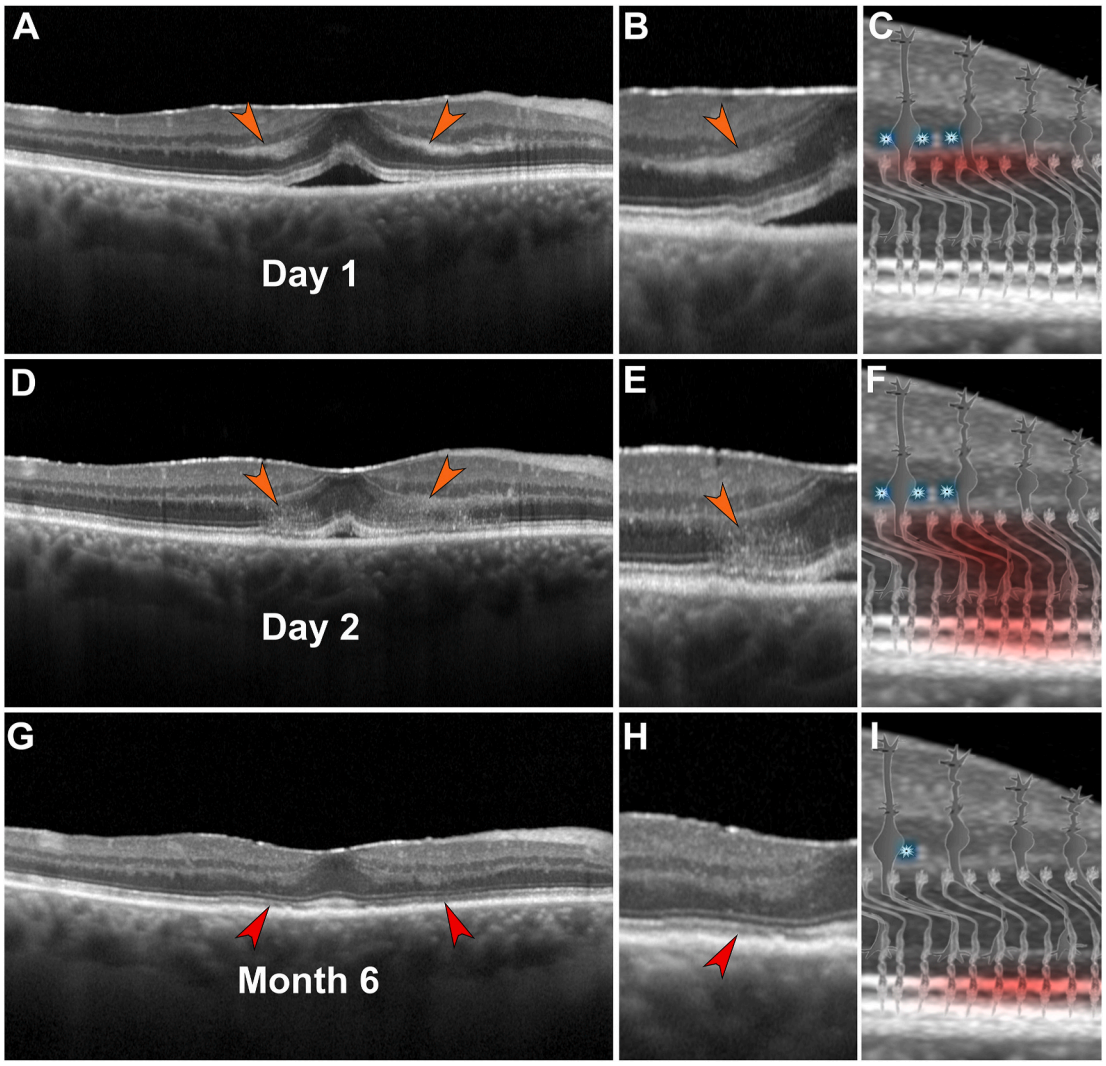

Fig. 11. Hyperacute features of acute macular neuroretinopathy (AMN) and schematic representation of the retrograde evolution of the Angular Sign of Henle Fiber Layer Hyperreflectivity (ASHH). Adapted from (Ramtohul et al., 2020b).

A. Spectral domain optical coherence tomography (OCT) horizontal B-scan through the fovea shows hyperreflective lesions (*orange arrowheads*) confined to the outer plexiform layer (OPL) and Henle fiber layer (HFL). Subretinal fluid is noted. There is no extension of the hyperreflective changes to the outer nuclear layer (ONL), ellipsoid (EZ), and interdigitation zones (IZ). The OCT image was acquired few hours after visual symptoms' onset.

B. Magnified view of the hyperreflective lesions confined to the OPL and HFL (*orange arrowhead*).

C. Schematic representation of the presumed hyperacute damages in AMN, including deep capillary plexus (DCP) disruption and photoreceptor synapse and axon insults. The same color-code and annotations as in Fig. 8 are used.

D. Tracked OCT B-scan shows retrograde extension of the hyperreflective lesions to the ONL, EZ, and IZ (*orange arrowheads*). The angular configuration of the hyperreflective lesions is apparent especially in the temporal side of the fovea. The OCT image was acquired the day after visual symptoms' onset.

E. Magnified view of ASHH (*orange arrowhead*).

F. Schematic representation of ASHH in AMN characterized by retrograde extension of the insult to the whole photoreceptor length. The same color-code and annotations as in Fig. 8 are used. Persistent DCP alteration can be observed.

G. Tracked OCT B-scan shows resolution of ASHH and persistent OPL, HFL, and ONL thinning with EZ/IZ attenuation (*red arrowheads*). The OCT image was acquired 6 months after symptoms' onset.

H. Magnified view of resolved ASHH. Note the thinning of the OPL, HFL, and ONL and attenuation of the EZ/IZ reflectivity (*red arrowhead*).

I. Schematic representation of resolved ASHH in AMN. Long-term DCP disruption can be detected but are usually more subtle on OCT-angiography and attenuation of the photoreceptor inner and outer segments is displayed. The same color-code and annotations as in Fig. 8 are used.

can include pachychoroid pigment epitheliopathy (Pang and Freund, 2014).

Acute fovealitis is a presumed inflammatory condition recently described by Ledesma-Gil and Spaide in a patient with acute foveal lesions involving the outer neurosensory retina (Ledesma-Gil and Spaide, 2022). Although acute fovealitis shares ophthalmoscopic and OCT features with ARPE, including foveal-centered ASHH, the absence of RPE involvement on OCT led the authors to suggest the name acute fovealitis (Ledesma-Gil and Spaide, 2022). Similar OCT features termed foveal outer retinal hyperreflectivity were previously described by Dolz-Marco et *al.* in patients with idiopathic multifocal choroiditis (Dolz-Marco et al., 2021). An additional case series of three patients with multimodal imaging findings compatible with acute fovealitis is described, although no established diagnostic criteria exist (Moraes et al., 2020). Acute fovealitis may also develop during COVID-19 infection (Munoz-Solano et al., 2022). Due to the paucity of reports, it remains unclear if acute fovealitis is a distinct entity or a variant of ARPE.

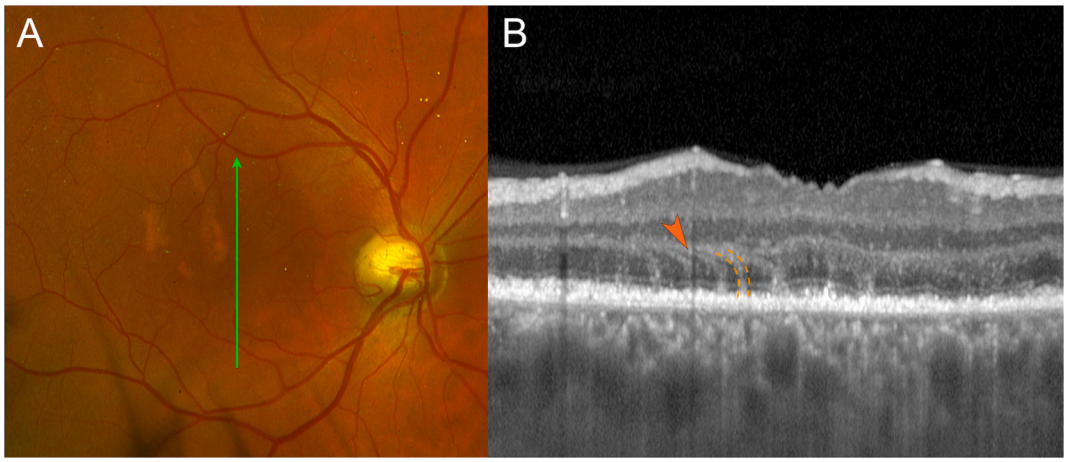

Fig. 12. Multimodal imaging of contusion maculopathy after blunt ocular trauma.
A. Pseudocolor fundus photography (Optos PLC, Dunfermline, UK) of the right eye shows areas of macular whitening consistent with commotio retinae. The green line indicates the position of the spectral domain OCT B-scan in (B).
B. Spectral domain OCT B-scan (Spectralis, Heidelberg Engineering, Heidelberg, Germany) shows multiple angular signs of Henle fiber layer hyperreflectivity (ASHH) (*orange arrowhead and between orange dashed lines*) associated with disruption of the ellipsoid zone, interdigitation zone, and retinal pigment epithelium band.

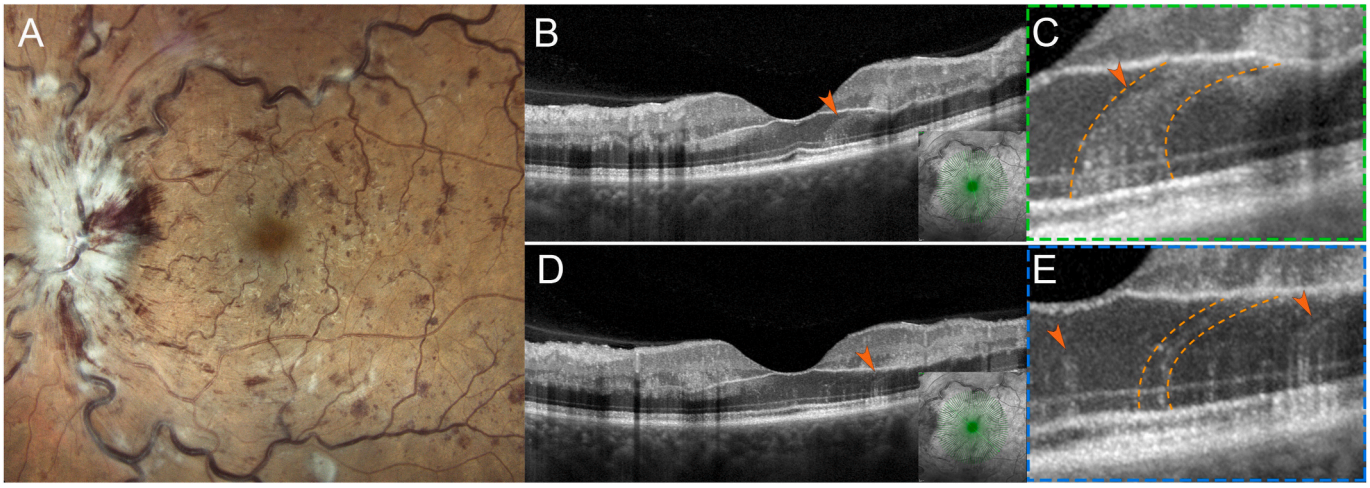

Fig. 13. Multimodal imaging of central retinal vein occlusion in a 42-year-old patient. Adapted from Iovino et al. (2021).
A. Confocal color fundus photography of the left eye shows optic disk edema, diffuse retinal hemorrhages, cotton wool spots, and venous dilation and tortuosity consistent with central retinal vein occlusion. Note the perivenular macular whitening.
B. High-Resolution OCT B-scan shows paracentral acute middle maculopathy lesions and one angular sign of Henle fiber layer hyperreflectivity (ASHH) (*orange arrowhead*). The inset is the near-infrared reflectance image with the green line indicating the position of the OCT-B scan.
C. Magnified view of ASHH on high-resolution OCT B-scan (*orange arrowhead and between orange dashed lines*).
D. High-Resolution OCT B-scan (Spectralis, Heidelberg Engineering, Heidelberg, Germany) shows paracentral acute middle maculopathy lesions and multiple thin ASHH (*orange arrowheads*). Note the vertically oriented ASHH centrally. The inset is the near-infrared reflectance image with the green line indicating the position of the OCT-B scan.
E. Magnified view of ASHH on High-Resolution OCT B-scan (*orange arrowheads and between orange dashed lines*).

4.7.1. Pathogenesis

Although the pathophysiology is unknown, ARPE is postulated to be caused by immune reaction targeting the RPE (Krill and Deutman, 1972). However, recent investigations using OCT demonstrate hyperreflective lesions affecting the outer neurosensory retina, suggesting that the latter, and not the RPE, may be the primary site of inflammation (Baillif et al., 2011; Cho et al., 2011; De Bats et al., 2013; Hall et al., 2012; Hsu et al., 2007; Iu et al., 2017; Krill and Deutman, 1972; Merkoudis and Granstam, 2013). Similarly, acute fovealitis may result from transient inflammation affecting the foveolar cellular components (cones and/or Müller cell cones) (Ledesma-Gil and Spaide, 2022). Anterograde and retrograde pathways of photoreceptor disruption are pathophysiologic candidates.

4.8. Acute annular outer retinopathy

Acute annular outer retinopathy (AAOR), first described by Gass and Stern in 1995, is supposed to be very rare variant of acute zonal occult outer retinopathy (AZOOR) (Gass and Stern, 1995). (Monson and Smith, 2011). The most prominent complaints include acute visual field defects, central vision loss, and photopsia (Monson and Smith, 2011). The characteristic ophthalmoscopic finding includes a progressively enlarging, gray-white outer retinal ring similar to the Wessely immune ring in herpetic corneal infection (Fekrat et al., 2000; Gass and Stern, 1995; Luckie et al., 1994). FA shows a hypofluorescent ring with a hyperfluorescent border, and ICGA demonstrates late hypofluorescence related to decreased RPE uptake (Fekrat et al., 2000; Harino et al., 2004), but both studies can be normal (Seetharam et al., 2015). OCT can

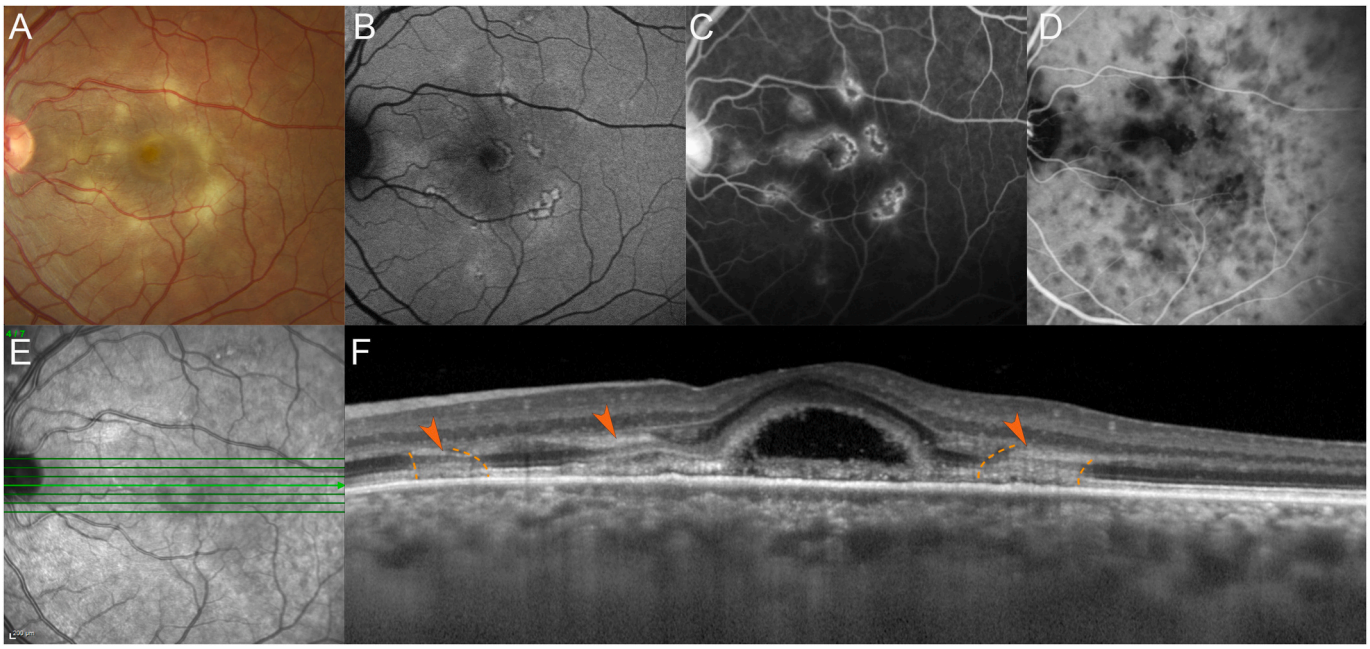

Fig. 14. Multimodal imaging of acute posterior multifocal placoid pigment epitheliopathy in a 31-year-old patient. Adapted from Mrejen et al. (2016).
A. Color fundus photography of the left eye shows multiple, yellowish, outer retinal lesions of the macula.
B. Blue-light fundus autofluorescence (HRA, Heidelberg Engineering, Heidelberg, Germany) shows hyperautofluorescent lesions surrounded by a thin hypoautofluorescent edge.
C. Late phase fluorescein angiography (HRA, Heidelberg Engineering, Heidelberg, Germany) shows hypofluorescent lesions with staining.
D. Late phase indocyanine green angiography (HRA, Heidelberg Engineering, Heidelberg, Germany) shows more numerous hypofluorescent lesions.
E. Near-infrared reflectance image shows discrete hyporeflective lesions. The green line indicates the location of the OCT B-scan in (F).
F. Spectral domain OCT B-scan (Spectralis, Heidelberg Engineering, Heidelberg, Germany) through the fovea shows bacillary layer detachment (BALAD) and multiple angular signs of Henle fiber layer hyperreflectivity (ASHH) (*orange arrowheads and between orange dashed lines*) typical of early acute disease. Note the choroidal thickening and loss of the normal choroidal architecture under the fovea.

illustrate paracentral ASHH correlating with the annular ring (Bemme et al., 2016; Seetharam et al., 2015). ASHH precede outer retinal atrophy, which suggests that early HFL damage may occur during the course of AAOR (Seetharam et al., 2015). No proven treatment of AAOR exists, although systemic antivirals, antibacterials, steroids, and immunosuppressive therapy have been studied with no consensus on efficacy (Fekrat et al., 2000; Monson and Smith, 2011; Seetharam et al., 2015). Spontaneous improvement may also occur (Fekrat et al., 2000).

4.8.1. Pathogenesis

The pathophysiology of AAOR is unknown but the characteristic enlarging, gray-white outer retinal ring similar to the Wessely immune ring noted in herpetic corneal infection led Gass and Stern to postulate that AAOR may be due to viral infection of the photoreceptor synapses and axons followed by a host immune response (retrograde pathway of photoreceptor disruption) (Gass and Stern, 1995).

4.9. Paraneoplastic autoimmune retinopathy

Cancer-associated retinopathy (CAR) is a paraneoplastic syndrome first described by Sawyer et *al.* in three cancer patients that developed blindness due to diffuse retinal degeneration (Sawyer et al., 1976). Symptoms classically include acute/subacute vision loss, photopsia, and visual field defects (Rahimy and Sarraf, 2013). For detailed information, we refer the reader to prior reviews (Rahimy and Sarraf, 2013; Touhami et al., 2019). Several OCT reports describe ASHH in eyes with CAR and paraneoplastic retinopathy (Chen et al., 2017; J. J. Lee et al., 2015; Russell et al., 2020). ASHH associated with retinal phlebitis can also develop in patients treated with programmed death 1 (PD-1) and death ligand 1 (PD-L1) inhibitors (Chen et al., 2022; Emens et al., 2019; Ramtohul and Freund, 2020). Patients with ASHH associated with paraneoplastic retinopathy typically develop extensive outer retinal atrophy (Chen et al., 2017, 2022; J. J. Lee et al., 2015). FAF may reveal zonal areas of hyperautofluorescence (Fig. 15) (Chen et al., 2017; Russell et al., 2020). Collaborative management with oncologic teams is required and additional steroid, immunosuppressive therapy or plasmapheresis can be considered (Chen et al., 2017, 2022; J. J. Lee et al., 2015).

4.9.1. Pathogenesis

The pathophysiology of paraneoplastic autoimmune retinopathy is unclear. Tumor-derived or systemic mediated auto-antibodies cross-reacting with retinal antigens and leading to cell apoptosis is the current accepted theory (Adamus et al., 2004). Disruption of the photoreceptor inner and outer segments and axons presumably cause HFL abnormalities as illustrated with ASHH on OCT. By contrast, PD-1 and PD-L1 inhibitors may incite a retinal phlebitis causing impairment of the most distal aspect of the DCP leading to disruption of the photoreceptor synapses and axons and extension of injury through the HFL to the photoreceptor inner and outer segments (retrograde pathway of photoreceptor disruption) (Ramtohul and Freund, 2020).

4.10. Handheld laser induced maculopathy

There are many reports of handheld laser induced maculopathy (HLIM) since the original publication by Zamir et al. (1999). For detailed information regarding laser characteristics, we refer the reader to recent reviews (Bhavsar et al., 2020; Tran et al., 2020). Symptoms of retinal phototoxicity include vision impairment within hours of exposure, central or paracentral scotomas, and metamorphopsia (Rusu et al., 2013). Eye pain due to anterior segment inflammation and iris atrophy can be additional clues for the diagnosis (Agarwal et al., 2022; Al-Amry

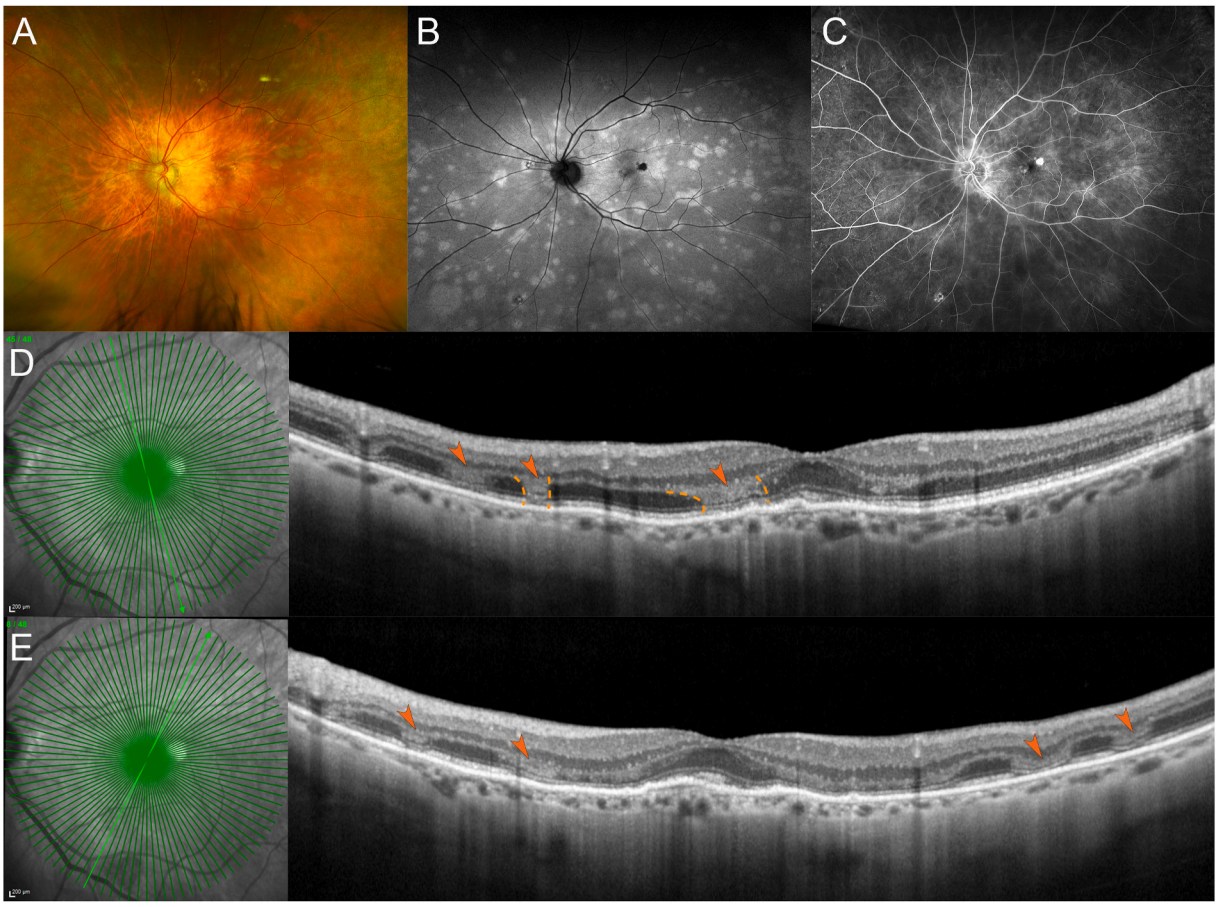

Fig. 15. Multimodal imaging of paraneoplastic retinopathy in an 86-year-old patient with a history of metastatic bladder cancer and neovascular age-related macular degeneration. Adapted from Russell et al. (2020).

A. Ultra-widefield pseudocolor fundus photography (Optos PLC, Dunfermline, UK) of the left eye shows multiple, yellowish, placoid lesions in the vicinity of the retinal vessels.

B. Green-light ultra-widefield fundus autofluorescence shows paravascular hyperautofluorescent lesions.

C. Late phase ultra-widefield fluorescein angiography shows mild leakage of the lesions.

D and E. Near-infrared reflectance images with corresponding spectral domain OCT B-scans (Spectralis, Heidelberg Engineering, Heidelberg, Germany) show multiple angular signs of Henle fiber layer hyperreflectivity (ASHH) (*orange arrowheads and between orange dashed lines*). Note that the angulation of the ASHH varies with eccentricities. The green lines in the near-infrared reflectance image indicate the location of the corresponding OCT B-scan.

et al., 2018; Bhavsar et al., 2020). On OCT, ASHH are very characteristic of HLIM and develop in approximately 13% of cases (Bhavsar et al., 2020), typically as a more acute sign of injury. Similar OCT lesions can be observed in photic maculopathy from arc welding (Park et al., 2021). Associated findings on OCT include focal EZ/IZ disruption, hyporeflective cavities in the outer retina, subretinal and intraretinal fluid, and RPE alterations (Bhavsar et al., 2015, 2020; Chen et al., 2021; Rusu et al., 2013). On NIR, hyperreflective lesions with dendritic-like radiations are characteristic findings, and FAF imaging typically shows vertical streak-like hyperautofluorescent lesions indicative of RPE injury (Fig. 16) (Bhavsar et al., 2015, 2020; Dhrami-Gavazi et al., 2015; Rusu et al., 2013). Distinctive signs on FA include early hyperfluorescence with late staining of the linear RPE streaks (Bhavsar et al., 2015, 2020). Focal staining of retinal vessels injured by laser can be misinterpreted as retinal vasculitis (Bhavsar et al., 2020). ICGA and OCTA can demonstrate choroidal ischemia which can explain the development of secondary CNV and may indicate the need for anti-VEGF therapy (Tran et al., 2020).

4.10.1. Pathogenesis

In HLIM, thermal injury of the HFL components and ischemia of the inner choroid and RPE may contribute to the genesis of ASHH (Bhavsar et al., 2020; Tran et al., 2020). Anterograde and retrograde pathways of photoreceptor disruption are pathophysiologic candidates.

4.11. Differential diagnosis

In this section, we briefly review alternative disorders associated with hyperreflective lesions migrating through or accumulating in the HFL, and provide key features to differentiate these findings from the typical ASHH on OCT. These hyperreflective lesions on OCT typically exhibit a trajectory following the direction of the HFL and the presumed underlying pathogenesis is different. While ASHH indicates an acute injury of the HFL originating from a retrograde or anterograde insult, hyperreflective materials within the HFL, including RPE cells, blood, or exudates, represents an entirely different pathogenesis. Adjunctive multimodal imaging features and analysis of the temporal sequence are useful to differentiate ASHH from hyperreflective lesions migrating through or accumulating in the HFL. Absence of outer retinal alteration may be observed after resolution of hyperreflective lesions accumulating or migrating through the HFL.

4.11.1. Retinal pigment epithelium plume

In AMD, the RPE plume is a distinctive reflective signature on OCT reminiscent of a windswept volcanic plume and representing a cluster of RPE cell organelles migrating anteriorly into the retina

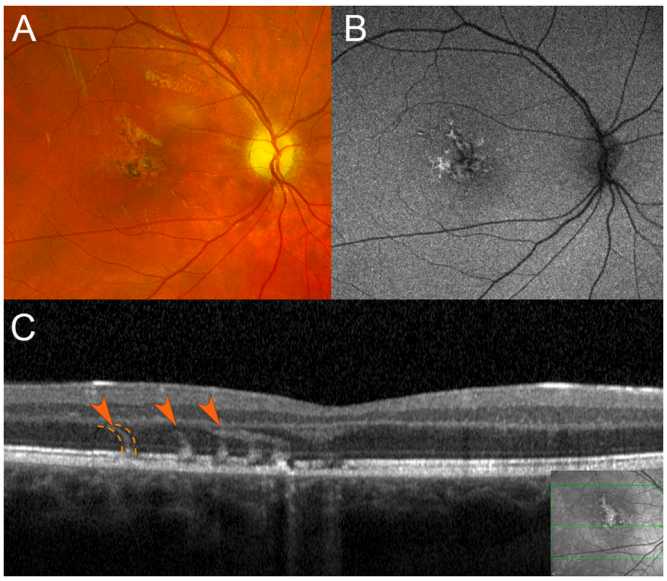

Fig. 16. Multimodal imaging of handheld-laser induced maculopathy in a 20-year-old patient. Courtesy of Dr. M. Engelbert.
A. Pseudocolor fundus image (Optos PLC, Dunfermline, UK) of the right eye shows pigmentary linear streaks and yellowish lesions in the macula.
B. Green-light fundus autofluorescence shows speckle hyperautofluorescent retinal pigment epithelium (RPE) lesions.
C. Spectral domain OCT B-scan (Spectralis, Heidelberg Engineering, Heidelberg, Germany) shows multiple angular signs of Henle fiber layer hyperreflectivity (ASHH) (*orange arrowheads and between orange dashed lines*). Note that the angulation of ASHH varies with eccentricities. Note the disruption of the ellipsoid zone, interdigitation zone, and RPE band. The inset is the near-infrared reflectance image with the green line indicating the location of the OCT B-scan.

(Balaratnasingam et al., 2017; Cao et al., 2021; Chen et al., 2016). The RPE plume is comprised of a collection of outer retinal hyperreflective foci representing RPE disruption and is an OCT biomarker for progression to RPE atrophy and late AMD (Cao et al., 2021; Christenbury et al., 2013; Nassisi et al., 2019; Ouyang et al., 2013a; Waldstein et al., 2020). Plumes develop because of RPE cell transdifferentiation (Cao et al., 2021). RPE plumes migrate in a pattern geometrically congruent with the local trajectory of the HFL (Balaratnasingam et al., 2017; Cao et al., 2021). The RPE plume is distinct from ASHH as the plume represents material (in this case pigment) tracking in a normal HFL while ASHH represents acute retrograde or anterograde injury to the HFL often with permanent disruption of the associated photoreceptor elements. RPE plumes originate from the RPE layer typically at the apex of large druse or drusenoid pigment epithelial detachment, or in association with acquired vitelliform lesions (Balaratnasingam et al., 2017; Cao et al., 2021; Chen et al., 2016). The apex may indicate the largest separation distance of the RPE from the underlying choroid resulting in RPE ischemia and impairment (Hilely et al., 2021). The lifecycle of RPE plume is complex and evolves considerably (Brinkmann et al., 2022; Cao et al., 2021). Similar RPE plumes can also develop in eyes with inherited retinal diseases, macular telangiectasia type 2 (MacTel 2), macular dystrophies (e.g. pattern dystrophy, Stargardt disease), and after macular grid laser, subthreshold laser, and pan retinal photocoagulation (Fig. 17) (Amoroso et al., 2021; Baumüller et al., 2010; Deák et al., 2012; Han et al., 2012; Sparrow et al., 2015). Outer retinal plumes presumably resulting from inward dispersion of photoreceptor debris can be noted in multiple evanescent white dot syndrome (Ramtohul et al., 2020c).

4.11.2. *Henle fiber layer hemorrhages*

Hemorrhage tracking in the HFL displays a characteristic radial and/or petaloid pattern of blood with feathery edges (Au et al., 2018, 2022; Baumal et al., 2021). Several authors postulate that the source of the blood is the DCP due to its anatomic position adjacent to the HFL (Au et al., 2018, 2022; Baumal et al., 2021). The OCT appearance of HFL hemorrhage varies from curvilinear, hyperreflective lesions clustered along the OPL to diffuse hyperreflective lesions tracking along the HFL (Fig. 18) (Au et al., 2018, 2022; Baumal et al., 2021). This spectrum of OCT changes is likely related to the severity and course of the HFL hemorrhage (Baumal et al., 2021). Underlying etiologies include local (e.g. retinal vein occlusion) and systemic (Valsalva, Terson's, intracranial hemorrhage) venous disorders, lacquers cracks associated with pathological myopia, non-proliferative MacTel 2, and type 1 aneurysmal macular neovascularization (i.e. polypoidal choroidal vasculopathy) (Asai et al., 2014; Au et al., 2018, 2022; Baumal et al., 2021; Lane et al., 2004).

4.11.3. *Vertical hyperreflective lesions in vitreoretinal lymphoma*

Deàk et *al.* were the first to describe with OCT vertical hyperreflective lesions extending from the inner retina to the RPE in patients

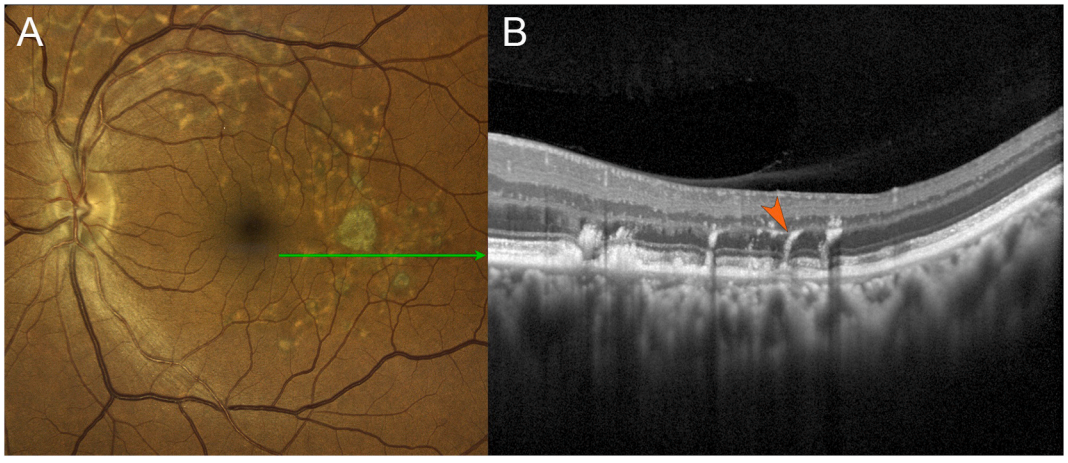

Fig. 17. Multimodal imaging of retinal pigment epithelium plumes in *ABCA4*-associated retinopathy (compound heterozygous mutations: [c.6215G > A (p.Ser2072Asn) and c.6499G > A (p.Val2167Ile)]).
A. Confocal color fundus photography of the left eye shows yellowish retinal flecks and paracentral macular atrophy. The green line indicates the position of the High-Resolution OCT B-scan in (B).
B. High-Resolution OCT B-scan (Spectralis, Heidelberg Engineering, Heidelberg, Germany) through the retinal flecks shows curvilinear, hyperreflective lesions migrating anteriorly in the Henle fiber layer above areas of focal retinal pigment epithelium thickening (*orange arrowhead*).

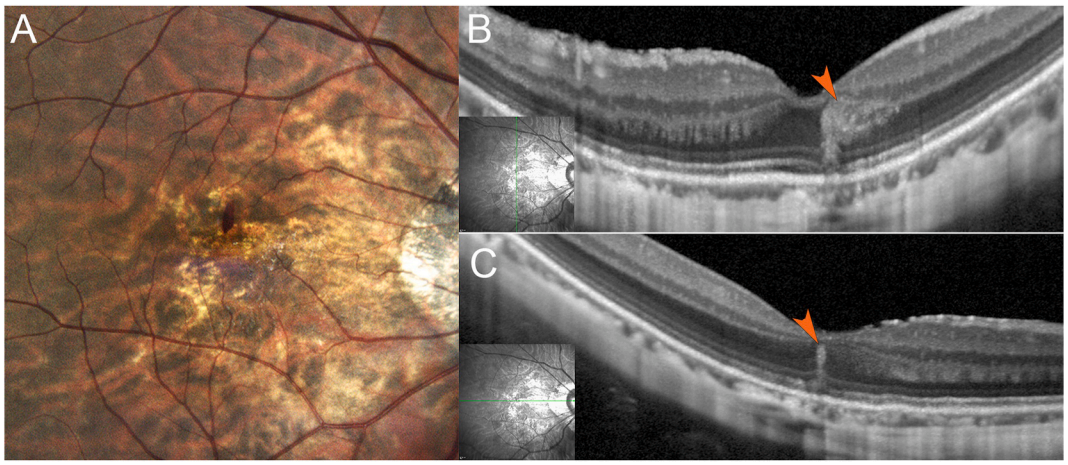

Fig. 18. Multimodal imaging of Henle fiber layer (HFL) hemorrhage associated with lacquers cracks in a 40-year-old female with myopic degeneration.
A. Confocal color fundus photography of the right eye shows a petaloid HFL hemorrhage pointing toward the fovea.
B. Vertical high-resolution OCT B-scan (Spectralis, Heidelberg Engineering, Heidelberg, Germany) shows hyperreflective HFL hemorrhage (*orange arrowhead*) radiating in the HFL. The inset is the near infrared reflectance image with the green line indicating the position of the OCT-B scan.
C. Horizontal high-resolution OCT B-scan (Spectralis, Heidelberg Engineering, Heidelberg, Germany) shows a different pattern of the HFL hemorrhage (*orange arrowhead*) which radiates vertically in the central HFL. The inset is the near-infrared reflectance image with the green line indicating the position of the OCT-B scan.

with vitreoretinal lymphoma (Deák et al., 2019). Controversies exist regarding the etiology of this OCT finding, which may represent early microinfiltrates of lymphoma cells (Pichi et al., 2021). It is unclear if the retinal capillary or the choroidal vasculature is the primary origin of these vertical hyperreflective lesions (Deák et al., 2019; Pichi et al., 2021). On OCT, the intensity of these lesions can vary greatly from hyperreflectivity comparable to that of the RPE layer to more subtle isoreflectivity (Fig. 19) (Deák et al., 2019). Vertical hyperreflective lesions are most commonly located along the vascular arcades and are rarely detectable in the fovea (Deák et al., 2019). Co-localization with sub-RPE deposits is reported (Deák et al., 2019). The natural course of these lesions is highly dynamic and characterized by spontaneous

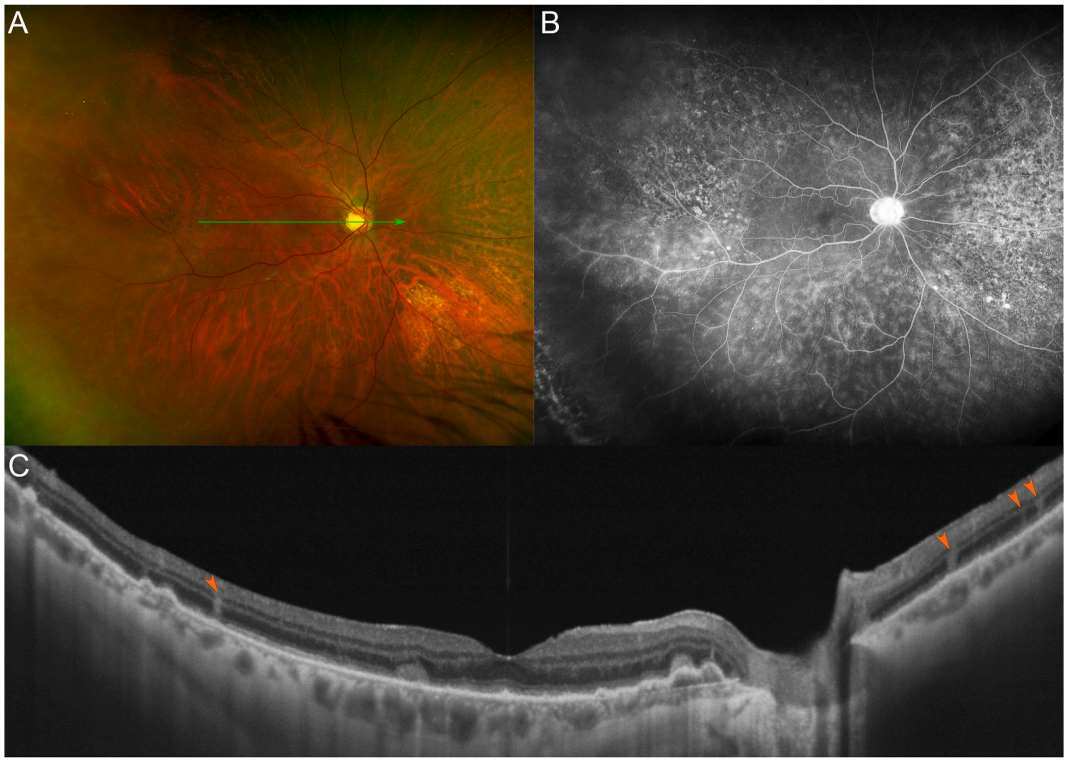

Fig. 19. Multimodal imaging of vertical hyperreflective lesions in primary vitreoretinal lymphoma. Adapted from Ramtohul et al. (2022b).
A. Ultra-widefield pseudocolor fundus photography (Optos PLC, Dunfermline, UK) of the right eye shows vitreous cells inferiorly, perivascular sheathing in the temporal periphery, and diffuse retinal pigment epithelium alterations. The green line indicates the location of the swept-source OCT B-scan in (C).
B. Mid-phase ultra-widefield fluorescein angiogram shows a leopard-spot pattern of hypo- and hyperfluorescence, and perivenular fern-like leakage in the inferior retina.
C. Swept-source OCT B-scan (Plex Elite 9000, Carl Zeiss Meditec, Inc, Dublin, CA) shows several vertical hyperreflective lesions (*orange arrowheads*). Note the presence of sub-retinal and sub-retinal pigment epithelium deposits indicative of lymphoma infiltrates.

resolution and development elsewhere (Deák et al., 2019).

4.11.4. Cytomegalovirus retinitis

Cytomegalovirus (CMV) can cause necrotizing retinitis in immunocompromised patients (Pichi et al., 2020). The virus is capable of infecting the RPE cells, Müller cells and inner retinal neurons after penetrating the eye from the retinal or choroidal vasculature (Pichi et al., 2020). On OCT, hyperreflective vertical lines connecting the RPE to the inner retinal layers are reported (Invernizzi et al., 2018; Pichi et al., 2020). This finding may represent infected Müller cells (Invernizzi et al., 2018; Pichi et al., 2020).

4.11.5. Vitreomacular tractions and macular holes

Preceding the development of a full-thickness macular hole, OCT investigations have identified a vertical, linear, hyperreflective lesion in the central fovea termed the hyperreflective stress line (J. M. Scharf et al., 2020) or foveal crack sign (Furashova and Matthé, 2020; Ishibashi et al., 2020). This lesion extends from the internal limiting membrane to the EZ and may be a biomarker of evolving vitreomacular traction (Fig. 20), although it can also be detected with OCT after surgery of macular hole (Ishibashi et al., 2020; J. M. Scharf et al., 2020). Therefore, this central vertical hyperreflective lesion may represent a central foveal seam due to mechanical disruption of the Müller cell cone but should not be confused with ASHH (Ishibashi et al., 2020; J. M. Scharf et al., 2020). Curved hyperreflective structures in the HFL and ONL likely representing gliosis of the outer Müller cell processes is reported in patients with macular holes (Bringmann et al., 2020).

5. Conclusions and perspectives

The HFL may be specifically disrupted in various retinal conditions and recognition of imaging patterns indicating HFL injury is critical to further understand the underlying pathophysiology and to guide accurate diagnosis. From a clinical and prognostic standpoint, identification of ASHH on OCT may guide diagnostic procedures and therapeutic interventions as ASHH is often observed in the early phases of macular disease. Resolved ASHH on OCT typically lead to various degrees of thinning of the OPL, HFL, and ONL with EZ/IZ alteration and this may account for persistent visual field defects and reduced visual acuity in some patients.

Introduction of ASHH on OCT as a descriptive term indicative of acute photoreceptor insult including HFL components may provide the opportunity to differentiate true AMN from AMN-like disorders such as dengue, whiplash and contusion maculopathy. Detection of ASHH on OCT should alert clinicians to the associated etiologies reviewed herein. Multimodal imaging can be powerful to further focus the diagnosis (e.g., APMPPE, HLIM) upon identification of ASHH on OCT. The etiology of ASHH may be the result of inflammatory, ischemic, thermal or mechanical insults involving the HFL components, leading to swelling of the photoreceptor axons and/or Müller cell elements thus making the HFL more prominent and more easily identified with OCT, but this requires further study with morphometric and histopathological analysis. This OCT sign should however, be differentiated from disorders that cause tracking of materials in the HFL (e.g., pigment in the RPE plume, HFL hemorrhage, macular star exudation and petaloid cystoid macular edema) in which primary injury to the HFL may not be present.

Many gray areas persist regarding the cellular and molecular mechanisms driving the embryology and functionality of the HFL. Key aspects of HFL oxygenation and metabolism in human retina remain unclear. The advent of more sophisticated imaging techniques, such as high-resolution OCT or visible-light OCT, may improve these crucial aspects (Pi et al., 2020). Understanding the embryologic steps resulting in functional photoreceptor axons and synapses are more than relevant nowadays with the advent of cell-based therapies for retinal diseases. Reproducing key aspects of human HFL development, integration and synaptogenesis remains major challenges and are still poorly understood.

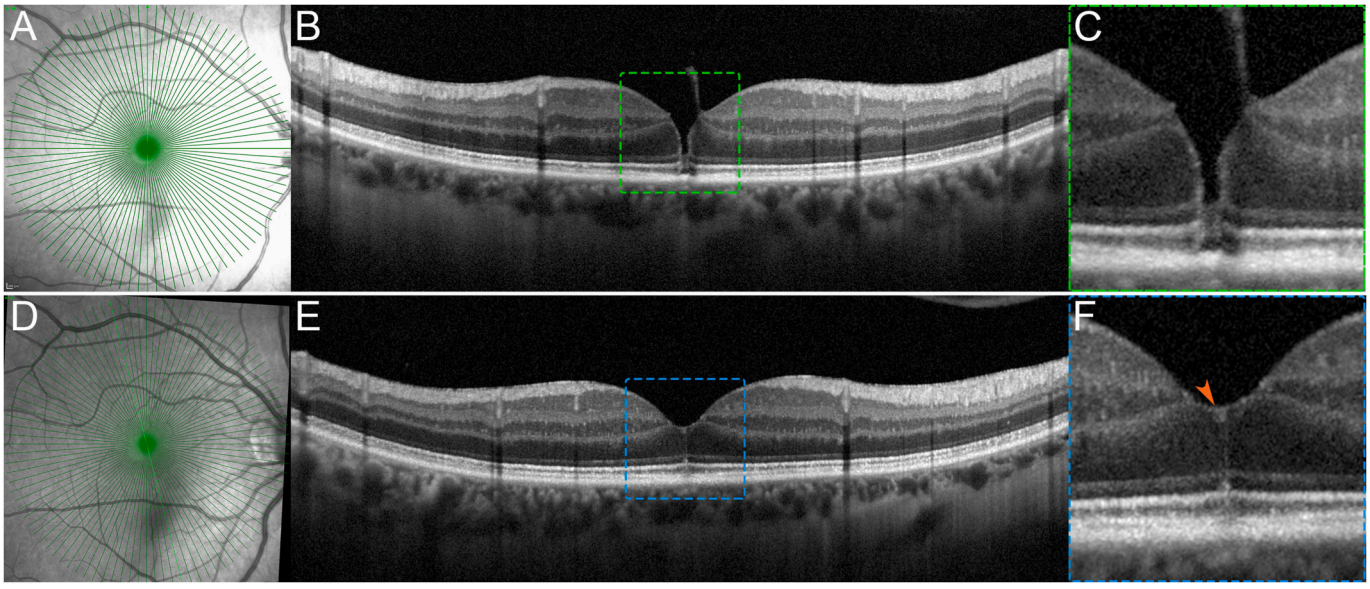

Fig. 20. High-resolution optical coherence tomography of hyperreflective stress line in a 55-year-old female with an impending macular hole.
A. Near-infrared reflectance image of the right eye at presentation. The green line indicates the location of the high-resolution OCT B-scan in (B).
B. High-resolution OCT B-scan (Spectralis, Heidelberg Engineering, Heidelberg, Germany) through the fovea shows an impending macular hole with vitreomacular traction. The green dashed box indicates the location of the magnified view in (C).
C. Magnified view of the impending macular hole. Note the linear hyperreflectivity at the borders of the macular hole.
D. Near-infrared reflectance image of the right eye at 2 weeks of follow-up. The green line indicates the location of the high-resolution OCT B-scan in (E).
E. High-Resolution OCT B-scan (Spectralis, Heidelberg Engineering, Heidelberg, Germany) through the fovea shows spontaneous resolution of the impeding macular hole. Note the hyperreflective stress line at the center of the fovea. The blue dashed box indicates the location of the magnified view in (F).
F. Magnified view of the hyperreflective stress line (*orange arrowhead*). Note the release of the vitreomacular traction.

Author statement

Prithvi Ramtohul: Conceptualization, Investigation, Writing – original draft, Writing – Reviewing & Editing. Percentage Contribution: 40%

Diogo Cabral: Investigation, Writing – original draft, Writing – Reviewing & Editing. Percentage Contribution: 5%

K. Bailey Freund: Conceptualization, Writing – original draft, Writing – Reviewing & Editing, Supervision. Percentage Contribution: 20%

SriniVas Sadda: Conceptualization, Writing – original draft, Writing – Reviewing & Editing, Supervision. Percentage Contribution: 5%

David Sarraf: Conceptualization, Investigation, Writing – original draft, Writing – Reviewing & Editing, Supervision. Percentage Contribution: 30%

Data availability

Data will be made available on request.

Acknowledgements

a. Funding/Support: Research To Prevent Blindness Inc (DS), New York, NY and the Macula Foundation Inc (KBF, PR), New York, NY. The Philippe Foundation (PR). Fundação Luso-Americana para o Desenvolvimento (FLAD, USA R&D@PhD – Proj 2020/0140) (DC).

b. Financial Disclosures: Prithvi Ramtohul: none; Diogo Cabral: none; SriniVas Sadda: Amgen (C), Allergan (C), Genentech-Roche (C), Oxurion (C), Novartis (C), Regeneron (C), Bayer (C), 4DMT (C), Centervue (C, S), Heidelberg (C, F, S), Optos (C, F, S), Carl Zeiss Meditec (F, S), Nidek (S), Topcon (S); K. Bailey Freund: Heidelberg Engineering (C), Zeiss (C), Bayer (C), Novartis (C), and Allergan (C), Genentech/Roche C. A (C, S). David Sarraf: Amgen (C, F), Genentech-Roche (C, 400F), Heidelberg (F), Novartis (C, F), Optovue (C, F), Regeneron (F), Bayer (C, F), Topcon (F).

References

Abramov, I., Gordon, J., Hendrickson, A., Hainline, L., Dobson, V., LaBossiere, E., 1982. The retina of the newborn human infant. Science 217, 265–267. https://doi.org/10.1126/science.6178160.

Adamus, G., Ren, G., Weleber, R.G., 2004. Autoantibodies against retinal proteins in paraneoplastic and autoimmune retinopathy. BMC Ophthalmol. 4, 5. https://doi.org/10.1186/1471-2415-4-5.

Agarwal, A., Aggarwal, K., Dogra, M., Kumar, A., Akella, M., Katoch, D., Bansal, R., Singh, R., Gupta, V., OCTA Study Group, 2019. Dengue-induced inflammatory, ischemic foveolitis and outer maculopathy: a swept-source imaging evaluation. Ophthalmol. Retina 3, 170–177. https://doi.org/10.1016/j.oret.2018.09.008.

Agarwal, A., Jindal, A.K., Anjani, G., Suri, D., Freund, K.B., Gupta, V., 2022. Self-Inflicted Laser-Induced Maculopathy Masquerading As Posterior Uveitis In A Patient With Suspected Igg4-Related Disease. Retin. Cases Brief Rep. 16, 226–232. https://doi.org/10.1097/ICB.0000000000000935.

Aggarwal, K., Agarwal, A., Katoch, D., Sharma, M., Gupta, V., 2017. Optical coherence tomography angiography features of acute macular neuroretinopathy in dengue fever. Indian J. Ophthalmol. 65, 1235–1238. https://doi.org/10.4103/ijo.IJO_485_17.

Agte, S., Junek, S., Matthias, S., Ulbricht, E., Erdmann, I., Wurm, A., Schild, D., Käs, J.A., Reichenbach, A., 2011. Müller glial cell-provided cellular light guidance through the vital Guinea-pig retina. Biophys. J. 101, 2611–2619. https://doi.org/10.1016/j.bpj.2011.09.062.

Ahmed, J., Braun, R.D., Dunn, R., Linsenmeier, R.A., 1993. Oxygen distribution in the macaque retina. Invest. Ophthalmol. Vis. Sci. 34, 516–521.

Ahn, S.J., Woo, S.J., Kim, K.E., Jo, D.H., Ahn, J., Park, K.H., 2013. Optical coherence tomography morphologic grading of macular commotio retinae and its association with anatomic and visual outcomes. Am. J. Ophthalmol. 156, 994–1001. https://doi.org/10.1016/j.ajo.2013.06.023 e1.

Akanda, M., Gangaputra, S., Kodati, S., Melamud, A., Sen, H.N., 2018. Multimodal imaging in dengue-fever-associated maculopathy. Ocul. Immunol. Inflamm. 26, 671–676. https://doi.org/10.1080/09273948.2017.1351571.

Al Mousa, M., Koch, F., 2016. Acute Borrelia infection inducing an APMPPE-like picture. J. Ophthalmic. Inflamm. Infect. 6, 22. https://doi.org/10.1186/s12348-016-0088-x.

Al-Amry, M.A., Alsulaiman, S.M., Ghazi, N.G., 2018. Anterior segment injury by a high-power handheld blue laser device. Ocul. Immunol. Inflamm. 26, 1174–1176. https://doi.org/10.1080/09273948.2017.1327603.

Alder, V.A., Cringle, S.J., Constable, I.J., 1983. The retinal oxygen profile in cats. Invest. Ophthalmol. Vis. Sci. 24, 30–36.

Ames, A., Li, Y.Y., Heher, E.C., Kimble, C.R., 1992. Energy metabolism of rabbit retina as related to function: high cost of Na+ transport. J. Neurosci. 12, 840–853.

Amini, N., Nowroozizadeh, S., Cirineo, N., Henry, S., Chang, T., Chou, T., Coleman, A.L., Caprioli, J., Nouri-Mahdavi, K., 2014. Influence of the disc-fovea angle on limits of RNFL variability and glaucoma discrimination. Invest. Ophthalmol. Vis. Sci. 55, 7332–7342. https://doi.org/10.1167/iovs.14-14962.

Amoroso, F., Mrejen, S., Pedinielli, A., Tabary, S., Souied, E.H., Gaudric, A., Cohen, S.Y., 2021. Intraretinal hyperreflective lines. Retina 41, 82–92. https://doi.org/10.1097/IAE.0000000000002806.

An, D., Yu, P., Freund, K.B., Yu, D.-Y., Balaratnasingam, C., 2020. Three-Dimensional characterization of the normal human parafoveal microvasculature using structural criteria and high-resolution confocal microscopy. Invest. Ophthalmol. Vis. Sci. 61 https://doi.org/10.1167/iovs.61.10.3, 3–3.

Anderson, K., Patel, K.R., Webb, L., Dutton, G.N., 1996. Acute posterior multifocal placoid pigment epitheliopathy associated with pulmonary tuberculosis. Br. J. Ophthalmol. 80, 186. https://doi.org/10.1136/bjo.80.2.186.

Anger, E.M., Unterhuber, A., Hermann, B., Sattmann, H., Schubert, C., Morgan, J.E., Cowey, A., Ahnelt, P.K., Drexler, W., 2004. Ultrahigh resolution optical coherence tomography of the monkey fovea. Identification of retinal sublayers by correlation with semithin histology sections. Exp. Eye Res. 78, 1117–1125. https://doi.org/10.1016/j.exer.2004.01.011.

Asai, T., Ikuno, Y., Nishida, K., 2014. Macular microstructures and prognostic factors in myopic subretinal hemorrhages. Invest. Ophthalmol. Vis. Sci. 55, 226–232. https://doi.org/10.1167/iovs.13-12658.

Ashraf, M., Goldstein, D., Fawzi, A., 2017. Optical coherence tomography angiography: potential artifacts in acute macular neuroretinopathy. JAMA Ophthalmol. 135, 675. https://doi.org/10.1001/jamaophthalmol.2017.0918.

Atas, F., Kaya, M., Saatci, A.O., 2021. Acute multifocal placoid pigment epitheliopathy-like presentation following the first dose of BNT162B2 COVID-19 vaccination. Ocul. Immunol. Inflamm. 1–4. https://doi.org/10.1080/09273948.2021.1995763.

Au, A., Hou, K., Baumal, C.R., Sarraf, D., 2018. Radial hemorrhage in Henle layer in macular telangiectasia type 2. JAMA Ophthalmol. 136, 1182–1185. https://doi.org/10.1001/jamaophthalmol.2018.2979.

Au, A., Jung, J., Johnson, M.W., Baumal, C., Daily, M.J., Gomolin, J.E.S., Gupta, R.R., Rahimy, E., Wu, L., Sadda, S.R., Sarraf, D., 2022. Henle fiber layer hemorrhage in macular telangiectasia type 2: is right eye dominance coincidence or consequence? Am. J. Ophthalmol. 241, 80–86. https://doi.org/10.1016/j.ajo.2022.04.002.

Avtar, R., Tandon, D., 2008. Mathematical modelling of intraretinal oxygen partial pressure. Trop. J. Pharmaceut. Res. 7, 1107–1116.

Aydoğan, T., Güney, E., Akçay, B.İ.S., Bozkurt, T.K., Ünlü, C., Ergin, A., 2015. Acute retinal pigment epitheliitis: spectral domain optical coherence tomography, fluorescein angiography, and autofluorescence findings. Case Rep. Med., 149497 https://doi.org/10.1155/2015/149497.

Azar, P., Gohd, R.S., Waltman, D., Gitter, K.A., 1975. Acute posterior multifocal placoid pigment epitheliopathy associated with an adenovirus type 5 infection. Am. J. Ophthalmol. 80, 1003–1005. https://doi.org/10.1016/0002-9394(75)90328-1.

Bach, L., Seefelder, P., 1914. Atlas zur Entwicklungsgeschichte des menschlichen. Auges. Wilhelm Englemann, Leipzig.

Bagci, A.M., Shahidi, M., Ansari, R., Blair, M., Blair, N.P., Zelkha, R., 2008. Thickness profiles of retinal layers by optical coherence tomography image segmentation. Am. J. Ophthalmol. 146, 679–687. https://doi.org/10.1016/j.ajo.2008.06.010.

Baillif, S., Wolff, B., Paoli, V., Gastaud, P., Mauget-Faÿsse, M., 2011. Retinal fluorescein and indocyanine green angiography and spectral-domain optical coherence tomography findings in acute retinal pigment epitheliitis. Retina 31, 1156–1163. https://doi.org/10.1097/IAE.0b013e3181fbcea5.

Balaratnasingam, C., Messinger, J.D., Sloan, K.R., Yannuzzi, L.A., Freund, K.B., Curcio, C. A., 2017. Histologic and optical coherence tomographic correlates in drusenoid pigment epithelium detachment in age-related macular degeneration. Ophthalmology 124, 644–656. https://doi.org/10.1016/j.ophtha.2016.12.034.

Baumal, C.R., Sarraf, D., Bryant, T., Gui, W., Muakkassa, N., Pichi, F., Querques, G., Choudhry, N., Teke, M.Y., Govetto, A., Invernizzi, A., Eliott, D., Gaudric, A., Cunha de Souza, E., Naysan, J., Lembo, A., Lee, G.C., Freund, K.B., 2021. Henle fibre layer haemorrhage: clinical features and pathogenesis. Br. J. Ophthalmol. 105, 374–380. https://doi.org/10.1136/bjophthalmol-2019-315443.

Baumal, C.R., Sarraf, D., Bryant, T., Gui, W., Muakkassa, N., Pichi, F., Querques, G., Choudhry, N., Teke, M.Y., Govetto, A., Invernizzi, A., Eliott, D., Gaudric, A., Cunha de Souza, E., Naysan, J., Lembo, A., Lee, G.C., Freund, K.B., 2020. Henle fibre layer haemorrhage: clinical features and pathogenesis. Br. J. Ophthalmol. https://doi.org/10.1136/bjophthalmol-2019-315443.

Baumüller, S., Charbel Issa, P., Scholl, H.P.N., Schmitz-Valckenberg, S., Holz, F.G., 2010. Outer retinal hyperreflective spots on spectral-domain optical coherence tomography in macular telangiectasia type 2. Ophthalmology 117, 2162–2168. https://doi.org/10.1016/j.ophtha.2010.02.014.

Baumüller, S., Holz, F.G., 2012. Early spectral-domain optical coherence tomography findings in acute macular neuroretinopathy. Retina 32, 409–410. https://doi.org/10.1097/IAE.0b013e31822f573a.

Bedggood, P., Nguyen, B., Lakkis, G., Turpin, A., McKendrick, A.M., 2017. Orientation of the temporal nerve fiber raphe in healthy and in glaucomatous eyes. Invest. Ophthalmol. Vis. Sci. 58, 4211–4217. https://doi.org/10.1167/iovs.17-21995.

Bemme, S., Pleyer, U., Salehi, N., Naxer, S., Callizo, J., Hoerauf, H., Feltgen, N., 2016. [Progressive scotoma with perception of photopsia]. Ophthalmologe 113, 66–70. https://doi.org/10.1007/s00347-015-0012-z.

Berger, E., Ghorayeb, G., Hogg, J., 2019. An atypical case of acute posterior multifocal placoid pigment epitheliopathy with recurrent strokes. Am. J. Ophthalmol. Case Rep. 16, 100574 https://doi.org/10.1016/j.ajoc.2019.100574.

Bhavsar, K.V., Lin, S., Rahimy, E., Joseph, A., Freund, K.B., Sarraf, D., Cunningham, E.T., 2016. Acute macular neuroretinopathy: a comprehensive review of the literature. Surv. Ophthalmol. 61, 538–565. https://doi.org/10.1016/j.survophthal.2016.03.003.

Bhavsar, K.V., Michel, Z., Greenwald, M., Cunningham, E.T., Freund, K.B., 2020. Retinal injury from handheld lasers: a review. Surv. Ophthalmol. https://doi.org/10.1016/j.survophthal.2020.06.006.

Bhavsar, K.V., Wilson, D., Margolis, R., Judson, P., Barbazetto, I., Freund, K.B., Cunningham, E.T., 2015. Multimodal imaging in handheld laser-induced maculopathy. Am. J. Ophthalmol. 159, 227–231. https://doi.org/10.1016/j.ajo.2014.10.020 e2.

Bigaut, K., Kremer, L., Hacquard, A., Wolff, B., Collongues, N., De Seze, J., 2019. A case of acute posterior multifocal placoid pigment epitheliopathy with aseptic meningitis and cerebral infarction. Rev. Neurol. (Paris) 175, 329–331. https://doi.org/10.1016/j.neurol.2018.06.011.

Bird, A.C., Hamilton, A.M., 1972. Placoid pigment epitheliopathy. Presenting with bilateral serous retinal detachment. Br. J. Ophthalmol. 56, 881–886. https://doi.org/10.1136/bjo.56.12.881.

Birol, G., Wang, S., Budzynski, E., Wangsa-Wirawan, N.D., Linsenmeier, R.A., 2007. Oxygen distribution and consumption in the macaque retina. Am. J. Physiol. Heart Circ. Physiol. 293, H1696–H1704. https://doi.org/10.1152/ajpheart.00221.2007.

Bone, R.A., Landrum, J.T., 1992. Distribution of macular pigment components, zeaxanthin and lutein, in human retina. Methods Enzymol. 213, 360–366. https://doi.org/10.1016/0076-6879(92)13137-m.

Bone, R.A., Landrum, J.T., 1984. Macular pigment in Henle fiber membranes: a model for Haidinger's brushes. Vis. Res. 24, 103–108. https://doi.org/10.1016/0042-6989(84)90094-4.

Bone, R.A., Landrum, J.T., 1983. Dichroism of lutein: a possible basis for Haidinger's brushes. Appl. Opt. 22, 775–776. https://doi.org/10.1364/ao.22.000775.

Bone, R.A., Landrum, J.T., Cains, A., 1992. Optical density spectra of the macular pigment in vivo and in vitro. Vis. Res. 32, 105–110. https://doi.org/10.1016/0042-6989(92)90118-3.

Bone, R.A., Landrum, J.T., Fernandez, L., Tarsis, S.L., 1988. Analysis of the macular pigment by HPLC: retinal distribution and age study. Invest. Ophthalmol. Vis. Sci. 29, 843–849.

Bone, R.A., Landrum, J.T., Friedes, L.M., Gomez, C.M., Kilburn, M.D., Menendez, E., Vidal, I., Wang, W., 1997. Distribution of lutein and zeaxanthin stereoisomers in the human retina. Exp. Eye Res. 64, 211–218. https://doi.org/10.1006/exer.1996.0210.

Bonnin, S., Mané, V., Couturier, A., Julien, M., Paques, M., Tadayoni, R., Gaudric, A., 2015. New insight into the macular deep vascular plexus imaged by optical coherence tomography angiography. Retina 35, 2347–2352. https://doi.org/10.1097/IAE.0000000000000839.

Borruat, F.X., Piguet, B., Herbort, C.P., 1998. Acute posterior multifocal placoid pigment epitheliopathy following mumps. Ocul. Immunol. Inflamm. 6, 189–193. https://doi.org/10.1076/ocii.6.3.189.4038.

Bos, P.J.M., Deutman, A.F., 1975. Acute macular neuroretinopathy. Am. J. Ophthalmol. 80, 573–584. https://doi.org/10.1016/0002-9394(75)90387-6.

Boss, J.D., Tosi, J., Glybina, I., Tewari, A., Abrams, G.W., 2017. Functional and morphological evaluation of traumatized eyes with berlin's edema affecting the macula using mfERG, microperimetry, and SD-OCT. Ophthalm. Surg. Lasers Imag. Retin. 48, 114–121. https://doi.org/10.3928/23258160-20170130-04.

Bridges, W.J., Saadeh, C., Gerald, R., 1995. Acute posterior multifocal placoid pigment epitheliopathy in a patient with systemic-onset juvenile rheumatoid arthritis: treatment with cyclosporin A and prednisone. Arthritis Rheum. 38, 446–447. https://doi.org/10.1002/art.1780380328.

Bringmann, A., Barth, T., Ziemssen, F., 2022a. Morphology of foveal hypoplasia: hyporeflective zones in the Henle fiber layer of eyes with high-grade foveal hypoplasia. PLoS One 17, e0266968. https://doi.org/10.1371/journal.pone.0266968.

Bringmann, A., Pannicke, T., Grosche, J., Francke, M., Wiedemann, P., Skatchkov, S.N., Osborne, N.N., Reichenbach, A., 2006. Müller cells in the healthy and diseased retina. Prog. Retin. Eye Res. 25, 397–424. https://doi.org/10.1016/j.preteyeres.2006.05.003.

Bringmann, A., Syrbe, S., Görner, K., Kacza, J., Francke, M., Wiedemann, P., Reichenbach, A., 2018. The primate fovea: structure, function and development. Prog. Retin. Eye Res. 66, 49–84. https://doi.org/10.1016/j.preteyeres.2018.03.006.

Bringmann, A., Unterlauft, J.D., Barth, T., Wiedemann, R., Rehak, M., Wiedemann, P., 2022b. Müller cells and astrocytes in tractional macular disorders. Prog. Retin. Eye Res. 86, 100977 https://doi.org/10.1016/j.preteyeres.2021.100977.

Bringmann, A., Unterlauft, J.D., Wiedemann, R., Barth, T., Rehak, M., Wiedemann, P., 2020. Two different populations of Müller cells stabilize the structure of the fovea: an optical coherence tomography study. Int. Ophthalmol. 40, 2931–2948. https://doi.org/10.1007/s10792-020-01477-3.

Brink, H.B., klein, Blokland, van, G.J., 1988. Birefringence of the human foveal area assessed in vivo with Mueller-matrix ellipsometry. J. Opt. Soc. Am. A 5, 49–57. https://doi.org/10.1364/JOSAA.5.000049.

Brinkmann, M., Bacci, T., Kar, D., Messinger, J.D., Sloan, K.R., Chen, L., Hamann, T., Wiest, M., Freund, K.B., Zweifel, S., Curcio, C.A., 2022. Histology and clinical lifecycle of acquired vitelliform lesion, a pathway to advanced age-related macular degeneration. Am. J. Ophthalmol. https://doi.org/10.1016/j.ajo.2022.02.006. S0002-9394(22)00062–9.

Britton, G., 1995. Structure and properties of carotenoids in relation to function. Faseb. J. 9, 1551–1558.

Burke, T.R., Chu, C.J., Salvatore, S., Bailey, C., Dick, A.D., Lee, R.W.J., Ross, A.H., Carreño, E., Medscape, 2017. Application of OCT-angiography to characterise the evolution of chorioretinal lesions in acute posterior multifocal placoid pigment epitheliopathy. Eye 31, 1399–1408. https://doi.org/10.1038/eye.2017.180.

Cabral, D., Fradinho, A.C., Pereira, T., Ramakrishnan, M.S., Bacci, T., An, D., Tenreiro, S., Seabra, M.C., Balaratnasingam, C., Freund, K.B., 2022. Macular vascular imaging and connectivity analysis using high-resolution optical coherence tomography. Transl. Vis. Sci. Technol. 11, 2. https://doi.org/10.1167/tvst.11.6.2.

Cabral, D., Pereira, T., Ledesma-Gil, G., Rodrigues, C., Coscas, F., Sarraf, D., Freund, K.B., 2020. Volume rendering of dense B-scan optical coherence tomography angiography to evaluate the connectivity of macular blood flow. Invest. Ophthalmol. Vis. Sci. 61, 44. https://doi.org/10.1167/iovs.61.6.44.

Cao, D., Leong, B., Messinger, J.D., Kar, D., Ach, T., Yannuzzi, L.A., Freund, K.B., Curcio, C.A., 2021. Hyperreflective foci, optical coherence tomography progression indicators in age-related macular degeneration, include transdifferentiated retinal pigment epithelium. Invest. Ophthalmol. Vis. Sci. 62, 34. https://doi.org/10.1167/iovs.62.10.34.

Cappello, E., Della Guardia, C., Cecchin, E., Morselli, S., 2021. Spectral domain optical coherence tomography findings in a case of whiplash maculopathy with incomplete resolution. Retin. Cases Brief Rep. 15, 421–425. https://doi.org/10.1097/ICB.0000000000000805.

Carr, J.M., Ashander, L.M., Calvert, J.K., Ma, Y., Aloia, A., Bracho, G.G., Chee, S.-P., Appukuttan, B., Smith, J.R., 2017. Molecular responses of human retinal cells to infection with dengue virus. Mediators Inflamm., 3164375 https://doi.org/10.1155/2017/3164375.

Carroll, W.J., Maganti, N., Gill, M.K., 2020. Hypoperfusion of the deep capillary plexus associated with acute on chronic cocaine use. Am. J. Ophthalmol. Case Rep. 18, 100684 https://doi.org/10.1016/j.ajoc.2020.100684.

Casalino, G., Arrigo, A., Romano, F., Munk, M.R., Bandello, F., Parodi, M.B., 2019. Acute macular neuroretinopathy: pathogenetic insights from optical coherence tomography angiography. Br. J. Ophthalmol. 103, 410–414. https://doi.org/10.1136/bjophthalmol-2018-312197.

Case, D., Seinfeld, J., Kumpe, D., Folzenlogen, Z., Jones, W., Simpson, J., Hughes, R., 2015. Acute Posterior Multifocal Placoid Pigment Epitheliopathy Associated with Stroke: A Case Report and Review of the Literature. J. Stroke Cerebrovasc. Dis. 24, e295-302 https://doi.org/10.1016/j.jstrokecerebrovasdis.2015.06.022.

Castro, P., Costa, A., Abreu, P., Penas, S., Faria, O., Azevedo, E., 2016. Acute posterior multifocal placoid pigment epitheliopathy presenting with multiple brain and spinal cord infarctions. J. Neurol. Sci. 361, 26–28. https://doi.org/10.1016/j.jns.2015.12.015.

Cense, B., Wang, Q., Lee, S., Zhao, L., Elsner, A.E., Hitzenberger, C.K., Miller, D.T., 2013. Henle fiber layer phase retardation measured with polarization-sensitive optical coherence tomography. Biomed. Opt Express 4, 2296. https://doi.org/10.1364/BOE.4.002296.

Chanthick, C., Suttitheptumrong, A., Rawarak, N., Pattanakitsakul, S.-N., 2018. Transcytosis involvement in transport system and endothelial permeability of vascular leakage during dengue virus infection. Viruses 10, E69. https://doi.org/10.3390/v10020069.

Chen, F.K., Chew, A.L., Zhang, D., Chen, S.-C., Chelva, E., Chandrasekera, E., Koay, E.M. H., Forrester, J., McLenachan, S., 2017. Acute progressive paravascular placoid neuroretinopathy with negative-type electroretinography in paraneoplastic retinopathy. Doc. Ophthalmol. 134, 227–235. https://doi.org/10.1007/s10633-017-9587-9.

Chen, K.C., Jung, J.J., Curcio, C.A., Balaratnasingam, C., Gallego-Pinazo, R., Dolz-Marco, R., Freund, K.B., Yannuzzi, L.A., 2016. Intraretinal hyperreflective foci in acquired vitelliform lesions of the macula: clinical and histologic study. Am. J. Ophthalmol. 164, 89–98. https://doi.org/10.1016/j.ajo.2016.02.002.

Chen, Q., Feng, C., Sun, C., Wang, W., Wang, M., Chen, L., Sun, X., Tian, G., 2022. Cancer-associated retinopathy after anti-programmed death 1 (PD-1) antibody for treating hepatocellular carcinoma–a case report of a Chinese patient. Am. J. Ophthalmol. Case Rep. 25, 101370 https://doi.org/10.1016/j.ajoc.2022.101370.

Chen, X., Dajani, O.A.W., Alibhai, A.Y., Duker, J.S., Baumal, C.R., 2021. LONG-TERM visual recovery in bilateral handheld laser pointer-induced maculopathy. Retin. Cases Brief Rep. 15, 536–539. https://doi.org/10.1097/ICB.0000000000000845.

Chinskey, N.D., Rahimy, E., Johnson, M.W., 2015. Acute macular neuroretinopathy following non-ocular trauma: a hypothesis regarding pathophysiologic mechanism. Ophthalm. Surg. Lasers Imag. Retin. 46, 1013–1020. https://doi.org/10.3928/23258160-20151027-05.

Chiquet, C., Lumbroso, L., Denis, P., Papo, T., Durieu, I., Lehoang, P., 1999. Acute posterior multifocal placoid pigment epitheliopathy associated with Wegener's granulomatosis. Retina 19, 309–313. https://doi.org/10.1097/00006982-199907000-00007.

Cho, H.J., Han, S.Y., Cho, S.W., Lee, D.W., Lee, T.G., Kim, C.G., Kim, J.W., 2014. Acute retinal pigment epitheliitis: spectral-domain optical coherence tomography findings in 18 cases. Invest. Ophthalmol. Vis. Sci. 55, 3314–3319. https://doi.org/10.1167/iovs.14-14324.

Cho, H.J., Lee, D.W., Kim, C.G., Kim, J.W., 2011. Spectral domain optical coherence tomography findings in acute retinal pigment epitheliitis. Can. J. Ophthalmol. 46, 498–500. https://doi.org/10.1016/j.jcjo.2011.09.012.

Cho, J.W., Sung, K.R., Lee, S., Yun, S.-C., Kang, S.Y., Choi, J., Na, J.H., Lee, Y., Kook, M. S., 2010. Relationship between visual field sensitivity and macular ganglion cell complex thickness as measured by spectral-domain optical coherence tomography. Invest. Ophthalmol. Vis. Sci. 51, 6401–6407. https://doi.org/10.1167/iovs.09-5035.

Christenbury, J.G., Folgar, F.A., O'Connell, R.V., Chiu, S.J., Farsiu, S., Toth, C.A., 2013. Progression of intermediate age-related macular degeneration with proliferation and inner retinal migration of hyperreflective foci. Ophthalmology 120, 1038–1045. https://doi.org/10.1016/j.ophtha.2012.10.018.

Chronopoulos, A., Lipski, A., Jonescu-Cuypers, C.-P., Thumann, G., 2014. Unusual bilateral traumatic maculopathy following whiplash injury. BMJ Case Rep 2014, bcr2014208068. https://doi.org/10.1136/bcr-2014-208068.

Chu, S., Nesper, P.L., Soetikno, B.T., Bakri, S.J., Fawzi, A.A., 2018. Projection-resolved OCT angiography of microvascular changes in paracentral acute middle maculopathy and acute macular neuroretinopathy. Invest. Opthalmol. Vis. Sci. 59, 2913. https://doi.org/10.1167/iovs.18-24112.

Cleary, M., Thompson, C.M., 2001. Diagnosis of eccentric fixation using a calibrated ophthalmoscope: defining clinically significant limits. Ophthalmic Physiol. Opt. 21, 461–469. https://doi.org/10.1046/j.1475-1313.2001.00613.x.

Colucciello, M., 2022. Acute retinal pigment epitheliitis: association with acute coxsackie A virus infection. Retin. Cases Brief Rep. https://doi.org/10.1097/ICB.0000000000001234.

Cornish, K.S., Reddy, A.R., McBain, V.A., 2014. Concentric macular rings sign in patients with foveal hypoplasia. JAMA Ophthalmol. 132, 1084. https://doi.org/10.1001/jamaophthalmol.2014.1715.

Cringle, S.J., Yu, D.-Y., 2002. A multi-layer model of retinal oxygen supply and consumption helps explain the muted rise in inner retinal PO(2) during systemic hyperoxia. Comp. Biochem. Physiol. Mol. Integr. Physiol. 132, 61–66. https://doi.org/10.1016/s1095-6433(01)00530-x.

Cringle, S.J., Yu, D.Y., Alder, V.A., 1991. Intraretinal oxygen tension in the rat eye. Graefes Arch. Clin. Exp. Ophthalmol. 229, 574–577. https://doi.org/10.1007/BF00203324.

Cringle, S.J., Yu, D.-Y., Yu, P.K., Su, E.-N., 2002. Intraretinal oxygen consumption in the rat in vivo. Invest. Ophthalmol. Vis. Sci. 43, 1922–1927.

Cuenca, N., Ortuño-Lizarán, I., Sánchez-Sáez, X., Kutsyr, O., Albertos-Arranz, H., Fernández-Sánchez, L., Martínez-Gil, N., Noailles, A., López-Garrido, J.A., López-Gálvez, M., Lax, P., Maneu, V., Pinilla, I., 2020. Interpretation of OCT and OCTA images from a histological approach: clinical and experimental implications. Prog. Retin. Eye Res. 77, 100828 https://doi.org/10.1016/j.preteyeres.2019.100828.

Curcio, C.A., Allen, K.A., 1990. Topography of ganglion cells in human retina. J. Comp. Neurol. 300, 5–25. https://doi.org/10.1002/cne.903000103.

Curcio, C.A., Messinger, J.D., Sloan, K.R., Mitra, A., McGwin, G., Spaide, R.F., 2011. Human chorioretinal layer thicknesses measured in macula-wide, high-resolution histologic sections. Invest. Ophthalmol. Vis. Sci. 52, 3943. https://doi.org/10.1167/iovs.10-6377.

Curcio, C.A., Sloan, K.R., Packer, O., Hendrickson, A.E., Kalina, R.E., 1987. Distribution of cones in human and monkey retina: individual variability and radial asymmetry. Science 236, 579–582. https://doi.org/10.1126/science.3576186.

Darugar, A., Mathian, A., LeHoang, P., Bodaghi, B., 2011. Acute posterior multifocal placoid pigment epitheliopathy as the initial manifestation of sarcoidosis. J. Ophthalmic Vis. Res. 6, 338–343.

Davenport, R.C., 1960. The eye and vision. Nature 186, 42–43. https://doi.org/10.1038/186042b0.

David, J.A., Fivgas, G.D., 2021. Acute macular neuroretinopathy associated with COVID-19 infection. Am. J. Ophthalmol. Case Rep. 24, 101232 https://doi.org/10.1016/j.ajoc.2021.101232.

De Bats, F., Wolff, B., Mauget-Faÿsse, M., Scemama, C., Kodjikian, L., 2013. B-scan and "en-face" spectral-domain optical coherence tomography imaging for the diagnosis and followup of acute retinal pigment epitheliitis. Case Rep. Med., 260237 https://doi.org/10.1155/2013/260237.

Deák, G.G., Bolz, M., Prager, S., Ritter, M., Kriechbaum, K., Scholda, C., Schmidt-Erfurth, U., 2012. Diabetic retinopathy research group vienna Photoreceptor layer regeneration is detectable in the human retina imaged by SD-OCT after laser treatment using subthreshold laser power. Invest. Ophthalmol. Vis. Sci. 53, 7019–7025. https://doi.org/10.1167/iovs.12-10196.

Deák, G.G., Goldstein, D.A., Zhou, M., Fawzi, A.A., Jampol, L.M., 2019. Vertical hyperreflective lesions on optical coherence tomography in vitreoretinal lymphoma. JAMA Ophthalmol. 137, 194–198. https://doi.org/10.1001/jamaophthalmol.2018.5835.

Degli Esposti, S., Rashad, M., Robertson, M., Riga, V., Singh, N., Moosajee, M., Michaelides, M., Webster, A.R., Mahroo, O.A., 2020. Comparison of white light and scanning laser ophthalmoscopy ultra-widefield pseudocolor reflectance images in foveal hypoplasia. Investig. Ophthalmol. Vis. Sci. 61, 5304.

Denniss, J., Turpin, A., McKendrick, A.M., 2019. Relating optical coherence tomography to visual fields in glaucoma: structure-function mapping, limitations and future applications. Clin. Exp. Optom. 102, 291–299. https://doi.org/10.1111/cxo.12844.

Deutman, A.F., Oosterhuis, J.A., Boen-Tan, T.N., Aan de Kerk, A.L., 1972. Acute posterior multifocal placoid pigment epitheliopathy. Pigment epitheliopathy of choriocapillaritis? Br. J. Ophthalmol. 56, 863–874. https://doi.org/10.1136/bjo.56.12.863.

Dhaliwal, R.S., Maguire, A.M., Flower, R.W., Arribas, N.P., 1993. Acute posterior multifocal placoid pigment epitheliopathy. An indocyanine green angiographic study. Retina 13, 317–325. https://doi.org/10.1097/00006982-199313040-00009.

Dhrami-Gavazi, E., Lee, W., Balaratnasingam, C., Kayserman, L., Yannuzzi, L.A., Freund, K.B., 2015. Multimodal imaging documentation of rapid evolution of retinal changes in handheld laser-induced maculopathy. Int. J. Retin. Vitr. 1, 14. https://doi.org/10.1186/s40942-015-0014-7.

Di Crecchio, L., Parodi, M.B., Saviano, S., Ravalico, G., 2001. Acute posterior multifocal placoid pigment epitheliopathy and ulcerative colitis: a possible association. Acta Ophthalmol. Scand. 79, 319–321. https://doi.org/10.1034/j.1600-0420.2001.790324.x.

Dolz-Marco, R., Kalevar, A., McDonald, H.R., Cunningham, E.T., Freund, K.B., 2021. Foveal outer retinal hyperreflectivity: a novel optical coherence tomography finding in idiopathic multifocal choroiditis. Retin. Cases Brief Rep. 15, 651–656. https://doi.org/10.1097/ICB.0000000000000878.

Dolz-Marco, R., Sarraf, D., Giovinazzo, V., Freund, K.B., 2017. Optical coherence tomography angiography SHOWS inner choroidal ischemia in acute posterior multifocal placoid pigment epitheliopathy. Retin. Cases Brief Rep. 11 (Suppl. 1), S136–S143. https://doi.org/10.1097/ICB.0000000000000473.

Drasdo, N., Millican, C.L., Katholi, C.R., Curcio, C.A., 2007. The length of Henle fibers in the human retina and a model of ganglion receptive field density in the visual field. Vis. Res. 47, 2901–2911. https://doi.org/10.1016/j.visres.2007.01.007.

Dreyer, R.F., Hopen, G., Gass, J.D., Smith, J.L., 1984. Leber's idiopathic stellate neuroretinitis. Arch. Ophthalmol. 102, 1140–1145. https://doi.org/10.1001/archopht.1984.01040030918013.

Dubis, A.M., Costakos, D.M., Subramaniam, C.D., Godara, P., Wirostko, W.J., Carroll, J., Provis, J.M., 2012. Evaluation of normal human foveal development using optical coherence tomography and histologic examination. Arch. Ophthalmol. 130, 1291. https://doi.org/10.1001/archophthalmol.2012.2270.

Duke-Elder, W.S., 1941. Text-Book of Ophthalmology, vol. III. CV Mosby Company, St. Louis, p. 2765.

Edge, R., McGarvey, D.J., Truscott, T.G., 1997. The carotenoids as anti-oxidants–a review. J. Photochem. Photobiol., B 41, 189–200. https://doi.org/10.1016/s1011-1344(97)00092-4.

El Sanhouri, A., Sisk, R.A., Petersen, M.R., 2012. Mortality from cerebral vasculitis associated with rapid steroid taper during treatment of acute posterior multifocal placoid pigment epitheliopathy. Arch. Ophthalmol. 130, 935–937. https://doi.org/10.1001/archophthalmol.2011.2522.

El-Markaby, H.S., Mohammed, T.H., El-Raggal, T.M., 2012. Acute posterior multifocal placoid pigment epitheliopathy: role of TNF blocker in severe cases. Retina 32, 2102–2107. https://doi.org/10.1097/IAE.0b013e31825620d6.

Elsner, A.E., Weber, A., Cheney, M.C., Vannasdale, D.A., 2008. Spatial distribution of macular birefringence associated with the Henle fibers. Vis. Res. 48, 2578–2585. https://doi.org/10.1016/j.visres.2008.04.031.

Elsner, A.E., Weber, A., Cheney, M.C., VanNasdale, D.A., Miura, M., 2007. Imaging polarimetry in patients with neovascular age-related macular degeneration. J. Opt. Soc. Am. Opt Image Sci. Vis. 24, 1468–1480. https://doi.org/10.1364/josaa.24.001468.

Elwyn, H., 1946. Diseases of the retina. Acad. Med. 21, 318.

Emens, L.A., Davis, S.L., Oliver, S.C.N., Lieu, C.H., Reddy, A., Solomon, S., He, L., Morley, R., Fassò, M., Pirzkall, A., Patel, H., O'Hear, C., Ferrara, D., 2019. Association of cancer immunotherapy with acute macular neuroretinopathy and diffuse retinal venulitis. JAMA Ophthalmol. 137, 96. https://doi.org/10.1001/jamaophthalmol.2018.5191.

Fang, P.P., Pfau, M., Holz, F.G., Finger, R.P., 2017. Persistent visual loss in dengue fever due to outer retinal damage. Clin. Exp. Ophthalmol. 45, 747–749. https://doi.org/10.1111/ceo.12960.

Fawzi, A.A., Pappuru, R.R., Sarraf, D., Le, P.P., McCannel, C.A., Sobrin, L., Goldstein, D. A., Honowitz, S., Walsh, A.C., Sadda, S.R., Jampol, L.M., Eliott, D., 2012. Acute macular neuroretinopathy: long-term insights revealed by multimodal imaging. Retina 32, 1500–1513. https://doi.org/10.1097/IAE.0b013e318263d0c3.

Fekrat, S., Wilkinson, C.P., Chang, B., Yannuzzi, L., Schatz, H., Haller, J.A., 2000. Acute annular outer retinopathy: report of four cases. Am. J. Ophthalmol. 130, 636–644. https://doi.org/10.1016/s0002-9394(00)00560-2.

Fine, B.S., Yanoff, M., 1979. Ocular Histology: A Text and Atlas. Medical Department, Harper & Row.

Finlay, B.L., Franco, E.C.S., Yamada, E.S., Crowley, J.C., Parsons, M., Muniz, J.A.P.C., Silveira, L.C.L., 2008. Number and topography of cones, rods and optic nerve axons in New and Old World primates. Vis. Neurosci. 25, 289–299. https://doi.org/10.1017/S0952523808080371.

Fogel Levin, M., Wong, A., Sarraf, D., 2022. Choroidal ischemia drives macular neovascularization in persistent placoid maculopathy. Am. J. Ophthalmol. Case Rep. 26, 101563 https://doi.org/10.1016/j.ajoc.2022.101563.

Fouquet, S., Vacca, O., Sennlaub, F., Paques, M., 2017. The 3D retinal capillary circulation in pigs reveals a predominant serial organization. Invest. Ophthalmol. Vis. Sci. 58, 5754–5763. https://doi.org/10.1167/iovs.17-22097.

Fragiotta, S., Leong, B.C.S., Kaden, T.R., Bass, S.J., Sherman, J., Yannuzzi, L.A., Freund, K.B., 2019. A proposed mechanism influencing structural patterns in X-linked retinoschisis and stellate nonhereditary idiopathic foveomacular retinoschisis. Eye 33, 724–728. https://doi.org/10.1038/s41433-018-0296-8.

Franze, K., Grosche, J., Skatchkov, S.N., Schinkinger, S., Foja, C., Schild, D., Uckermann, O., Travis, K., Reichenbach, A., Guck, J., 2007. Müller cells are living optical fibers in the vertebrate retina. Proc. Natl. Acad. Sci. U. S. A. 104, 8287–8292. https://doi.org/10.1073/pnas.0611180104.

Freund, K.B., Sarraf, D., Leong, B.C.S., Garrity, S.T., Vupparaboina, K.K., Dansingani, K. K., 2018. Association of optical coherence tomography angiography of collaterals in retinal vein occlusion with major venous outflow through the deep vascular complex. JAMA Ophthalmol. 136, 1262–1270. https://doi.org/10.1001/jamaophthalmol.2018.3586.

Friedenwald, J.S., 1952. An Atlas and Textbook of Ophthalmic Pathology.

Furashova, O., Matthé, E., 2020. Foveal crack sign as a predictive biomarker for development of macular hole in fellow eyes of patients with full-thickness macular holes. Sci. Rep. 10, 19932 https://doi.org/10.1038/s41598-020-77078-y.

Gao, W., Cense, B., Zhang, Y., Jonnal, R.S., Miller, D.T., 2008. Measuring retinal contributions to the optical Stiles-Crawford effect with optical coherence tomography. Opt Express 16, 6486–6501. https://doi.org/10.1364/OE.16.006486.

Garrity, S.T., Paques, M., Gaudric, A., Freund, K.B., Sarraf, D., 2017. Considerations in the understanding of venous outflow in the retinal capillary plexus. Retina 37, 1809–1812. https://doi.org/10.1097/IAE.0000000000001784.

Gass, J.D., 1977. Diseases of the optic nerve that may simulate macular disease. Trans. Sect. Ophthalmol. Am. Acad. Ophtalmol. Otolaryngol. 83, 763–770.

Gass, J.D., 1968. Acute posterior multifocal placoid pigment epitheliopathy. Arch. Ophthalmol. 80, 177–185. https://doi.org/10.1001/archopht.1968.00980050179005.

Gass, J.D., Stern, C., 1995. Acute annular outer retinopathy as a variant of acute zonal occult outer retinopathy. Am. J. Ophthalmol. 119, 330–334. https://doi.org/10.1016/s0002-9394(14)71176-6.

Gaudric, A., Audo, I., Vignal, C., Couturier, A., Boulanger-Scemama, É., Tadayoni, R., Cohen, S.Y., 2022. Non-vasogenic cystoid maculopathies. Prog. Retin. Eye Res. 101092 https://doi.org/10.1016/j.preteyeres.2022.101092.

Georgakopoulos, C.D., Antonopoulos, I., Makri, O.E., Vasilakis, P., Liossis, S.-N.C., Andonopoulos, A.P., 2016. Acute posterior multifocal placoid pigment epitheliopathy in a patient with familial Mediterranean fever. Clin. Exp. Optom. 99, 385–387. https://doi.org/10.1111/cxo.12401.

Gibelalde, A., Bidaguren, A., Ostolaza, J.I., Cortázar, L., Irigoyen, C., 2009. [Pigmentary epitheliopathy multifocal acute placoid associated with paralysis of VI cranial par]. Arch. Soc. Esp. Oftalmol. 84, 159–162. https://doi.org/10.4321/s0365-66912009000300010.

Goldenberg, D., Habot-Wilner, Z., Loewenstein, A., Goldstein, M., 2012. Spectral domain optical coherence tomography classification of acute posterior multifocal placoid. Pigment Epitheliopath.: Retina 32, 1403–1410. https://doi.org/10.1097/IAE.0b013e318234cafc.

Goldhardt, R., Patel, H., Davis, J.L., 2016. Acute posterior multifocal placoid pigment epitheliopathy following dengue fever: a new association for an old disease. Ocul. Immunol. Inflamm. 24, 610–614. https://doi.org/10.3109/09273948.2015.1125513.

Gong, D., Zou, X., Zhang, X., Yu, W., Qu, Y., Dong, F., 2016. The influence of age and central foveal thickness on foveal zone size in healthy people. Ophthalm. Surg. Lasers Imag. Retin. 47, 142–148. https://doi.org/10.3928/23258160-20160126-07.

Gramatikov, B.I., 2017. Detecting central fixation by means of artificial neural networks in a pediatric vision screener using retinal birefringence scanning. Biomed. Eng. Online 16, 52. https://doi.org/10.1186/s12938-017-0339-6.

Gramatikov, B.I., Zalloum, O.H.Y., Wu, Y.K., Hunter, D.G., Guyton, D.L., 2007. Directional eye fixation sensor using birefringence-based foveal detection. Appl. Opt. 46, 1809–1818. https://doi.org/10.1364/ao.46.001809.

Gramatikov, B.I., Zalloum, O.H.Y., Wu, Y.K., Hunter, D.G., Guyton, D.L., 2006. Birefringence-based eye fixation monitor with no moving parts. J. Biomed. Opt. 11, 34025 https://doi.org/10.1117/1.2209003.

Greenfield, D.S., Bagga, H., Knighton, R.W., 2003. Macular thickness changes in glaucomatous optic neuropathy detected using optical coherence tomography. Arch. Ophthalmol. 121, 41–46. https://doi.org/10.1001/archopht.121.1.41.

Griffin, S.M., McDonald, H.R., Johnson, R.N., Jumper, J.M., Fu, A.D., Cunningham, E.T., Kiang, L., Ng, C.C., Lujan, B.J., 2021. Fingerprint sign of the henle fiber layer. Retina 41, 381–386. https://doi.org/10.1097/IAE.0000000000002875.

Guardiola, G.A., Villegas, V.M., Cruz-Villegas, V., Schwartz, S.G., 2022. Acute macular neuroretinopathy in dengue virus serotype 1. Am. J. Ophthalmol. Case Rep. 25, 101250 https://doi.org/10.1016/j.ajoc.2021.101250.

Haidinger, W., 1844. Ueber das directe Erkennen des polarisirten Lichts und der Lage der Polarisationsebene. Ann. Phys. 139, 29–39. https://doi.org/10.1002/andp.18441390903.

Hall, E.F., Ahmad, B., Schachat, A.P., 2012. Spectral-domain optical coherence tomography findings in acute retinal pigment epitheliitis. Retin. Cases Brief Rep. 6, 309–312. https://doi.org/10.1097/ICB.0b013e3182378bd7.

Hammer, M.E., Grizzard, W.S., Travies, D., 1989. Death associated with acute, multifocal, placoid pigment epitheliopathy. Case report. Arch. Ophthalmol. 107, 170–171. https://doi.org/10.1001/archopht.1989.01070010176014.

Hammond, B.R., Fletcher, L.M., Roos, F., Wittwer, J., Schalch, W., 2014. A double-blind, placebo-controlled study on the effects of lutein and zeaxanthin on photostress recovery, glare disability, and chromatic contrast. Invest. Ophthalmol. Vis. Sci. 55, 8583–8589. https://doi.org/10.1167/iovs.14-15573.

Han, D.P., Croskrey, J.A., Dubis, A.M., Schroeder, B., Rha, J., Carroll, J., 2012. Adaptive optics and spectral- domain optical coherence tomography of human photoreceptor structure after short-duration [corrected] pascal macular grid and panretinal laser photocoagulation. Arch. Ophthalmol. 130, 518–521. https://doi.org/10.1001/archophthalmol.2011.2878.

Hardarson, S.H., 2013. Retinal oximetry. Acta Ophthalmol. 91, 1–47. https://doi.org/10.1111/aos.12086. Thesis 2.

Harino, S., Nagaya, C., Matsuda, S., Iwahashi, Y., Uyama, M., Cekiç, O., Hashimoto, M., 2004. Indocyanine green angiographic findings in a case of acute annular outer retinopathy. Retina 24, 796–799. https://doi.org/10.1097/00006982-200410000-00018.

Hart, J.C., Blight, R., 1979. Commotio retinae. Arch. Ophthalmol. 97, 1738. https://doi.org/10.1001/archopht.1979.01020020296025.

Haugh, L.M., Linsenmeier, R.A., Goldstick, T.K., 1990. Mathematical models of the spatial distribution of retinal oxygen tension and consumption, including changes upon illumination. Ann. Biomed. Eng. 18, 19–36. https://doi.org/10.1007/BF02368415.

He, Y., Chen, X., Tsui, I., Vajzovic, L., Sadda, S.R., 2022. Insights into the developing fovea revealed by imaging. Prog. Retin. Eye Res. 90, 101067 https://doi.org/10.1016/j.preteyeres.2022.101067.

Hemenger, R.P., 1982. Dichroism of the macular pigment and Haidinger's brushes. J. Opt. Soc. Am. 72, 734–737. https://doi.org/10.1364/josa.72.000734.

Hendrickson, A., 2016. Development of retinal layers in prenatal human retina. Am. J. Ophthalmol. 161, 29–35. https://doi.org/10.1016/j.ajo.2015.09.023 e1.

Hendrickson, A., 2005. Organization of the adult primate fovea. In: Penfold, P.L., Provis, J.M. (Eds.), Macular Degeneration. Springer, Berlin, Heidelberg, pp. 1–23. https://doi.org/10.1007/3-540-26977-0_1.

Hendrickson, A., Possin, D., Vajzovic, L., Toth, C.A., 2012. Histologic development of the human fovea from midgestation to maturity. Am. J. Ophthalmol. 154, 767–778. https://doi.org/10.1016/j.ajo.2012.05.007 e2.

Hendrickson, A.E., Yuodelis, C., 1984. The morphological development of the human fovea. Ophthalmology 91, 603–612. https://doi.org/10.1016/s0161-6420(84)34247-6.

Hilely, A., Au, A., Freund, K.B., Loewenstein, A., Souied, E.H., Zur, D., Sacconi, R., Borrelli, E., Peiretti, E., Iovino, C., Sugiura, Y., Ellabban, A.A., Monés, J., Waheed, N. K., Ozdek, S., Yalinbas, D., Thiele, S., de Moura Mendonça, L.S., Lee, M.Y., Lee, W.K., Turcotte, P., Capuano, V., Filali Ansary, M., Chakravarthy, U., Lommatzsch, A., Gunnemann, F., Pauleikhoff, D., Ip, M.S., Querques, G., Holz, F.G., Spaide, R.F., Sadda, S., Sarraf, D., 2021. Non-neovascular age-related macular degeneration with subretinal fluid. Br. J. Ophthalmol. 105, 1415–1420. https://doi.org/10.1136/bjophthalmol-2020-317326.

Hogan, M.J., Feeney, L., 1963. The ultrastructure of the retinal vessels: III. Vascular-Glial relationships. J. Ultra. Res. 9, 47–64.

Holt, W.S., Regan, C.D., Trempe, C., 1976. Acute posterior multifocal placoid pigment epitheliopathy. Am. J. Ophthalmol. 81, 403–412. https://doi.org/10.1016/0002-9394(76)90294-4.

Hood, D.C., 2017. Improving our understanding, and detection, of glaucomatous damage: an approach based upon optical coherence tomography (OCT). Prog. Retin. Eye Res. 57, 46–75. https://doi.org/10.1016/j.preteyeres.2016.12.002.

Hood, D.C., Anderson, S.C., Wall, M., Kardon, R.H., 2007. Structure versus function in glaucoma: an application of a linear model. Invest. Ophthalmol. Vis. Sci. 48, 3662–3668. https://doi.org/10.1167/iovs.06-1401.

Hood, D.C., Kardon, R.H., 2007. A framework for comparing structural and functional measures of glaucomatous damage. Prog. Retin. Eye Res. 26, 688–710. https://doi.org/10.1016/j.preteyeres.2007.08.001.

Howe, L.J., Woon, H., Graham, E.M., Fitzke, F., Bhandari, A., Marshall, J., 1995. Choroidal hypoperfusion in acute posterior multifocal placoid pigment epitheliopathy. An indocyanine green angiography study. Ophthalmology 102, 790–798. https://doi.org/10.1016/s0161-6420(95)30955-4.

Hsu, C.T., Harlan, J.B., Goldberg, M.F., Dunn, J.P., 2003. Acute posterior multifocal placoid pigment epitheliopathy associated with a systemic necrotizing vasculitis. Retina 23, 64–68. https://doi.org/10.1097/00006982-200302000-00010.

Hsu, J., Fineman, M.S., Kaiser, R.S., 2007. Optical coherence tomography findings in acute retinal pigment epitheliitis. Am. J. Ophthalmol. 143, 163–165. https://doi.org/10.1016/j.ajo.2006.07.052.

Hunter, D.G., Patel, S.N., Guyton, D.L., 1999. Automated detection of foveal fixation by use of retinal birefringence scanning. Appl. Opt. 38, 1273. https://doi.org/10.1364/AO.38.001273.

Invernizzi, A., Agarwal, A., Ravera, V., Oldani, M., Staurenghi, G., Viola, F., 2018. Optical coherence tomography findings in cytomegalovirus retinitis: a longitudinal study. Retina 38, 108–117. https://doi.org/10.1097/IAE.0000000000001503.

Iovino, C., Au, A., Ramtohul, P., Bacci, T., AlBahlal, A., Khan, A.M., Al-Abdullah, A.A., Wendel, R., Chhablani, J., Sadda, S., Freund, K.B., Sarraf, D., 2021. Coincident PAMM and AMN and insights into a common pathophysiology. Am. J. Ophthalmol. 236, 136–146. https://doi.org/10.1016/j.ajo.2021.07.004.

Irsch, K., Gramatikov, B.I., Wu, Y.-K., Guyton, D.L., 2014. Improved eye-fixation detection using polarization-modulated retinal birefringence scanning, immune to corneal birefringence. Opt Express 22, 7972–7988. https://doi.org/10.1364/OE.22.007972.

Isenberg, S.J., 1986. Macular development in the premature infant. Am. J. Ophthalmol. 101, 74–80. https://doi.org/10.1016/0002-9394(86)90467-8.

Ishibashi, T., Iwama, Y., Nakashima, H., Ikeda, T., Emi, K., 2020. Foveal crack sign: an OCT sign preceding macular hole after vitrectomy for rhegmatogenous retinal detachment. Am. J. Ophthalmol. 218, 192–198. https://doi.org/10.1016/j.ajo.2020.05.030.

Iu, L.P.L., Lee, R., Fan, M.C.Y., Lam, W.-C., Chang, R.T., Wong, I.Y.H., 2017. Serial spectral-domain optical coherence tomography findings in acute retinal pigment epitheliitis and the correlation to visual acuity. Ophthalmology 124, 903–909. https://doi.org/10.1016/j.ophtha.2017.01.043.

Jacklin, H.N., 1977. Acute posterior multifocal placoid pigment epitheliopathy and thyroiditis. Arch. Ophthalmol. 95, 995–997. https://doi.org/10.1001/archopht.1977.04450060081006.

Jadon, T., Sadda, S., Singh, G., Narayan, P., Chhblani, J., Venkatesh, P., 2022. Novel retinal imaging abnormalities in Alport syndrome. Retin. Cases Brief Rep. https://doi.org/10.1097/ICB.0000000000001265.

Jaramillo, A., Gaete, G., Romero, P., Orellana, P., Illanes, S., 2009. Acute pontine infarct in a 16-year-old man with acute posterior multifocal placoid pigment epitheliopathy. A case report. J. Stroke Cerebrovasc. Dis. 18, 164–166. https://doi.org/10.1016/j.jstrokecerebrovasdis.2008.08.004.

Junghans, A., Sies, H., Stahl, W., 2001. Macular pigments lutein and zeaxanthin as blue light filters studied in liposomes. Arch. Biochem. Biophys. 391, 160–164. https://doi.org/10.1006/abbi.2001.2411.

Kelley, J.S., Hoover, R.E., George, T., 1978. Whiplash maculopathy. Arch. Ophthalmol. 96, 834–835. https://doi.org/10.1001/archopht.1978.03910050440007.

Kersten, D.H., Lessell, S., Carlow, T.J., 1987. Acute posterior multifocal placoid pigment epitheliopathy and late-onset meningo-encephalitis. Ophthalmology 94, 393–396. https://doi.org/10.1016/s0161-6420(87)33434-7.

Kesim, C., Bektas, S.N., Kulali, Z., Yildiz, E., Ersoz, M.G., Sahin, A., Gunduz-Demir, C., Hasanreisoglu, M., 2022. Henle fiber layer mapping with directional optical coherence tomography. Retina. https://doi.org/10.1097/IAE.0000000000003514.

Khachik, F., Bernstein, P.S., Garland, D.L., 1997. Identification of lutein and zeaxanthin oxidation products in human and monkey retinas. Invest. Ophthalmol. Vis. Sci. 38, 1802–1811.

Khmelinskii, I., Golubeva, T., Korneeva, E., Inyushin, M., Zueva, L., Makarov, V., 2017. Spectral selectivity model for light transmission by the intermediate filaments in Müller cells. J. Photochem. Photobiol., B 173, 282–290. https://doi.org/10.1016/j.jphotobiol.2017.06.001.

Kim, J.H., Lee, S.H., Han, J.Y., Kang, H.G., Byeon, S.H., Kim, S.S., Koh, H.J., Lee, S.C., Kim, M., 2019. Comparison of individual retinal layer thicknesses between highly myopic eyes and normal control eyes using retinal layer segmentation analysis. Sci. Rep. 9, 14000 https://doi.org/10.1038/s41598-019-50306-w.

Kim, N.R., Lee, E.S., Seong, G.J., Kim, J.H., An, H.G., Kim, C.Y., 2010. Structure-function relationship and diagnostic value of macular ganglion cell complex measurement using Fourier-domain OCT in glaucoma. Invest. Ophthalmol. Vis. Sci. 51, 4646–4651. https://doi.org/10.1167/iovs.09-5053.

Kim, S., Lee, J.Y., Kim, S.-O., Kook, M.S., 2015. Macular structure-function relationship at various spatial locations in glaucoma. Br. J. Ophthalmol. 99, 1412–1418. https://doi.org/10.1136/bjophthalmol-2014-306538.

Kim, T.Y., Lee, M.W., Baek, S.K., Lee, Y.H., 2020. Comparison of retinal layer thicknesses of highly myopic eyes and normal eyes. Kor. J. Ophthalmol. 34, 469–477. https://doi.org/10.3341/kjo.2020.0012.

Kline, D.C., Vitale, A., Warner, J.E., 2007. Acute multifocal placoid pigment epitheliopathy associated with cavernous sinus thrombosis. Ocul. Immunol. Inflamm. 15, 443–446. https://doi.org/10.1080/09273940701732271.

Klufas, M.A., Phasukkijwatana, N., Iafe, N.A., Prasad, P.S., Agarwal, A., Gupta, V., Ansari, W., Pichi, F., Srivastava, S., Freund, K.B., Sadda, S.R., Sarraf, D., 2017. Optical coherence tomography angiography reveals choriocapillaris flow reduction in placoid chorioretinitis. Ophthalmol. Retina 1, 77–91. https://doi.org/10.1016/j.oret.2016.08.008.

Knox, D.L., 2021. Acute posterior multifocal placoid pigment epitheliopathy complicated by fatal cerebral vasculitis. J. Neuro Ophthalmol. 41, e817–e819. https://doi.org/10.1097/WNO.0000000000000987.

Kohno, T., Ishibashi, T., Inomata, H., Ikui, H., Taniguchi, Y., 1983. Experimental macular edema of commotio retinae: preliminary report. Jpn. J. Ophthalmol. 27, 149–156.

Kraemer, L.S., Montgomery, J.R., Baker, K.M., Colyer, M.H., 2022. Acute posterior multifocal placoid pigment epitheliopathy after immunization with multiple vaccines. Retin. Cases Brief Rep. 16, 16–19. https://doi.org/10.1097/ICB.0000000000000959.

Krill, A.E., Deutman, A.F., 1972. Acute retinal pigment epitheliitus. Am. J. Ophthalmol. 74, 193–205. https://doi.org/10.1016/0002-9394(72)90535-1.

Laatikainen, L.T., Immonen, I.J., 1988. Acute posterior multifocal placoid pigment epitheliopathy in connection with acute nephritis. Retina 8, 122–124. https://doi.org/10.1097/00006982-198808020-00007.

Labin, A.M., Safuri, S.K., Ribak, E.N., Perlman, I., 2014. Müller cells separate between wavelengths to improve day vision with minimal effect upon night vision. Nat. Commun. 5, 4319. https://doi.org/10.1038/ncomms5319.

Landrum, J.T., Bone, R.A., 2001. Lutein, zeaxanthin, and the macular pigment. Arch. Biochem. Biophys. 385, 28–40. https://doi.org/10.1006/abbi.2000.2171.

Lane, R.G., Nelson, M.L., Belmont, J.B., 2004. Petalloid foveal hemorrhage in a patient with high myopia. Arch. Ophthalmol. 122, 660–661. https://doi.org/10.1001/archopht.122.4.660.

Leber, T., 1916. Pseudonephritic retinal disease, stellate retinitis; the angiopathic retinal affection after severe skull injury. Graefe-Saemisch Handb Ges Augenheilkd 7, 1319.

Ledesma-Gil, G., Spaide, R.F., 2022. Acute fovealitis. Retin. Cases Brief Rep. 16, 133–135. https://doi.org/10.1097/ICB.0000000000000973.

Lee, D.J., Woertz, E.N., Visotcky, A., Wilk, M.A., Heitkotter, H., Linderman, R.E., Tarima, S., Summers, C.G., Brooks, B.P., Brilliant, M.H., Antony, B.J., Lujan, B.J., Carroll, J., 2018a. The Henle fiber layer in albinism: comparison to normal and relationship to outer nuclear layer thickness and foveal cone density. Invest. Ophthalmol. Vis. Sci. 59, 5336–5348. https://doi.org/10.1167/iovs.18-24145.

Lee, H., Purohit, R., Patel, A., Papageorgiou, E., Sheth, V., Maconachie, G., Pilat, A., McLean, R.J., Proudlock, F.A., Gottlob, I., 2015a. In vivo foveal development using optical coherence tomography. Invest. Ophthalmol. Vis. Sci. 56, 4537. https://doi.org/10.1167/iovs.15-16542.

Lee, J.J., Vrabec, T.R., Baldassano, V.F., 2015b. Cancer-associated retinopathy with unusual retinal whitening. Retin. Cases Brief Rep. 9, 21–24. https://doi.org/10.1097/ICB.0000000000000083.

Lee, J.-W., Morales, E., Sharifipour, F., Amini, N., Yu, F., Afifi, A.A., Coleman, A.L., Caprioli, J., Nouri-Mahdavi, K., 2017. The relationship between central visual field sensitivity and macular ganglion cell/inner plexiform layer thickness in glaucoma. Br. J. Ophthalmol. 101, 1052–1058. https://doi.org/10.1136/bjophthalmol-2016-309208.

Lee, W.J., Kim, T.J., Kim, Y.K., Jeoung, J.W., Park, K.H., 2018b. Serial combined wide-field optical coherence tomography maps for detection of early glaucomatous structural progression. JAMA Ophthalmol. 136, 1121–1127. https://doi.org/10.1001/jamaophthalmol.2018.3160.

Li, D., Akiyama, H., Kishi, S., 2018a. Optical coherence tomography patterns and outcomes of contusion maculopathy caused by impact of sporting equipment. BMC Ophthalmol. 18, 174. https://doi.org/10.1186/s12886-018-0843-x.

Li, K.X., Young, B.K., Miller, J.M.L., Besirli, C.G., 2021. Concentric macular rings without ocular pathology. Ophthalm. Surg. Lasers Imag. Retin. 52, 353–355. https://doi.org/10.3928/23258160-20210528-09.

Li, M., Huisingh, C., Messinger, J., Dolz-Marco, R., Ferrara, D., Freund, K.B., Curcio, C.A., 2018b. Histology of geographic atrophy secondary to age-related macular degeneration: a multilayer approach. Retina 38, 1937–1953. https://doi.org/10.1097/IAE.0000000000002182.

Li, M., Zhang, X., Ji, Y., Ye, B., Wen, F., 2015. Acute macular neuroretinopathy in dengue fever: short-term prospectively followed up case series. JAMA Ophthalmol. 133, 1329–1333. https://doi.org/10.1001/jamaophthalmol.2015.2687.

Li, Y.-H., Chang, Y.-C., Wu, W.-C., 2019. Spectral-domain optical coherence tomography finding of acute retinal pigment epitheliitis. Taiwan J Ophthalmol 9, 276–279. https://doi.org/10.4103/tjo.tjo_23_19.

Linsenmeier, R.A., 1986. Effects of light and darkness on oxygen distribution and consumption in the cat retina. J. Gen. Physiol. 88, 521–542. https://doi.org/10.1085/jgp.88.4.521.

Linsenmeier, R.A., Braun, R.D., 1992. Oxygen distribution and consumption in the cat retina during normoxia and hypoxemia. J. Gen. Physiol. 99, 177–197. https://doi.org/10.1085/jgp.99.2.177.

Linsenmeier, R.A., Zhang, H.F., 2017. Retinal oxygen: from animals to humans. Prog. Retin. Eye Res. 58, 115–151. https://doi.org/10.1016/j.preteyeres.2017.01.003.

Loduca, A.L., Zhang, C., Zelkha, R., Shahidi, M., 2010. Thickness mapping of retinal layers by spectral-domain optical coherence tomography. Am. J. Ophthalmol. 150, 849–855. https://doi.org/10.1016/j.ajo.2010.06.034.

Lowder, C.Y., Foster, R.E., Gordon, S.M., Gutman, F.A., 1996. Acute posterior multifocal placoid pigment epitheliopathy after acute group A streptococcal infection. Am. J. Ophthalmol. 122, 115–117. https://doi.org/10.1016/s0002-9394(14)71974-9.

Luckie, A., Ai, E., Del Piero, E., 1994. Progressive zonal outer retinitis. Am. J. Ophthalmol. 118, 583–588. https://doi.org/10.1016/s0002-9394(14)76573-0.

Lujan, B.J., Roorda, A., Croskrey, J.A., Dubis, A.M., Cooper, R.F., Bayabo, J.-K., Duncan, J.L., Antony, B.J., Carroll, J., 2015. Directional optical coherence tomography provides accurate outer nuclear layer and henle fiber layer measurements. Retina 35, 1511–1520. https://doi.org/10.1097/IAE.0000000000000527.

Lujan, B.J., Roorda, A., Knighton, R.W., Carroll, J., 2011. Revealing Henle's fiber layer using spectral domain optical coherence tomography. Invest. Ophthalmol. Vis. Sci. 52, 1486–1492. https://doi.org/10.1167/iovs.10-5946.

Luneau, K., Newman, N.J., Srivastava, S., Biousse, V., 2009. A case of acute posterior multifocal placoid pigment epitheliopathy with recurrent stroke. J. Neuro Ophthalmol. 29, 111–118. https://doi.org/10.1097/WNO.0b013e318199bfd9.

Maamari, R.N., Stunkel, L., Kung, N.H., Ferguson, C.J., Tanabe, J., Schmidt, R.E., Dahiya, S., Dhand, A., Van Stavern, G.P., Rajagopal, R., Harocopos, G.J., 2019. Acute posterior multifocal placoid pigment epitheliopathy complicated by fatal cerebral vasculitis. J. Neuro Ophthalmol. 39, 260–267. https://doi.org/10.1097/WNO.0000000000000750.

Makarov, V., Zueva, L., Golubeva, T., Korneeva, E., Khmelinskii, I., Inyushin, M., 2017. Quantum mechanism of light transmission by the intermediate filaments in some specialized optically transparent cells. Neurophotonics 4, 011005. https://doi.org/10.1117/1.NPh.4.1.011005.

Maldonado, R.S., O'Connell, R.V., Sarin, N., Freedman, S.F., Wallace, D.K., Cotten, C.M., Winter, K.P., Stinnett, S., Chiu, S.J., Izatt, J.A., Farsiu, S., Toth, C.A., 2011. Dynamics of human foveal development after premature birth. Ophthalmology 118, 2315–2325. https://doi.org/10.1016/j.ophtha.2011.05.028.

Mann, I., 1964. The Development of the Human Eye. Grune & Stratton.

Mansour, A.M., Green, W.R., Hogge, C., 1992. Histopathology of commotio retinae. Retina 12, 24–28. https://doi.org/10.1097/00006982-199212010-00006.

Matamala, J.M., Feuerhake, W., Verdugo, R., 2013. Delayed recurrent stroke in a young patient with acute posterior multifocal placoid pigment epitheliopathy. J. Stroke Cerebrovasc. Dis. 22, e630–e634. https://doi.org/10.1016/j.jstrokecerebrovasdis.2012.09.014.

Matsuo, T., Horikoshi, T., Nagai, C., 2002. Acute posterior multifocal placoid pigment epitheliopathy and scleritis in a patient with pANCA-positive systemic vasculitis. Am. J. Ophthalmol. 133, 566–568. https://doi.org/10.1016/s0002-9394(01)01369-1.

Merkoudis, N., Granstam, E., 2013. Acute retinal pigment epitheliitis: optical coherence tomography findings at onset and follow-up. Acta Ophthalmol. 91, e84–e85. https://doi.org/10.1111/j.1755-3768.2012.02442.x.

Michaelson, I.C., 1954. Retinal circulation in man and animals. Am. J. Ophthalmol. 38, 419–420.

Miraftabi, A., Amini, N., Morales, E., Henry, S., Yu, F., Afifi, A., Coleman, A.L., Caprioli, J., Nouri-Mahdavi, K., 2016. Macular SD-OCT outcome measures: comparison of local structure-function relationships and dynamic range. Invest. Ophthalmol. Vis. Sci. 57, 4815–4823. https://doi.org/10.1167/iovs.16-19648.

Mishra, S., Goel, S., Nangia, P., Senger, D., Shah, A.V., Saurabh, K., Roy, R., 2019. Acute macular neuroretinopathy after blunt ocular trauma: a rare association. Indian J. Ophthalmol. 67, 566–568. https://doi.org/10.4103/ijo.IJO_1251_18.

Missaka, R.F.B.G., Goldbaum, M., Machado, C.G., Cunningham, E.T., Souto, F.M.S., Lavezzo, M.M., da Nóbrega, P.F.C., Sakata, V.M., Oyamada, M.K., Hirata, C.E., Yamamoto, J.H., 2022. Fingerprint sign in Vogt-Koyanagi-Harada disease: a case series. Int. J. Retina Vitreous 8, 7. https://doi.org/10.1186/s40942-021-00356-y.

Miura, M., Elsner, A.E., Cheney, M.C., Usui, M., Iwasaki, T., 2007. Imaging polarimetry and retinal blood vessel quantification at the epiretinal membrane. J. Opt. Soc. Am. Opt Image Sci. Vis. 24, 1431–1437. https://doi.org/10.1364/josaa.24.001431.

Miura, M., Elsner, A.E., Weber, A., Cheney, M.C., Osako, M., Usui, M., Iwasaki, T., 2005. Imaging polarimetry in central serous chorioretinopathy. Am. J. Ophthalmol. 140, 1014–1019. https://doi.org/10.1016/j.ajo.2005.06.033.

Mohammadzadeh, V., Rabiolo, A., Fu, Q., Morales, E., Coleman, A.L., Law, S.K., Caprioli, J., Nouri-Mahdavi, K., 2020. Longitudinal macular structure-function relationships in glaucoma. Ophthalmology 127, 888–900. https://doi.org/10.1016/j.ophtha.2020.01.023.

Monson, D.M., Smith, J.R., 2011. Acute zonal occult outer retinopathy. Surv. Ophthalmol. 56, 23–35. https://doi.org/10.1016/j.survophthal.2010.07.004.

Moraes, R.T., Vianna, R.N.G., Cunha de Souza, E., Moraes, L.S., 2020. Clinical variants of presumed acute fovealitis. Retin. Cases Brief Rep. https://doi.org/10.1097/ICB.0000000000001080.

Mottes, J., Ortolan, D., Ruffato, G., 2022. Haidinger's brushes: psychophysical analysis of an entoptic phenomenon. Vis. Res. 199, 108076 https://doi.org/10.1016/j.visres.2022.108076.

Mrejen, S., Gallego-Pinazo, R., Freund, K.B., Paques, M., 2013. Recognition of Henle's fiber layer on OCT images. Ophthalmology 120, e32–e33. https://doi.org/10.1016/j.ophtha.2013.01.039 e1.

Mrejen, S., Sarraf, D., Chexal, S., Wald, K., Freund, K.B., 2016. Choroidal involvement in acute posterior multifocal placoid pigment epitheliopathy. Ophthalm. Surg. Lasers Imag. Retin. 47, 20–26. https://doi.org/10.3928/23258160-20151214-03.

Munk, M.R., Jampol, L.M., Cunha Souza, E., de Andrade, G.C., Esmaili, D.D., Sarraf, D., Fawzi, A.A., 2016. New associations of classic acute macular neuroretinopathy. Br. J. Ophthalmol. 100, 389–394. https://doi.org/10.1136/bjophthalmol-2015-306845.

Munoz-Solano, J., Fernández-Avellaneda, P., Gallego-Pinazo, R., Dolz-Marco, R., 2022. Atypical acute fovealitis in COVID-19 context. Am. J. Ophthalmol. Case Rep. 101641 https://doi.org/10.1016/j.ajoc.2022.101641.

Na, J.H., Kook, M.S., Lee, Y., Baek, S., 2012. Structure-function relationship of the macular visual field sensitivity and the ganglion cell complex thickness in glaucoma. Invest. Ophthalmol. Vis. Sci. 53, 5044–5051. https://doi.org/10.1167/iovs.11-9401.

Narayanan, K., Wadhwa, S., 1998. Photoreceptor morphogenesis in the human retina: a scanning electron microscopic study. Anat. Rec. 252, 133–139. https://doi.org/10.1002/(SICI)1097-0185 (199809)252:1<133::AID-AR11>3.0.CO;2-P.

Nassisi, M., Lei, J., Abdelfattah, N.S., Karamat, A., Balasubramanian, S., Fan, W., Uji, A., Marion, K.M., Baker, K., Huang, X., Morgenthien, E., Sadda, S.R., 2019. OCT risk factors for development of late age-related macular degeneration in the fellow eyes of patients enrolled in the HARBOR study. Ophthalmology 126, 1667–1674. https://doi.org/10.1016/j.ophtha.2019.05.016.

Nentwich, M.M., Leys, A., Cramer, A., Ulbig, M.W., 2013. Traumatic retinopathy presenting as acute macular neuroretinopathy. Br. J. Ophthalmol. 97, 1268–1272. https://doi.org/10.1136/bjophthalmol-2013-303354.

Ng, A.W., Teoh, S.C., 2015. Dengue eye disease. Surv. Ophthalmol. 60, 106–114. https://doi.org/10.1016/j.survophthal.2014.07.003.

Ng, X.L., Betzler, B.K., Testi, I., Ho, S.L., Tien, M., Ngo, W.K., Zierhut, M., Chee, S.P., Gupta, V., Pavesio, C.E., de Smet, M.D., Agrawal, R., 2021. Ocular adverse events after COVID-19 vaccination. Ocul. Immunol. Inflamm. 29, 1216–1224. https://doi.org/10.1080/09273948.2021.1976221.

Ni, S., Khan, S., Nguyen, T.-T.P., Ng, R., Lujan, B.J., Tan, O., Huang, D., Jian, Y., 2022. Volumetric directional optical coherence tomography. Biomed. Opt Express 13, 950–961. https://doi.org/10.1364/BOE.447882.

Nilforushan, N., Nassiri, N., Moghimi, S., Law, S.K., Giaconi, J., Coleman, A.L., Caprioli, J., Nouri-Mahdavi, K., 2012. Structure-function relationships between spectral-domain OCT and standard achromatic perimetry. Invest. Ophthalmol. Vis. Sci. 53, 2740–2748. https://doi.org/10.1167/iovs.11-8320.

Nolan, J.M., Loughman, J., Akkali, M.C., Stack, J., Scanlon, G., Davison, P., Beatty, S., 2011. The impact of macular pigment augmentation on visual performance in normal subjects: compass. Vis. Res. 51, 459–469. https://doi.org/10.1016/j.visres.2010.12.016.

Nouri-Mahdavi, K., Fatehi, N., Caprioli, J., 2019. Longitudinal macular structure-function relationships in glaucoma and their sources of variability. Am. J. Ophthalmol. 207, 18–36. https://doi.org/10.1016/j.ajo.2019.04.034.

Oh, J., Jung, J.-H., Moon, S.W., Song, S.J., Yu, H.G., Cho, H.Y., 2011. Commotio retinae with spectral-domain optical coherence tomography. Retina 31, 2044–2049. https://doi.org/10.1097/IAE.0b013e31820f4bb4.

O'Halloran, H.S., Berger, J.R., Lee, W.B., Robertson, D.M., Giovannini, J.A., Krohel, G.B., Meckler, R.J., Selhorst, J.B., Lee, A.G., Nicolle, D.A., O'Day, J., 2001. Acute multifocal placoid pigment epitheliopathy and central nervous system involvement: nine new cases and a review of the literature. Ophthalmology 108, 861–868. https://doi.org/10.1016/s0161-6420(01)00565-6.

Olguín-Manríquez, F., Cernichiaro-Espinosa, L., Olguín-Manríquez, A., Manríquez-Arias, R., Flores-Villalobos, E.O., Kawakami-Campos, P.A., 2021. Unilateral acute posterior multifocal placoid pigment epitheliopathy in a convalescent COVID-19 patient. Int. J. Retina Vitreous 7, 41. https://doi.org/10.1186/s40942-021-00312-w.

Oliveira, M.A., Simão, J., Martins, A., Farinha, C., 2020. Management of acute posterior multifocal placoid pigment epitheliopathy (APMPPE): insights from multimodal imaging with OCTA. Case Rep. Ophthalmol. Med., 7049168 https://doi.org/10.1155/2020/7049168.

Ong, S.S., Ahmed, I., Scott, A.W., 2021. Association of acute macular neuroretinopathy or paracentral acute middle maculopathy with sickle cell disease. Ophthalmol. Retina 5, 1146–1155. https://doi.org/10.1016/j.oret.2021.01.003.

Ooi, K.G.-J., Inglis, H., Paramanathan, N., Downie, J.A., Hennessy, M.P., 2016. Dengue fever-associated maculopathy and panuveitis in Australia. Case Rep. Ophthalmol. Med., 5704695 https://doi.org/10.1155/2016/5704695.

Ooto, S., Hangai, M., Tomidokoro, A., Saito, H., Araie, M., Otani, T., Kishi, S., Matsushita, K., Maeda, N., Shirakashi, M., Abe, H., Ohkubo, S., Sugiyama, K., Iwase, A., Yoshimura, N., 2011. Effects of age, sex, and axial length on the three-dimensional profile of normal macular layer structures. Invest. Ophthalmol. Vis. Sci. 52, 8769–8779. https://doi.org/10.1167/iovs.11-8388.

Otani, T., Yamaguchi, Y., Kishi, S., 2011. Improved visualization of Henle fiber layer by changing the measurement beam angle on optical coherence tomography. Retina 31, 497–501. https://doi.org/10.1097/IAE.0b013e3181ed8dae.

Ouyang, Y., Heussen, F.M., Hariri, A., Keane, P.A., Sadda, S.R., 2013a. Optical coherence tomography–based observation of the natural history of drusenoid lesion in eyes with dry age-related macular degeneration. Ophthalmology 120, 2656–2665. https://doi.org/10.1016/j.ophtha.2013.05.029.

Ouyang, Y., Walsh, A.C., Keane, P.A., Heussen, F.M., Pappuru, R.K., Sadda, S.R., 2013b. Different phenotypes of the appearance of the outer plexiform layer on optical coherence tomography. Graefe's Arch. Clin. Exp. Ophthalmol. 251, 2311–2317.

Packer, O., Hendrickson, A.E., Curcio, C.A., 1990. Developmental redistribution of photoreceptors across theMacaca nemestrina (pigtail macaque) retina. J. Comp. Neurol. 298, 472–493. https://doi.org/10.1002/cne.902980408.

Pang, C.E., Freund, K.B., 2014. Pachychoroid pigment epitheliopathy may masquerade as acute retinal pigment epitheliitis. Invest. Ophthalmol. Vis. Sci. 55, 5252. https://doi.org/10.1167/iovs.14-14959.

Park, D.-W., Alonzo, B., Faridi, A., Bhavsar, K.V., 2021. Multimodal imaging of photic maculopathy from arc welding. Retin. Cases Brief Rep. 15, 468–472. https://doi.org/10.1097/ICB.0000000000000823.

Park, J.J., Soetikno, B.T., Fawzi, A.A., 2016. Characterization of the middle capillary plexus using optical coherence tomography angiography in healthy and diabetic eyes. Retina 36, 2039–2050. https://doi.org/10.1097/IAE.0000000000001077.

Parsons, M.A., Talbot, J.F., Mudhar, H.S., Rutty, G.N., 2005. The pathology of whiplash maculopathy and retinopathy : illustrated observations derived from a fatal roller-coaster accident. Forensic Sci. Med. Pathol. 1, 19–25. https://doi.org/10.1385/FSMP:1:1:019.

Patel, Y.P., Saraf, S.S., Desai, A., Desai, U.R., 2016. Roller coaster retinopathy: case report of symptomatic bilateral intraretinal hemorrhages after shaking injury in an otherwise healthy adult. Retin. Cases Brief Rep. 10, 259–262. https://doi.org/10.1097/ICB.0000000000000245.

Pease, P.L., Adams, A.J., Nuccio, E., 1987. Optical density of human macular pigment. Vis. Res. 27, 705–710. https://doi.org/10.1016/0042-6989(87)90067-8.

Perry, V.H., Cowey, A., 1988. The lengths of the fibres of Henle in the retina of macaque monkeys: implications for vision. Neuroscience 25, 225–236. https://doi.org/10.1016/0306-4522(88)90021-8.

Pham, T.Q., Chua, B., Gorbatov, M., Mitchell, P., 2007. Optical coherence tomography findings of acute traumatic maculopathy following motor vehicle accident. Am. J. Ophthalmol. 143, 348–350. https://doi.org/10.1016/j.ajo.2006.09.024.

Pi, S., Hormel, T.T., Wei, X., Cepurna, W., Wang, B., Morrison, J.C., Jia, Y., 2020. Retinal capillary oximetry with visible light optical coherence tomography. Proc. Natl. Acad. Sci. U. S. A. 117, 11658–11666. https://doi.org/10.1073/pnas.1918546117.

Pichi, F., Dolz-Marco, R., Francis, J.H., Au, A., Davis, J.L., Fawzi, A., Gattousi, S., Goldstein, D.A., Keane, P.A., Miserocchi, E., Marchese, A., Ohno-Matsui, K., Sagoo, M.S., Smith, S.D., Sobol, E.K., Tasiopoulou, A., Yang, X., Shields, C.L., Freund, K.B., Sarraf, D., 2021. Advanced OCT analysis of biopsy-proven vitreoretinal lymphoma. Am. J. Ophthalmol. 238, 16–26. https://doi.org/10.1016/j.ajo.2021.11.023.

Pichi, F., Invernizzi, A., Tucker, W.R., Munk, M.R., 2020. Optical coherence tomography diagnostic signs in posterior uveitis. Prog. Retin. Eye Res. 75, 100797 https://doi.org/10.1016/j.preteyeres.2019.100797.

Pillar, S., Gepstein, R., Gal-Or, O., Kramer, M., 2021. Acute posterior multifocal placoid pigment epitheliopathy associated with CN III palsy. Am. J. Ophthalmol. Case Rep. 22, 101102 https://doi.org/10.1016/j.ajoc.2021.101102.

Polyak, S.L., 1957. The Vertebrate Visual System; its Origin, Structure, and Function and its Manifestations in Disease with an Analysis of its Role in the Life of Animals and in the Origin of Man. Preceded by a Historical Review of Investigations of the Eye, and of the Visual Pathways and Centers of the Brain. Univof Chicago Press, Chicago.

Polyak, S.L., 1941. The Retina; the Anatomy and the Histology of the Retina in Man, Ape, and Monkey, Including the Consideration of Visual Functions, the History of Physiological Optics, and the Histological Laboratory Technique. Univ. of Chicago Press, Chicago.

Pournaras, C.J., Riva, C.E., Tsacopoulos, M., Strommer, K., 1989. Diffusion of O2 in the retina of anesthetized miniature pigs in normoxia and hyperoxia. Exp. Eye Res. 49, 347–360. https://doi.org/10.1016/0014-4835(89)90045-6.

Preti, R.C., Zacharias, L.C., Cunha, L.P., Monteiro, M.L.R., 2022. Acute macular neuroretinopathy as the presenting manifestation of COVID-19 infection. Retin. Cases Brief Rep. 16, 12–15. https://doi.org/10.1097/ICB.0000000000001050.

Provis, J.M., Diaz, C.M., Dreher, B., 1998. Ontogeny of the primate fovea: a central issue in retinal development. Prog. Neurobiol. 54, 549–580. https://doi.org/10.1016/s0301-0082(97)00079-8.

Quinn, N., Csincsik, L., Flynn, E., Curcio, C.A., Kiss, S., Sadda, S.R., Hogg, R., Peto, T., Lengyel, I., 2019. The clinical relevance of visualising the peripheral retina. Prog. Retin. Eye Res. 68, 83–109. https://doi.org/10.1016/j.preteyeres.2018.10.001.

Rahimy, E., Sarraf, D., 2013. Paraneoplastic and non-paraneoplastic retinopathy and optic neuropathy: evaluation and management. Surv. Ophthalmol. 58, 430–458. https://doi.org/10.1016/j.survophthal.2012.09.001.

Ramrath, L., Moreno, G., Mueller, H., Bonin, T., Huettmann, G., Schweikard, A., 2008. Towards multi-directional OCT for speckle noise reduction. Med. Imag. Comput. Comput. Assist. Interv. 11, 815–823. https://doi.org/10.1007/978-3-540-85988-8_97.

Ramtohul, P., Cabral, D., Curcio, C.A., Freund, K.B., 2022a. High-resolution spectral domain optical coherence tomography of congenital grouped albinotic spots. Retina 42 (9), e41–e42. https://doi.org/10.1097/IAE.0000000000003552.

Ramtohul, P., Comet, A., Denis, D., 2020a. Multimodal imaging correlation of the concentric macular rings sign in foveal hypoplasia: a distinctive Henle fiber layer geometry. Ophthalmol. Retina 4, 946–953. https://doi.org/10.1016/j.oret.2020.03.022.

Ramtohul, P., Comet, A., Denis, D., 2020b. Optical coherence tomography angiography recovery pattern of acute macular neuroretinopathy. JAMA Ophthalmol. 138, 221–223. https://doi.org/10.1001/jamaophthalmol.2019.5066.

Ramtohul, P., Denis, D., 2019. Concentric macular rings sign in chediak-higashi syndrome. Ophthalmology 126, 1616. https://doi.org/10.1016/j.ophtha.2019.07.005.

Ramtohul, P., Denis, D., Gascon, P., 2021a. Bacillary layer detachment in acute posterior multifocal placoid pigment epitheliopathy: a multimodal imaging analysis. Retina 41, e12–e14. https://doi.org/10.1097/IAE.0000000000003014.

Ramtohul, P., Engelbert, M., Malclès, A., Gigon, E., Miserocchi, E., Modorati, G., Cunha de Souza, E., Besirli, C.G., Curcio, C.A., Freund, K.B., 2021b. Bacillary layer detachment: multimodal imaging and histologic evidence of a novel optical coherence tomography terminology: literature review and proposed theory. Retina 41, 2193–2207. https://doi.org/10.1097/IAE.0000000000003217.

Ramtohul, P., Freund, K.B., 2020. Clinical and morphological characteristics of anti-programmed death ligand 1-associated retinopathy: expanding the spectrum of acute macular neuroretinopathy. Ophthalmol. Retina 4, 446–450. https://doi.org/10.1016/j.oret.2019.11.006.

Ramtohul, P., Gascon, P., Denis, D., 2020c. Outer retinal plume signature in multiple evanescent white dot syndrome. Ophthalmol. Retina 4, 766. https://doi.org/10.1016/j.oret.2020.03.023.

Ramtohul, P., Iovino, C., Au, A., Bacci, T., Pichi, F., Corradetti, G., Corvi, F., Manoharan, N., Marin, A.I., Tadayoni, R., Sadda, S., Freund, K.B., Sarraf, D., 2022b. Clinical and morphologic characteristics of perivenular fern-like leakage on ultra-widefield fluorescein angiography. Ophthalmol. Retina. https://doi.org/10.1016/j.oret.2022.05.001. S2468-6530(22)00232–9.

Rao, H.L., Zangwill, L.M., Weinreb, R.N., Leite, M.T., Sample, P.A., Medeiros, F.A., 2011. Structure-function relationship in glaucoma using spectral-domain optical coherence tomography. Arch. Ophthalmol. 129, 864–871. https://doi.org/10.1001/archophthalmol.2011.145.

Raza, A.S., Cho, J., de Moraes, C.G.V., Wang, M., Zhang, X., Kardon, R.H., Liebmann, J. M., Ritch, R., Hood, D.C., 2011. Retinal ganglion cell layer thickness and local visual field sensitivity in glaucoma. Arch. Ophthalmol. 129, 1529–1536. https://doi.org/10.1001/archophthalmol.2011.352.

Reichenbach, A., Bringmann, A., 2020. Glia of the human retina. Glia 68, 768–796. https://doi.org/10.1002/glia.23727.

Reichenbach, A., Schneider, H., Leibnitz, L., Reichelt, W., Schaaf, P., Schümann, R., 1989. The structure of rabbit retinal Müller (glial) cells is adapted to the surrounding retinal layers. Anat. Embryol. 180, 71–79. https://doi.org/10.1007/BF00321902.

Ron, I., Pecht, I., Sheves, M., Cahen, D., 2010. Proteins as solid-state electronic conductors. Acc. Chem. Res. 43, 945–953. https://doi.org/10.1021/ar900161u.

Rotsos, T., Symeonidis, C., Kanakis, M., Andreanos, K., 2021. A fingerprint hidden inside the eye. A unique pattern of outer retina splitting as seen on en-face OCT and OCT-angiography. Am. J. Ophthalmol. Case Rep. 23, 101184 https://doi.org/10.1016/j.ajoc.2021.101184.

Roy, R., Saurabh, K., Thomas, N.R., 2021. Multicolor imaging in a case of acute retinal pigment epitheliitis. Retin. Cases Brief Rep. 15, 45–48. https://doi.org/10.1097/ICB.0000000000000726.

Russell, J.F., Pichi, F., Scott, N.L., Hartley, M.J., Bell, D., Agarwal, A., Leong, B., Holland, G.N., Freund, K.B., Sarraf, D., 2020. Masqueraders of multiple evanescent white dot syndrome (MEWDS). Int. Ophthalmol. 40, 627–638. https://doi.org/10.1007/s10792-019-01223-4.

Rusu, I., Sherman, J., Gallego-Pinazo, R., Lam, M., Freund, K.B., 2013. Spectral-domain optical coherence tomography and fundus autofluorescence findings in a case of laser pointer-induced maculopathy. Retin. Cases Brief Rep. 7, 371–375. https://doi.org/10.1097/ICB.0b013e3182965291.

Sarraf, D., Rahimy, E., Fawzi, A.A., Sohn, E., Barbazetto, I., Zacks, D.N., Mittra, R.A., Klancnik, J.M., Mrejen, S., Goldberg, N.R., Beardsley, R., Sorenson, J.A., Freund, K. B., 2013. Paracentral acute middle maculopathy: a new variant of acute macular neuroretinopathy associated with retinal capillary ischemia. JAMA Ophthalmol. 131, 1275–1287. https://doi.org/10.1001/jamaophthalmol.2013.4056.

Sato, S., Hirooka, K., Baba, T., Tenkumo, K., Nitta, E., Shiraga, F., 2013. Correlation between the ganglion cell-inner plexiform layer thickness measured with cirrus HD-OCT and macular visual field sensitivity measured with microperimetry. Invest. Ophthalmol. Vis. Sci. 54, 3046–3051. https://doi.org/10.1167/iovs.12-11173.

Sawyer, R.A., Selhorst, J.B., Zimmerman, L.E., Hoyt, W.F., 1976. Blindness caused by photoreceptor degeneration as a remote effect of cancer. Am. J. Ophthalmol. 81, 606–613. https://doi.org/10.1016/0002-9394(76)90125-2.

Scharf, J., Freund, K.B., Sadda, S., Sarraf, D., 2020a. Paracentral acute middle maculopathy and the organization of the retinal capillary plexuses. Prog. Retin. Eye Res., 100884 https://doi.org/10.1016/j.preteyeres.2020.100884.

Scharf, J.M., Hilely, A., Preti, R.C., Grondin, C., Chehaibou, I., Greaves, G., Tran, K., Wang, D., Ip, M.S., Hubschman, J.P., Gaudric, A., Sarraf, D., 2020b. Hyperreflective stress lines and macular holes. Invest. Ophthalmol. Vis. Sci. 61, 50. https://doi.org/10.1167/iovs.61.4.50.

Schnitzer, J., 1988. Astrocytes in mammalian retina. Prog. Retin. Res. 7, 209–231.

Seetharam, S.S., Jampol, L.M., Gill, M.K., 2015. New insights into acute annular outer retinopathy. Retin. Cases Brief Rep. 9, 1–6. https://doi.org/10.1097/ICB.0000000000000070.

Sepulveda, Juan A., et al., 2016. Individual differences in foveal shape: feasibility of individual maps between structure and function within the macular region. Investig. Ophthalmol. Vis. Sci. 57 (11) https://doi.org/10.1167/iovs.16-19288, 4772-8.

Seth, D., Mishra, K.P., Ghai, R., Mishra, R., Kumar, A., 2022. Mathematical model for oxygen diffusion in the retina. Mater. Today Proc.

Sherman, M.E., Priestley, B.S., 1962. The Haidinger brush phenomenon: a new clinical use. Am. J. Ophthalmol. 54, 807–812. https://doi.org/10.1016/0002-9394(62)94165-x.

Shimizu, K., Ujiie, K., 1978. Structure of Ocular Vessels. Igaku-Shoin Medical Publishers.

Sigona, M., Morphis, G., Edmunds, M.R., 2015. Bilateral reversible macular edema following road traffic collision. Can. J. Ophthalmol. 50, e53–e54. https://doi.org/10.1016/j.jcjo.2015.03.011.

Sipperley, J.O., Quigley, H.A., Gass, D.M., 1978. Traumatic retinopathy in primates. The explanation of commotio retinae. Arch. Ophthalmol. 96, 2267–2273. https://doi.org/10.1001/archopht.1978.03910060563021.

Sisk, R.A., Parekh, P.K., Riemann, C.D., 2020. Fingerprint macula artifact on Optos fundus imaging in nystagmus. Ophthalmology 127, 96. https://doi.org/10.1016/j.ophtha.2019.09.020.

Sjöstrand, J., Olsson, V., Popovic, Z., Conradi, N., 1999a. Quantitative estimations of foveal and extra-foveal retinal circuitry in humans. Vis. Res. 39, 2987–2998. https://doi.org/10.1016/s0042-6989(99)00030-9.

Sjöstrand, J., Popovic, Z., Conradi, N., Marshall, J., 1999b. Morphometric study of the displacement of retinal ganglion cells subserving cones within the human fovea. Graefes Arch. Clin. Exp. Ophthalmol. 237, 1014–1023. https://doi.org/10.1007/s004170050338.

Sjöstrand, J., Rosén, R., Nilsson, M., Popovic, Z., 2017. Arrested foveal development in preterm eyes: thickening of the outer nuclear layer and structural redistribution within the fovea. Invest. Ophthalmol. Vis. Sci. 58, 4948–4958. https://doi.org/10.1167/iovs.17-22333.

Smelser, G.K., Ozanics, V., Rayborn, M., Sagun, D., 1973. The fine structure of the retinal transient layer of Chievitz. Invest. Ophthalmol. 12, 504–512.

Snodderly, D.M., Auran, J.D., Delori, F.C., 1984a. The macular pigment. II. Spatial distribution in primate retinas. Invest. Ophthalmol. Vis. Sci. 25, 674–685.

Snodderly, D.M., Brown, P.K., Delori, F.C., Auran, J.D., 1984b. The macular pigment. I. Absorbance spectra, localization, and discrimination from other yellow pigments in primate retinas. Invest. Ophthalmol. Vis. Sci. 25, 660–673.

Snodderly, D.M., Weinhaus, R.S., 1990. Retinal vasculature of the fovea of the squirrel monkey, Saimiri sciureus: three-dimensional architecture, visual screening, and relationships to the neuronal layers. J. Comp. Neurol. 297, 145–163. https://doi.org/10.1002/cne.902970111.

Snodderly, D.M., Weinhaus, R.S., Choi, J.C., 1992. Neural-vascular relationships in central retina of macaque monkeys (Macaca fascicularis). J. Neurosci. 12, 1169–1193.

Snyder, A.W., Pask, C., 1973. The Stiles-Crawford effect–explanation and consequences. Vis. Res. 13, 1115–1137. https://doi.org/10.1016/0042-6989(73)90148-x.

Soe, H.J., Khan, A.M., Manikam, R., Samudi Raju, C., Vanhoutte, P., Sekaran, S.D., 2017. High dengue virus load differentially modulates human microvascular endothelial barrier function during early infection. J. Gen. Virol. 98, 2993–3007. https://doi.org/10.1099/jgv.0.000981.

Souza-Santos, F., Lavinsky, D., Moraes, N.S., Castro, A.R., Cardillo, J.A., Farah, M.E., 2012. Spectral-domain optical coherence tomography in patients with commotio retinae. Retina 32, 711–718. https://doi.org/10.1097/IAE.0b013e318227fd01.

Sparrow, J.R., Marsiglia, M., Allikmets, R., Tsang, S., Lee, W., Duncker, T., Zernant, J., 2015. Flecks in recessive Stargardt disease: short-wavelength Autofluorescence, near-infrared autofluorescence, and optical coherence tomography. Invest. Ophthalmol. Vis. Sci. 56, 5029–5039. https://doi.org/10.1167/iovs.15-16763.

Staurenghi, G., Sadda, S., Chakravarthy, U., Spaide, R.F., 2014. Proposed lexicon for anatomic landmarks in normal posterior segment spectral-domain optical coherence tomography. Ophthalmology 121, 1572–1578. https://doi.org/10.1016/j.ophtha.2014.02.023.

Steptoe, P., Pearce, I., Beare, N., Sreekantam, S., Mohammed, B., Barry, R., Steeples, L., Denniston, A., Murray, P., 2022. Proposing a Neurotropic Etiology for Acute Posterior Multifocal Placoid Pigment Epitheliopathy and Relentless Placoid Chorioretinitis. Front. Ophthalmol. https://doi.org/10.3389/fopht.2021.802962, 1, 1.

Stiles, W.S., Crawford, B.H., Parsons, J.H., 1933. The luminous efficiency of rays entering the eye pupil at different points. Proc. R. Soc. Lond. - Ser. B Contain. Pap. a Biol. Character 112, 428–450. https://doi.org/10.1098/rspb.1933.0020.

Stringham, J.M., Fuld, K., Wenzel, A.J., 2004. Spatial properties of photophobia. Invest. Ophthalmol. Vis. Sci. 45, 3838–3848. https://doi.org/10.1167/iovs.04-0038.

Stringham, J.M., Garcia, P.V., Smith, P.A., McLin, L.N., Foutch, B.K., 2011. Macular pigment and visual performance in glare: benefits for photostress recovery, disability glare, and visual discomfort. Invest. Ophthalmol. Vis. Sci. 52, 7406–7415. https://doi.org/10.1167/iovs.10-6699.

Stringham, J.M., Hammond, B.R., 2007. The glare hypothesis of macular pigment function. Optom. Vis. Sci. 84, 859–864. https://doi.org/10.1097/OPX.0b013e3181559c2b.

Su, D.H.-W., Bacsal, K., Chee, S.-P., Flores, J.V.P., Lim, W.-K., Cheng, B.C.-L., Jap, A.H.-E., Dengue Maculopathy Study Group, 2007. Prevalence of dengue maculopathy in patients hospitalized for dengue fever. Ophthalmology 114, 1743–1747. https://doi.org/10.1016/j.ophtha.2007.03.054.

Sujak, A., Gabrielska, J., Grudziński, W., Borc, R., Mazurek, P., Gruszecki, W.I., 1999. Lutein and zeaxanthin as protectors of lipid membranes against oxidative damage: the structural aspects. Arch. Biochem. Biophys. 371, 301–307. https://doi.org/10.1006/abbi.1999.1437.

Thanos, A., Faia, L.J., Yonekawa, Y., Randhawa, S., 2016. Optical coherence tomographic angiography in acute macular neuroretinopathy. JAMA Ophthalmol. 134, 1310. https://doi.org/10.1001/jamaophthalmol.2016.3513.

Tong, K.K., Lujan, B.J., Zhou, Y., Lin, M.C., 2016. Directional optical coherence tomography reveals reliable outer nuclear layer measurements. Optom. Vis. Sci. 93, 714–719. https://doi.org/10.1097/OPX.0000000000000861.

Touhami, S., Audo, I., Terrada, C., Gaudric, A., LeHoang, P., Touitou, V., Bodaghi, B., 2019. Neoplasia and intraocular inflammation: from masquerade syndromes to immunotherapy-induced uveitis. Prog. Retin. Eye Res. https://doi.org/10.1016/j.preteyeres.2019.05.002. S1350946218300740.

Toussaint, D., Kuwabara, T., Cogan, D.G., 1961. Retinal vascular patterns. II. Human retinal vessels studied in three dimensions. Arch. Ophthalmol. 65, 575–581. https://doi.org/10.1001/archopht.1961.01840020577022.

Tran, K., Wang, D., Scharf, J., Sadda, S., Sarraf, D., 2020. Inner choroidal ischaemia and CNV due to handheld laser-induced maculopathy: a case report and review. Eye 34, 1958–1965. https://doi.org/10.1038/s41433-020-0830-3.

Trieschmann, M., van Kuijk, F.J.G.M., Alexander, R., Hermans, P., Luthert, P., Bird, A.C., Pauleikhoff, D., 2008. Macular pigment in the human retina: histological evaluation of localization and distribution. Eye 22, 132–137. https://doi.org/10.1038/sj.eye.6702780.

Turbeville, S.D., Cowan, L.D., Gass, J.D.M., 2003. Acute macular neuroretinopathy: a review of the literature. Surv. Ophthalmol. 48, 1–11. https://doi.org/10.1016/s0039-6257(02)00398-3.

Turpin, A., Chen, S., Sepulveda, J.A., McKendrick, A.M., 2015. Customizing structure-function displacements in the macula for individual differences. Invest. Ophthalmol. Vis. Sci. 56, 5984–5989. https://doi.org/10.1167/iovs.15-17384.

Vajzovic, L., Hendrickson, A.E., O'Connell, R.V., Clark, L.A., Tran-Viet, D., Possin, D., Chiu, S.J., Farsiu, S., Toth, C.A., 2012. Maturation of the human fovea: correlation of spectral-domain optical coherence tomography findings with histology. Am. J. Ophthalmol. 154, 779–789. https://doi.org/10.1016/j.ajo.2012.05.004 e2.

van Blokland, G.J., 1985. Ellipsometry of the human retina in vivo: preservation of polarization. J. Opt. Soc. Am. A 2, 72–75. https://doi.org/10.1364/josaa.2.000072.

Van Buskirk, E.M., Lessell, S., Friedman, E., 1971. Pigmentary epitheliopathy and erythema nodosum. Arch. Ophthalmol. 85, 369–372. https://doi.org/10.1001/archopht.1971.00990050371025.

VanNasdale, D.A., Elsner, A.E., Weber, A., Miura, M., Haggerty, B.P., 2009. Determination of foveal location using scanning laser polarimetry. J. Vis. 9, 21. https://doi.org/10.1167/9.3.21, 1–17.

Vecino, E., Rodriguez, F.D., Ruzafa, N., Pereiro, X., Sharma, S.C., 2016. Glia-neuron interactions in the mammalian retina. Prog. Retin. Eye Res. 51, 1–40. https://doi.org/10.1016/j.preteyeres.2015.06.003.

Villard, F., Thumann, G., Malclès, A., 2019. Bilateral loss of vision a few hours after a motor vehicle crash. JAMA Ophthalmol. 137, 1080–1081. https://doi.org/10.1001/jamaophthalmol.2019.2674.

Waldstein, S.M., Vogl, W.-D., Bogunovic, H., Sadeghipour, A., Riedl, S., Schmidt-Erfurth, U., 2020. Characterization of drusen and hyperreflective foci as biomarkers for disease progression in age-related macular degeneration using artificial intelligence in optical coherence tomography. JAMA Ophthalmol. 138, 740–747. https://doi.org/10.1001/jamaophthalmol.2020.1376.

Walls, G.L., 1942. The Vertebrate Eye and its Adaptive Radiation. Cranbrook Institute of Science, Bloomfield Hills, Mich. https://doi.org/10.5962/bhl.title.7369.

Wang, M., Hood, D.C., Cho, J.-S., Ghadiali, Q., De Moraes, C.G., De Moraes, G.V., Zhang, X., Ritch, R., Liebmann, J.M., 2009. Measurement of local retinal ganglion cell layer thickness in patients with glaucoma using frequency-domain optical coherence tomography. Arch. Ophthalmol. 127, 875–881. https://doi.org/10.1001/archophthalmol.2009.145.

Wang, Q., Wei, W.B., Wang, Y.X., Yan, Y.N., Yang, J.Y., Zhou, W.J., Chan, S.Y., Xu, L., Jonas, J.B., 2020. Thickness of individual layers at the macula and associated factors: the Beijing Eye Study 2011. BMC Ophthalmol. 20, 49. https://doi.org/10.1186/s12886-019-1296-6.

Wangsa-Wirawan, N.D., Linsenmeier, R.A., 2003. Retinal oxygen: fundamental and clinical aspects. Arch. Ophthalmol. 121, 547–557. https://doi.org/10.1001/archopht.121.4.547.

Wartak, A., Augustin, M., Haindl, R., Beer, F., Salas, M., Laslandes, M., Baumann, B., Pircher, M., Hitzenberger, C.K., 2017. Multi-directional optical coherence tomography for retinal imaging. Biomed. Opt Express 8, 5560–5578. https://doi.org/10.1364/BOE.8.005560.

Wässle, H., Boycott, B.B., 1991. Functional architecture of the mammalian retina. Physiol. Rev. 71, 447–480. https://doi.org/10.1152/physrev.1991.71.2.447.

Wässle, H., Grünert, U., Röhrenbeck, J., Boycott, B.B., 1989. Cortical magnification factor and the ganglion cell density of the primate retina. Nature 341, 643–646. https://doi.org/10.1038/341643a0.

Weinstein, J.M., Bresnick, G.H., Bell, C.L., Roschmann, R.A., Brooks, B.R., Strother, C.M., 1988. Acute posterior multifocal placoid pigment epitheliopathy associated with cerebral vasculitis. J. Clin. Neuro Ophthalmol. 8, 195–201.

Wenzel, A.J., Fuld, K., Stringham, J.M., Curran-Celentano, J., 2006. Macular pigment optical density and photophobia light threshold. Vis. Res. 46, 4615–4622. https://doi.org/10.1016/j.visres.2006.09.019.

Wilson, C.A., Choromokos, E.A., Sheppard, R., 1988. Acute posterior multifocal placoid pigment epitheliopathy and cerebral vasculitis. Arch. Ophthalmol. 106, 796–800. https://doi.org/10.1001/archopht.1988.01060130866042.

Wolf, M.D., Folk, J.C., Nelson, J.A., Peeples, M.E., 1992. Acute, posterior, multifocal, placoid, pigment epitheliopathy and Lyme disease. Arch. Ophthalmol. 110, 750. https://doi.org/10.1001/archopht.1992.01080180020004.

Wolf, M.D., Folk, J.C., Panknen, C.A., Goeken, N.E., 1990. HLA-B7 and HLA-DR2 antigens and acute posterior multifocal placoid pigment epitheliopathy. Arch. Ophthalmol. 108, 698–700. https://doi.org/10.1001/archopht.1990.01070070084040.

Xu, X., Yannuzzi, N.A., Fernández-Avellaneda, P., Echegaray, J.J., Tran, K.D., Russell, J. F., Patel, N.A., Hussain, R.M., Sarraf, D., Freund, K.B., 2019. Differentiating veins from arteries on optical coherence tomography angiography by identifying deep capillary plexus vortices. Am. J. Ophthalmol. 207, 363–372. https://doi.org/10.1016/j.ajo.2019.06.009.

Yamada, E., 1969. Some structural features of the fovea centralis in the human retina. Arch. Ophthalmol. 82, 151–159. https://doi.org/10.1001/archopht.1969.00990020153002.

Ye, J., Shen, M., Huang, S., Fan, Y., Yao, A., Pan, C., Shi, X., Lu, F., Shao, Y., 2019. Visual acuity in pathological myopia is correlated with the photoreceptor myoid and ellipsoid zone thickness and affected by choroid thickness. Invest. Ophthalmol. Vis. Sci. 60, 1714–1723. https://doi.org/10.1167/iovs.18-26086.

Yu, D.Y., Cringle, S., Yu, P.K., Su, E.N., Sun, W., Guo, W., Morgan, W.H., Yu, X.B., Balaratnasingam, C., 2009. Retinal Cellular Metabolism and its Regulation and Control. Oxford University Press, New York.

Yu, D.-Y., Cringle, S.J., 2005. Retinal degeneration and local oxygen metabolism. Exp. Eye Res. 80, 745–751. https://doi.org/10.1016/j.exer.2005.01.018.

Yu, D.-Y., Cringle, S.J., 2001. Oxygen distribution and consumption within the retina in vascularised and avascular retinas and in animal models of retinal disease. Prog. Retin. Eye Res. 20, 175–208. https://doi.org/10.1016/S1350-9462(00)00027-6.

Yu, D.Y., Cringle, S.J., Alder, V., Su, E.N., 1999. Intraretinal oxygen distribution in the rat with graded systemic hyperoxia and hypercapnia. Invest. Ophthalmol. Vis. Sci. 40, 2082–2087.

Yu, D.-Y., Cringle, S.J., Su, E.-N., 2005. Intraretinal oxygen distribution in the monkey retina and the response to systemic hyperoxia. Invest. Ophthalmol. Vis. Sci. 46, 4728–4733. https://doi.org/10.1167/iovs.05-0694.

Yu, D.-Y., Cringle, S.J., Yu, P.K., Balaratnasingam, C., Mehnert, A., Sarunic, M.V., An, D., Su, E.-N., 2019. Retinal capillary perfusion: spatial and temporal heterogeneity. Prog. Retin. Eye Res. 70, 23–54. https://doi.org/10.1016/j.preteyeres.2019.01.001.

Yu, D.-Y., Cringle, S.J., Yu, P.K., Su, E.-N., 2007. Intraretinal oxygen distribution and consumption during retinal artery occlusion and graded hyperoxic ventilation in the rat. Invest. Ophthalmol. Vis. Sci. 48, 2290–2296. https://doi.org/10.1167/iovs.06-1197.

Yu, P.K., Balaratnasingam, C., Cringle, S.J., McAllister, I.L., Provis, J., Yu, D.-Y., 2010. Microstructure and network organization of the microvasculature in the human macula. Invest. Ophthalmol. Vis. Sci. 51, 6735. https://doi.org/10.1167/iovs.10-5415.

Yunker, J.J., Ready, E.L., Tucker, C.L., Morris, R.E., Witherspoon, C.D., 2008. Acute posterior multifocal placoid pigment epitheliopathy and thalamic infarction. Retin. Cases Brief Rep. 2, 209–212. https://doi.org/10.1097/ICB.0b013e3180653d27.

Yuodelis, C., Hendrickson, A., 1986. A qualitative and quantitative analysis of the human fovea during development. Vis. Res. 26, 847–855. https://doi.org/10.1016/0042-6989(86)90143-4.

Yuzawa, M., Kawamura, A., Matsui, M., 1994. Indocyanine green video angiographic findings in acute posterior multifocal placoid pigment epitheliopathy. Acta Ophthalmol. 72, 128–133. https://doi.org/10.1111/j.1755-3768.1994.tb02753.x.

Zamir, E., Kaiserman, I., Chowers, I., 1999. Laser pointer maculopathy. Am. J. Ophthalmol. 127, 728–729. https://doi.org/10.1016/s0002-9394(99)00017-3.

Zueva, L., Golubeva, T., Korneeva, E., Makarov, V., Khmelinskii, I., Inyushin, M., 2016. Foveolar Müller cells of the Pied Flycatcher: morphology and distribution of the intermediate filaments regarding the cell transparency. Microsc. Microanal. 22, 379–386. https://doi.org/10.1017/S1431927616000507.

Zueva, L., Golubeva, T., Korneeva, E., Resto, O., Inyushin, M., Khmelinskii, I., Makarov, V., 2020. Electron microscopy study of the central retinal fovea in Pied flycatcher: evidence of a mechanism of light energy transmission through the retina. Heliyon 6, e04146. https://doi.org/10.1016/j.heliyon.2020.e04146.

Zueva, L., Golubeva, T., Korneeva, E., Resto, O., Inyushin, M., Khmelinskii, I., Makarov, V., 2019. Quantum mechanism of light energy propagation through an avian retina. J. Photochem. Photobiol., B 197, 111543. https://doi.org/10.1016/j.jphotobiol.2019.111543.